Investigations on some technologically important polymer nanocomposite films and semi crystalline Polypyrrole films

Thesis submitted to

Cochin University of Science and Technology

in partial fulfillment of the requirements

for the award of the degree of

Doctor of Philosophy

By

Jeeju P P

Department of Physics

Cochin University of Science and Technology

Cochin – 682 022, Kerala, India

June 2012

Investigations on some technologically important polymer nanocomposite films and semi crystalline Polypyrrole films

Author: T 557

Jeeju P. P.
(Associate Professor, Department of Physics,
S N M College, Maliankara)
Teacher Fellow, Division for Research in Advanced Materials
Department of Physics,
Cochin University of Science and Technology,
Cochin-682 022, Kerala, India
Email: jecjupp@gmail.com, jeejusukesan@yahoo.com

Research Advisor:

Dr. S Jayalekshmi
Professor, Department of Physics,
Cochin University of Science and Technology,
Cochin-682 022, Kerala, India
Email:jayalekshmi@cusat.ac.in

Department of Physics,
Cochin University of Science andTechnology,
Cochin-682 022, Kerala, India

June 2012

Cover design: Revathi S

Department of Physics
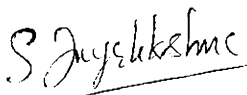## Cochin University of Science and Tecnology
Cochin - 682022

Dr.S.Jayalekshmi
Professor

Certificate

Certified that the research work presented in the thesis entitled **"Investigations on some technologically important polymer nanocomposite films and semi crystalline Polypyrrole films"** is an authentic record of the bonafide research work done by Smt. Jeeju P. P, under my guidance and supervision at the Department of Physics, Cochin University of Science and Technology, Cochin–22, India, and no part of it has been included in any other thesis submitted previously for the award of any degree.

Cochin – 22

Prof. S Jayalekshmi
(Supervising Guide)

Declaration

I hereby declare that the work presented in the thesis entitled **"Investigations on some technologically important polymer nanocomposite films and semi crystalline Polypyrrole films"** is based on the original research work done by me under the guidance of Dr. S. Jayalekshmi, Professor, Department of Physics, Cochin University of Science and Technology, Cochin–22, India and no part of it has been included in any other thesis submitted previously for the award of any degree.

Cochin–22
8 June 2012.

Jeeju P P

Dedicated to

My beloveds

Acknowledgements

Jeeju P P

▌▌▌ CONTENTS ▌▌▌

Preface
List of publications
Papers presented in International/National conferences

Chapter 3

Optical properties of highly transparent, thermally stable, spin coated Zinc Oxide (ZnO)/Polystyrene (PS) nanocomposite films .... 113 - 153

Chapter 4

Size-dependent optical properties of transparent, spin-coated Zinc oxide/ Polystyrene nanocomposite films ...... 155 - 173

Chapter 5

Size dependent nonlinear optical properties of Zinc Oxide-Polystyrene nanocomposite films .... 177 - 192

Chapter 6

On the linear and nonlinear optical properties of thermally stable, ZnO/PS-PMMA nanocomposite films .... 193 - 216

Chapter 7
Novel polypyrrole films with excellent crystallinity
and good thermal stability .... 217 - 236

Chapter 8
Conclusions and future prospects.................................... 237 - 246

Nanostructured materials and related technologies are being extensively pursued during the past few years owing to their innovative applications in all walks of science and technology. The work presented in the thesis deals with the realization of novel polymer nanocomposites with enhanced functionalities and prospects of applications in the fields related to nanophotonics. The development of inorganic/polymer nanocomposites is a rapidly expanding multidisciplinary research area with profound industrial applications. The incorporation of suitable inorganic nanoparticles can endow the resulting nanocomposites with excellent electrical, optical and mechanical properties.

The first part of the thesis deals with the synthesis and characterization of ZnO nanoparticles and transparent ZnO/polymer nanocomposite films. Zinc oxide (ZnO) is a technologically important transparent conducting oxide material noted for its efficient blue-green luminescence and excitonic ultraviolet (UV) laser action at room temperature. These attributes make ZnO/polymer nanocomposite materials potentially interesting for photonic applications in the UV region of the spectrum. Polystyrene (PS) and poly methyl methacrylate (PMMA), which are transparent and flexible thermoplastics with excellent film forming properties are used for the synthesis of ZnO/polymer nanocomposites. The optical characterization of these materials provides rich information about various optical and electronic phenomena, vital for various device fabrication technologies. In the present work, extensive investigations on the size dependent linear and nonlinear optical properties of ZnO/PS and ZnO/PS-PMMA blend

nanocomposite films have been carried out. ZnO shows quantum confinement effects in the experimentally accessible range of sizes. The immiscibility of heterophases of the polymer and ZnO constituents has been resolved by ultrasonicating the mixture, which has ensured the homogeneous dispersion of ZnO nanoparticles in the polymer matrix.

Comprehensive characterization of the ZnO/polymer nanocomposite materials has been undertaken using a wide range of techniques such as XRD, FT-IR, AFM, FESEM, TEM, HRTEM, Raman spectroscopy, TGA, UV-Vis- NIR absorption spectroscopy, Photoluminescence, and Z-scan. The homogeneous ZnO/PS nanocomposite films of about 1μm thickness exhibit enhanced UV- shielding effects in the UVA (400-315 nm), UVB (315-280 nm) and part of UVC (280-100 nm) regions even at low percentage of ZnO loading. The excellent UV shielding effects observed in the ZnO/PS and ZnO/PS-PMMA nanocomposite films offer ample prospects of applications as efficient UV-protection coatings. The nonlinear optical properties of ZnO/PS, ZnO/PMMA and ZnO/PS-PMMA nanocomposite films have been investigated in detail using Z-scan technique. All the nanocomposite films exhibit good optical limiting behavior. Out of the three polymer nanocomposite film systems investigated, the ZnO/PS-PMMA system shows the highest optical limiting efficiency and can be of application as efficient optical limiters to protect sensors from damage due to high intense radiations.

The second part of the thesis deals with the synthesis of polypyrrole (PPy, a conducting polymer) films with appreciable crystallinity and high electrical conductivity. The polypyrrole films prepared from the solution in m-cresol are found to show quite high extent of crystallinity in the XRD

analysis, which has not been reported earlier. Crystallinity influences many of the polymer properties and hence, while selecting polymers for specific applications, it plays an important role. The percentage crystallinity of the PPy films has been determined using XRD and Differential scanning calorimetry (DSC) analysis. There are no earlier reports related to the synthesis of PPy films with exceptionally good crystallinity and the quantitative assessment of the percentage crystallinity. It is the first time that PPy films with high degree of crystallinity have been synthesized and reported. Raman, DSC and TGA studies of the PPy films also give ample support to the observed high extent of crystallinity in the XRD data. These PPy films can be considered as semi crystalline in which highly crystalline regions and amorphous regions co-exist. Semi-crystallinity in polymers is significant because semi crystalline polymers combine the strength of crystalline nature with the flexibility of the amorphous one. The present work is quite significant from this point of view.

The thesis entitled "Investigations on some technologically important polymer nanocomposite films and semi crystalline Polypyrrole films" consists of eight chapters. The **first chapter** gives a general introduction to nanotechnology, nanocomposites and conducting polymers. It also emphasizes the significance of ZnO among other semiconductor materials, which forms the inorganic filler in the polymer nanocomposites of the present study. This chapter also gives general ideas on the properties and applications of conducting polymers with special reference to polypyrrole. The objectives of the present investigations are also clearly addressed in this chapter.

The **second chapter** deals with the theoretical aspects and details of all the experimental techniques used in the present work for the synthesis of polymer nanocomposites and polypyrrole samples and their various characterizations.

Chapter 3 is based on the preparation and properties of ZnO/Polystyrene nanocomposite film samples. The optical properties of these nanocomoposite films are discussed in detail.

Chapter 4 deals with the detailed investigations on the dependence of the optical properties of ZnO/PS nanocomposite films on the size of the nanostructured ZnO filler material. The excellent UV shielding properties of these nanocomposite films form the highlight of this chapter.

Chapter 5 gives a detailed analysis of the nonlinear optical properties of ZnO/PS nanocomposite films using Z scan technique. The effect of ZnO particle size in the composite films on the nonlinear properties is discussed.

The linear and nonlinear optical properties of ZnO/PS, ZnO/PMMA and ZnO/ PS- PMMA nanocomposite films are described and compared in **chapter 6**. The excellent optical limiting and efficient UV shielding characteristics observed in ZnO/PS-PMMA nanocomposite blend films form the highlights of these investigations.

In **chapter 7**, the synthesis and characterization of polypyrrole films with exceptionally high extent of crystallinity are described. These semi crystalline polypyrrole films, synthesized by a dedoping-redoping process show excellent crystallinity not reported earlier.

The general conclusions and the scope for future investigations are included in **chapter 8**

The major highlights of the present investigations are,

1. Successful synthesis of homogeneous, transparent, spin coated ZnO/PS nanocomposite films , using pure ZnO without any surfactants ,which exhibit good UV shielding properties by absorbing about 90% of UVA, UVB and part of UVC radiations, in the range from 395 to 190 nm with 10% ZnO loading in the composite

2. The identification of ZnO/PS-PMMA blend nanocomposite films as prospective nanocomposites for efficient optical limiting and UV shielding applications. The main factor contributing towards the excellent optical characteristics of this polymer blend nanocomposite is the presence of an interpenetrating (IPN) network of PS and PMMA in the polymer blend. This is a very interesting observation which extends ample scope for detailed further investigations.

3. The synthesis of polypyrrole films with exceptionally high extent of crystallinity comparable to crystalline inorganic solids, which has not been reported earlier.

4. It is the first time that polypyrrole films with exceptionally high crystallinity have been synthesized and reported. Crystallinity influences many of the polymer properties, and thus plays an important role while selecting polymers for specific applications. The present work on highly crystalline polypyrrole films is quite significant from this point of view.

List of Publications

In peer reviewed journals – Related to the work presented in the thesis

1. Jeeju.P.P, S.Jayalekshmi,*On the interesting optical properties of highly transparent, thermally stable, spin coated Polystyrene (PS) /Zinc Oxide (ZnO) nanocomposite films,* **Journal of Applied Polymer Science, 120, 1361-1365 (2011)**

2. **Jeeju, P, P,** Sajimol. A.M, Sreevalsa. V.G, S.J.Varma, S. Jayalekshmi, *Size dependent optical properties of transparent, spin coated Polystyrene/Zinc Oxide nanocomposite films,* **Polym Int. 60: 1263–1268 (2011)**

3. **P.P.Jeeju,** S. J.Varma, P.A.Francis Xavier, A.M.Sajimol, S.Jayalekshmi, *Novel polypyrrole films with excellent crystallinity and good thermal stability,* **Mater. Chem. Phys, 134 (2012) pp. 803-808**

4. **P. P. Jeeju,** S. Jayalekshmi, K. Chandrasekharan, P. Sudheesh, *Enhanced linear and nonlinear optical properties of thermally stable ZnO/PS-PMMA nanocomposite films,* **Thin solid films** (Under revision)

5. **P. P. Jeeju,** S. Jayalekshmi, K. Chandrasekharan, P. Sudheesh, *Size dependent nonlinear optical properties of spin coated Zinc Oxide-Polystyrene nanocomposite films,* (Under review)

Other publications in peer reviewed journals

1. S.J.Varma, Jerin George, **P.P. Jeeju,** S. Jayalekshmi, *Quantum confinement effects in highly conducting, ultrathin Polyaniline films pursued through spectroscopic investigations,* **Journal of Luminescence, 132, Issue: 3, 801-805 (2012)**

2. V.G. Sreevalsa; **P.P. Jeeju**; M. Sajimol Augustine; K M. Anilkumar; S.Jayalekshmi; *L-Histidine Modified Biocompatible Zinc Oxide Nanocrystals,* **Journal of Experimental Nanoscience,** DOI: 10.1080/ 17458080.2011.624553   .

3. M. Sajimol Augustine; **P.P. Jeeju** ;V.G. Sreevalsa , S. Jayalekshmi, *Excellent UV absorption in spin-coated thin films of oleic acid modified zinc oxide nanorods embedded in Polyvinyl alcohol,* **Journal of Physics and Chemistry of Solids, 73, Issue 3, 396–401 (2012)**

4. **P.P. Jeeju**, P.A. Francis Xavier, A.M. Sajimol, V.G. Sreevalsa, S.Jayalekshmi, *Micelle-assisted synthesis of polypyrrole nanoparticles and their characterization,* **Science & Society (ISSN 0973-0206) .9 (2), 113-120 (2011)**

5. V.G Sreevalsa, **P.P Jeeju**, M. Sajimol Augustine and S. Jayalekshmi, *Studies on L-citrulline Capped Zinc Oxide Nanocrystals,* **Science & Society (ISSN 0973-0206) .9 (2), 183-188 (2011)**

6. M. Sajimol Augustine, P. Indu, V.G Sreevalsa, **P.P Jeeju** and S. Jayalekshmi, *Solvent Dependent Optical Properties of Highly Luminescent Nanocrystals of ZnS Doped with Manganese,* **Science & Society (ISSN 0973-0206) .9 (2), 109-112 (2011)**

Papers presented in International/National Conferences

1. **Jeeju P. P.** , Sreekanth J Varma, Amritesh M, S Jayalekshmi *"Polypyrrole Nanorods with appreciable Crystallinity and good Optical Absorption Characteristics"* International conference on frontiers in Nano Science and Technology. Cochin Nano -2009, January 3-6, Cochin, Kerala, India.

2. **Jeeju P. P.** , S Jayalekshmi , *"On the interesting optical properties of ZnO nano crystals embedded in polystyrene matrix"* National seminar on Quantum chemistry and Nano techniques;19-20 Nov 2009   S NM College Maliankara, Ernakulum, Kerala.

3. **Jeeju P. P.**, Asha K, S Jayalekshmi, *"Synthesis and study of size dependent optical properties of ZnO nano particles"* National seminar on Nano structured materials and Nano photonics; 4-5 Jan 2010, St.Teresa's college, Ernakulam, Kerala.

4. **Jeeju P. P.** , S Jayalekshmi, *"Transparent PS-ZnO/ Nano composite films with good UV shielding properties"* International conference on Advancements in Polymeric Materials APM-2010, Trends and Technology, 20-22 Feb 2010, CIPET, Bhuvaneswar.

5. **Jeeju P. P**, S J. Varma, Francis Xavier P.A, S.Jayalekshmi, *Polypyrrole films with excellent   crystallinity and good thermal stability*, International conference on Recent Trends   in Materials Science and Technology ICMST-2010, October 29-31, 2010 IIST, Trivandrum.

6. **Jeeju P. P.**, Asha K, S Jayalekshmi, *Investigations on the size dependent optical properties of PS/ZnO nanocomposite films*, International Symposium for Research Scholars on Metallurgy, Materials Science and Engineering ISRS-2010, December 20-22, 2010, Dept. of Metallurgical and Materials Engineering, IIT Madras.

7. **Jeeju P.P.**, Sreevalsa.V.G, Sajimol.A.M and S.Jayalekshmi, *Enhanced UV-shielding properties of ZnO/PS-PMMA nanocomposite films,* The Third International conference on frontiers in Nano Science and Technology. Cochin Nano - 2011, August 14-17, Cochin, Kerala.

8. **P.P. Jeeju**, P.A. Francis Xavier, A.M. Sajimol, V.G. Sreevalsa, S.Jayalekshmi, *Micelle-assisted synthesis of polypyrrole nanoparticles and their characterization,* National symposium on Nano Science and Technology Nanostech – 2011, 1-2 September, Nirmala College Muvattupuzha, Kerala.

9. S.J.Varma, Jerin George, Francis Xavier.P.A, **Jeeju P.P.**, S.Jayalekshmi, *A quest for quantum confinement in conducting Polyaniline through spectroscopic investigations,* International conference on Recent Trends in Materials and Technology ICMST, October 29-31, 2010 IIST, Trivandrum.

10. Francis Xavier.P.A, Bobins Augustine, S J Varma, **Jeeju P. P.**, Amrithesh M and S Jayalekshmi *Functionalization of multiwalled carbon nanotube as a route to synthesize highly conducting polymer-nanocomposites,* International conference on Recent Trends in Materials Science and Technology ICMST-2010, October 29-31, 2010 IIST, Trivandrum.

11. Francis Xavier.P.A, Amrithesh M, S J Varma, **Jeeju P. P.**, S Jayalekshmi, *Studies on Polyaniline-Functionalised Carbon Nanotube Composite Films with Exceptionally High DC Electrical Conductivity,* International Symposium for Research Scholars on Metallurgy, Materials Science and Engineering ISRS-2010, December 20-22, 2010, Dept. of Metallurgical and Materials Engineering, IIT Madras.

12. M. Sajimol Augustine, **P.P. Jeeju**, V.G Sreevalsa, S.Jayalekshmi, *Highly luminescent PANI/ZnO Nanocomposite Films Prepared from Oleic Acid Capped ZnO Nanoparticles,* The Third International conference on frontiers in Nano Science and Technology. Cochin Nano - 2011, August 14-17, Cochin, Kerala.

13. Sreevalsa.V.G. **Jeeju P.P.**, Sajimol Augustine. M., Jayalekshmi. S., *Effect of various capping agents on the optical properties of Zinc oxide nanocrystals,* The Third International conference on frontiers in Nano Science and Technology. Cochin Nano - 2011, August 14-17, Cochin, Kerala.

14. V.G. Sreevalsa, **P.P. Jeeju**, M. Sajimol Augustine and S. Jayalekshmi, *Studies on L-citrulline Capped Zinc Oxide Nanocrystals,* National symposium on Nano Science and Technology Nanostech – 2011, 1-2 September, Nirmala College Muvattupuzha, Kerala.

15. M. Sajimol Augustine, P. Indu, V.G Sreevalsa, **P.P. Jeeju** and S. Jayalekshmi, *Solvent Dependent Optical Properties of Highly Luminescent Nanocrystals of ZnS Doped with Manganese,* National symposium on Nano Science and Technology Nanostech – 2011, 1-2 September, Nirmala College Muvattupuzha, Kerala.

.....ഇാര.....

Chapter **1**

Introduction

This chapter serves as a general introduction to the thesis. Investigations on semiconductor nanocrystals, polymer nanocomposites and crystalline conducting polymers, form the essence of the thesis. In this chapter, the basic concepts and relevance of nanotechnology, with emphasis on semiconductor nano crystals and polymer nanocomposites and the significance and potential of electrically conducting polymers are discussed. The motivation for carrying out the present studies, the importance of the materials chosen and the objectives of the present work are also addressed in this section.

1.1 Motivation

Physics of systems of reduced dimensionality is a fascinating area, from the point of view of both physicists and material scientists. Nanotechnology is based on the realization of the fact that at nanoscale, material properties are size dependent. It is in this context that nanoscale semiconductor devices are being given increased attention, and their novel electrical and optical properties subjected to extensive research from different angles of approach. The most notable size effect is the significant blue shift of optical absorption edges and emission peaks with decreasing size due to quantum confinement. This leads to remarkable size-dependent modifications in the optical (linear and nonlinear) properties with scope for applications in the area of photonics. The present study deals with i) the synthesis of nanosized zinc oxide (ZnO) and ZnO/polymer nanocomposite films for possible UV shielding and optical limiting applications, and ii) the realization of highly crystalline polypyrrole films.

Nanotechnology is recognized as one of the most promising avenues of technology development for the 21st century. In the materials industry, the development of ceramic and polymer nanocomposites is a rapidly expanding multidisciplinary research activity.

In recent years, the design and synthesis of new inorganic/organic optical materials have been widely attempted in order to combine the advantageous properties of inorganic elements and polymer matrices to suit specific applications [1-4].

Polymer/Inorganic nanocomposites represent a new class of materials, alternative to conventional filled polymers. The incorporation of inorganic nanoparticles can endow the resulting nanocomposites with excellent electrical, optical and mechanical properties. Among all the functional materials to be synthesized on the nanoscale, metal oxides are particularly attractive due to their unique properties covering almost all aspects of material science and solid-state physics.

Semiconductor nanoparticles exhibit a change in their electronic properties relative to those of the bulk material. As the size of the solid becomes smaller, the band gap becomes larger [5]. This allows material scientists the unique opportunity to change the properties of a material simply by controlling its particle size, which leads to the realization of a host of novel devices. The size dependence of the optical properties of quantum dots has been one of the prime subjects of extensive research activity during the last decade. Chemically synthesized semiconductor nanocomposites represent a class of color tunable, flexible systems, in which the strong quantum confinement effect of the carriers leads to unique, size dependent linear and nonlinear optical properties [6].

Zinc oxide (ZnO) is a technologically important material, which shows efficient blue-green luminescence and excitonic ultraviolet (UV) laser action at room temperature with a band gap energy of 3.37 eV, and exciton binding energy of 60 meV. These attributes make ZnO/polymer composite materials potentially interesting for photonic applications in the UV region of the spectrum. ZnO can also be used in UV light emitting diodes, transparent UV protection coatings, luminescent devices, solar cells and piezoelectric devices. Extensive investigations

have already been carried out on composites of ZnO nanoparticles with polymers such as poly(hydroxyl ethyl methacrylate), poly(methyl methacrylate), polyimide,. Nylon-6, poly(ethylene glycol), poly(ethylene oxide), etc.[7-12]. In the process of preparing these optical nanohybrid materials, it is very important to control the dispersion homogeneity of the nanoparticles over the entire matrix, because this has a great influence on the optical characteristics and many other functions of the nanohybrid materials [13]. Polystyrene (PS) and Poly methyl methacrylate (PMMA), which possess favorable processing conditions, are excellent host materials for functional particles. In order to see the modified properties of ZnO/polymer nanocomposites and to find out appropriate matrices for modified functionalities, investigations on various properties of different ZnO/ polymer nanocomposite systems become essential.

Organic conducting polymers (OCPs) are endowed with the unique characteristics to show the mechanical properties of the polymer and the electrical properties of the conductor, which offer high prospects of potential technological applications. Conducting polymers such as polypyrrole, polyaniline, polypthiophene, polyindoles and polyacetylenes can be easily synthesized, which show excellent ambient stability and exhibit a very rapid and reversible adsorption/desorption kinetics.

Conjugated conducting polymers have been successfully used as components in anticorrosion coatings, in organic light-emitting diodes, in electromagnetic shielding, plastic circuitry, and biosensors due to their high conductivity, low density, and reasonably high processability [14]. Polypyrrole (PPy) as a conducting polymer has potential applications in electrical and electronic devices because of its high

electrical conductivity, environmental stability and redox activity. There have been many attempts to endow electrically conductive PPy with processibility. For the as-prepared PPy of chemical polymerization, its application has been limited due to the difficulty in processing, very poor solubility and infusibility. Hence, many efforts have been carried out to synthesize soluble PPy [15] and its copolymers [16, 17]. PPy-based composites and nanostuctured PPy are expected to possess novel properties and offer prospects of new applications beyond conventional PPy.

1.2 Nanotechnology

Nanotechnology is considered as one of the most important future technologies involving several disciplines of science such as physics, chemistry, materials science, medical science, computer science, biotechnology etc [18]. Nanotechnology (nanotech) is the study of manipulating matter on an atomic and molecular scale, and generally, deals with structures sized between 1 and 100 nm at least in one dimension. Nanostructured materials have become a subject of intensive research owing to their extraordinary properties compared to their bulk counter parts. The last two decades have witnessed substantial progress in the synthesis, characterization and understanding of this class of materials. In 1959, the great physicist of our time, Professor Richard Feynman gave the first illuminating talk on nano technology, which was entitled as "There's Plenty of Room at the Bottom". He consciously explored the possibility of "direct manipulation" of the individual atoms to be effective as a more powerful form of 'synthetic chemistry'. Two main approaches are used in nanotechnology. In the "bottom-up"

approach, materials and devices are built from molecular components, which assemble themselves chemically by principles of molecular recognition. In the "top-down" approach, nano-objects are constructed from larger entities without atomic-level control [19]. In the material world, particularly in ceramics, the trend is always to prepare finer powder for the ultimate processing and better sintering to achieve dense materials with dense, fine-grained microstructure of the particulates with better and useful properties for various applications.

Nanostructured materials exhibit properties, quite different from their microstructured counterparts. For instance, mechanical properties of the material are improved through nanostructuring. Optical properties change drastically due to the quantum confinement effects with changing particle size. For example, the color of cadmium telluride changes from red to blue as the particle size changes from 11.5 to 1.2 nm. In the coming years, nanotechnology will have a profound effect in all major areas of science and technology including medicine, computer science, clean and green energy and automobile industry.

1.2.1 Quantum Nanostructures

Three limiting classes of nano structures emerge based on whether only one, two, or all dimensions fall in the nanometer scale. These are

(a) **Quantum Wells:** When only one dimension is reduced to nanometer range and the other two remain large, the resulting material is called a quantum well. (Example: a thin film having thickness in the nanometer range or nano film).The quantum confinement effects take place when the well thickness becomes

comparable to the de-Broglie wavelength of the charge carriers in the material [20, 21].

The charge carriers can have only discrete energy values. This 'well' is like a cage in which the carrier particles can be trapped, in much the same way as light can be trapped between the mirrors. By creating 'layers of different semiconductors', it is possible to make particular 'layers' to act as 'traps' for carriers. These 'trapped particles' can be considered to be in the state of 'quantum confinement'. These particles are constrained or confined in the forward-backward directions, i.e. a 2D-confinement. These nanostructures are now widely used to make 'Semiconductor Lasers' and other useful devices including HEMT (High Electron Mobility Transistors). The thickness of quantum well is typically 5-20 nm.

(b) **Quantum Wires:** When any two dimensions are reduced to the nanometer range, there is confinement in two dimensions and the resulting nanostructure is known as the quantum wire. In condensed matter physics, a quantum wire is an electrically conducting wire, in which quantum effects are affecting transport properties. Nanowires are used as interconnections for the transport of electrons in nanoelectronic devices. Various metals such as cobalt, gold, and copper are used to fabricate quantum nanowires. Various laboratory techniques such as suspension, deposition, vapour liquid solid (VLS) phase growth etc. are used for fabricating nanowire structures.

(c) **Quantum Dots:** If all the three dimensions of a material are reduced to the nanometer size, which can produce quantum

confinement effects, such structures are known as quantum dots. In this case, the motion of conduction band electrons and excitons are confined in all three spatial directions [22].

The quantum dots have discrete energy spectra [23] and the corresponding wave functions are localized within the quantum dots, but are extended over many periods of crystal lattice. Quantum dots can be as small as 2 to 10 nanometers in size corresponding to 10 to 50 atoms in diameter and 100 to 100,000 atoms within the quantum dot volume. The most common method of synthesis of quantum dots is the wet chemical colloidal process.

1.2.2 Quantum Mechanical background of Nanoparticles and Quantum Confinement Effects

As the size of the material particles approaches nanometer scale ($1nm = 10^{-9}m$) the laws of quantum mechanics come into play. The basic concept of quantum confinement comes from the interplay of two fundamental principles of quantum mechanics; namely

- The electronic system must obey the Schrodinger equation

- It should also follow the de-Broglie momentum wavelength relationship

From a review of the Schrodinger equation as applied to the theory of electrons in solids, it is found that, the solution to the wave equation for a periodic potential predicts energy bands with gaps. The simplest approximation, which yields sensible results and provides insights into more complicated solutions, is the so-called parabolic band approximation. The eigen values for these approximations are

$$E(k) = (hk)^2 / 8\,\pi^2 m_{e,h} \;\text{---} (1.1)$$

where $m_{e,h}$ - Effective mass of electron or hole

k – Wave vector determined by the symmetry and spacing of lattice.

Figure 1.1 shows the schematic plot of energy versus k in a bulk semi conductor for both electron and hole states.
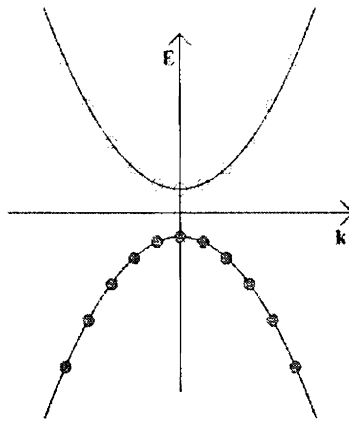
Figure 1.1: E-k diagram in bulk semiconductor

The gap between the two parabolas is the so-called band gap found in all semi conductors and is directly related to the optical properties of a given material. The region below the lower parabola is typically called the valence band and energy states in this region are generally filled in semiconductors. The region inside the upper parabola is called conduction band (CB) and is generally empty. However, the electron may be excited into the conduction band by a photon, which then leaves a hole in the valence band region. This electron hole pair exists as an exciton. In fact, the exciton can be considered as an exotic atom with its own atomic or Bohr radius.

1.2.3 Exciton

The exciton can be defined as a bound state of an electron in conduction band and a hole in valence band. In low dimensional structures, the Coulomb relational effects or the excitonic effects become more prominent than in bulk structures, leading to peculiar optical characteristics combined with the geometrical confinement effects.

The number of excitons and the optical response are related in a material. Under a weak excitation condition, only an electron and a hole are created, which forms a bound state due to Coulomb's attraction. This is just a two-body problem, which can be solved with the use of effective mass approximation. However in the case of stronger excitation, where many electrons and holes are excited, semiconductor body effects should be taken into account and the inter particle Coulomb interaction plays an important role.

The dimensionality of exciton systems depends on the ratio of particle size R to the exciton effective Bohr radius R_B. For designing novel materials with new optical properties there is a greater significance for the geometrical confinement of excitons, dielectric image charge effects and single electron band structures.

1.2.4 Quantum Confinement of excitons in 3D quantum dots

Quantum confinement describes the confinement of the excitons with in the physical boundaries of the material. The effective Coulomb potential includes the dielectric image charge effect arising from the difference in dielectric constant of the material and the surroundings. This is a confinement effect of Coulomb interaction. If the surrounding

material has a smaller dielectric constant and a larger energy gap than the relevant material, the electron hole Coulomb interaction in the relevant material works very effectively through the surroundings with reduced screening. As a result, the exciton binding energy is expected to increase much more than in normal low-dimensional systems without this effect. Quantum confinement effects arise as soon as the dimensions of the material become comparable to the Bohr radius of exciton wave function, leading to significant changes in the electronic and optical properties.

In the case of spherical quantum dots with diameter D $=2R$, one can see the consequence of quantum confinement. For simplicity consider an infinite spherical well, in which the Hamiltonian operator, by neglecting the Coulomb interaction is

$$H = - (h^2/8\pi^2 m_e) \Delta_e - (h^2/8\pi^2 m_h) \Delta_h + V_e (r_e) + V_h (r_h) \text{ -------- (1.2)}$$

where the potential

$$V_i (r_i) \quad = 0 \text{ for } r_i < R \quad i = e,h$$
$$= \infty \text{ for } r_i > R$$

In case of single electron one can take

$$\Psi (r_e, r_h) = \varphi (r_e) \varphi (r_h) \text{ --- (1.3)}$$

The Schrodinger equation for an infinite spherical well has been well studied and its solutions can be found out as follows. The normalized solution is given in terms of spherical harmonics (Y_{lm}) and Bessel functions (J_l) [26],

$$\Phi^i_{nlm} (r) = Y_{lm}(2/R^3)^{1/2} [J_l (\chi_{nl}) / J_{l+1} (\chi_{nl})] \text{ ---------------------- (1.4)}$$

The χ_{nl} are the zeroes of the Bessel functions.

The Bessel function J_l (χ_{nl} r/R) must also vanish at the surface of quantum dot sphere. With these conditions the energies of electrons or holes are given by

$$E_{nl}^{e, h} = (h^2/8 \ \pi^2 m_{e, h}) \ (\chi_{nl}/R)^2 \ \text{------------------------------------} (1.5)$$

The additional term shown in eqn. (1.5) is added on to the energy gap E_g predicted for the bulk due to the quantum confinement of electron or hole. Thus the photon energy required to produce the electron – hole pair (exciton) is

$$H_e = E_g + (h^2/8\pi^2 m_{e, h}) \ (\chi_{nl}/R)^2 \ \text{------------------------------} (1.6)$$

This produces an effective band gap shift that is proportional to $(1/R^2)$ in the quantum regime [27]. When the size of quantum dot decreases, the band gap increases. This gives rise to the beautiful array of photoluminescent colors in the quantum dots of different sizes dissolved in solution. The widening of band gap due to the size reduction will affect the optical transitions in the material. Therefore, the optical transitions such as absorption, emission, photo luminescence etc are blue shifted compared to the bulk material or a larger sized quantum dot.

Depending upon the size of nanocrystallites constituting the nanostructured material, there are generally different regimes of quantum confinement as given below.

- Strong-confinement regime: $D < 2R_B$

- Intermediate-confinement regime: $D \sim 2R_B$

- Weak-confinement regime: $D > 2R_B$

The optical properties are mostly affected in the strong confinement regime. This will result in the considerable blue shift of optical band gap with decrease in size [28-31]. This is an interesting area of research, which makes it possible to tune the properties of quantum dots just by tailoring the size, to suit any application.

1.3 Nanocomposites

Nanotechnology has quite high impact in developing new classes of materials with enhanced functionality and a wide range of applications. Nanocomposites belong to this class and form an exciting research field for both fundamental studies and application oriented investigations. Nanocomposites can be defined as multiphase materials, where one or more of the phases have at least one dimension less than 100 nm. The phases can be inorganic, organic, or both, with amorphous, semi-crystalline or crystalline phases or combinations of these phases. Most nanocomposites, which are of proven technological importance, are composed of two phases. Micro structurally these are classified into three. (a) Nano layered composites, composed of alternating layers of nanoscale dimension. (b) Nano filamentary composites composed of matrices with embedded (generally aligned) nanoscale diameter filaments. (c) Nano particulate composites composed of matrices with embedded nanoscale particles. In terms of their engineering applications, nanocomposites can be classified either as functional materials (based on their electrical, magnetic and optical behavior) or as structural materials

(based on their mechanical properties) [32]. Organic-inorganic composites with nanoscale dimensions are of growing interest because of their unique properties, and numerous potential applications in the 'enhancement of conductivity [33 ,34], toughness [35], optical activity [36 ,37], catalytic activity [38], chemical selectivity [39 ,40] etc. In these materials, inorganic and organic components are mixed or hybridized at nanometer scale, virtually at any composition leading to the formation of nanocomposite materials [41].

The introduction of inorganic nanomaterial into polymer matrix has resulted in polymer nanostructured materials exhibiting high performance polymer characteristics beyond what traditional polymer composites possess. The driving force behind the fabrication of novel nanocomposites is to achieve high functional properties for many applications. Nanocomposites can be of the form of porous media, colloids, gels and co- polymers. The electrical, optical, mechanical, electro chemical and catalytic properties of nanocomposites will differ markedly from those of component materials. These special properties shown by nanocomposites are attributed to many effects. The properties of nanocomposite materials depend not only on the properties of their individual components but also on their morphology and interfacial characteristics. The interfaces play an important role in enhancing or limiting the overall properties of the system. Due to large surface area of the nanostructures, nanocomposites present many interfaces between the constituent intermixed phases. The special properties arise due to the interaction of the different phases at the interfaces. An excellent example of this phenomenon is the improved mechanical behaviour of carbon

nano tube filled polymer composites. Nanocomposite materials are currently significant in a broad area of applications. For example, rubber-clay nanocomposites are widely used as additives to vehicle tyres and some metal-ceramic nanocomposites are used for surgical implants, as wear and heat resistant coatings or as lubricants. Research institutions and companies are engaged in the exploration of efficient methods for developing nanocomposites in large volumes, and at lower costs. According to the matrix used, nanocomposites are classified into four types [42].

(a) Ceramic matrix nanocomposites

It consists of ceramic matrix reinforced with sub-micron metal or ceramic particles [43]. Most of the ceramic materials pose some grave problems including relatively low fracture toughness and strength, degradation of mechanical properties at high temperatures and poor resistance to creep fatigue and thermal shock. These problems can be overcome by using ceramic matrix nanocomposites. Ceramic matrix nanocomposite coatings can be utilized in the transport sectors as well as in the biomedical sector. Other potential applications are as catalysts, foams or coatings for machine tools.

(b) Metal matrix nanocomposites

Metal matrix nanocomposites (MMNCs) are formed by embedding nano scale ceramics or other hard particles into soft metal matrix. The properties of the matrix material can be substantially improved or strengthened. The properties of MMNCs would be

improved considerably even with a very low volume fraction [44] of the embedded nanomaterial.

Metal matrix nanocomposites have been used for aerospace applications due to their low weight and tailorable properties. The MMNCs exhibit greater improvements in their physical and mechanical properties as compared to composites with micron-sized reinforcements.

(c) Polymer matrix nanocomposites

For most current applications of polymers, performance requirements as well as cost and processing considerations necessitate the introduction of additives and fillers into the polymer matrices. The nano particles offer small interparticle separations in a polymer matrix and often very high length to width or aspect ratio [45]. The appropriate addition of nano particles to a polymer matrix can improve its performance to a very large extent. The production of polymer matrix nanocomposites is based on the intercalation of the molecular chains of the matrix polymer between the layers of the filler. The structural integrity of the layers is thereby destroyed, and the filler material resolves into individual layers (delamination). The delamination process leads to the dispersion of layers within the matrix.

(d) Natural nano biocomposite

Biocomposites are composite materials comprising one or more phases derived from a biological origin. In terms of reinforcements, this could include plant fibers such as cotton, flux, hemp and the

like or fibers from recycled wood or waste paper or even by-products from wood crops. Regenerated cellulose fibers are also included in this definition, since ultimately they too come from renewable resources, as are natural nanofibrils of cellulose or chitin. Matrices may be polymers, ideally derived from renewable resources such as vegetable oils or starches.

Nanofibrils are extracted from natural plant materials using fungi attack and steam explosion techniques and are subsequently combined with various polymers derived from plant materials to form nano-bio-composites. Nano bio composites are used in artificial limbs and dental restorative materials.

1.3.1 Polymer nanocomposites – Basic ingredients

There has been a great deal of interest in polymer nanocomposites (PNCs) over the last few years. Nanoparticles and nanolayers have very high surface-to-volume and aspect ratios and this makes them ideal for use in polymeric materials. Such structures combine the best properties of each component to possess enhanced mechanical & superconducting properties for advanced applications. There are different types of commercially available nanoparticles that can be incorporated into the polymer matrix to form polymer nanocomposites.

The correct selection of particles is essential to ensure effective penetration of the polymer or its precursor into the interlayer spacing of the reinforcement material and result in the desired exfoliated or intercalated product. In the intercalated type, the polymer chains are alternately present with the inorganic layers in a fixed compositional ratio and have a well-defined number of polymer layers in the

intralamellar space whereas in exfoliated nanocomposites, the number of polymer chains between the layers is almost continuously variable. The intercalated nanocomposites are useful for electronic and charge transport properties. On the other hand, exfoliated nanocomposites possess superior mechanical properties [46].
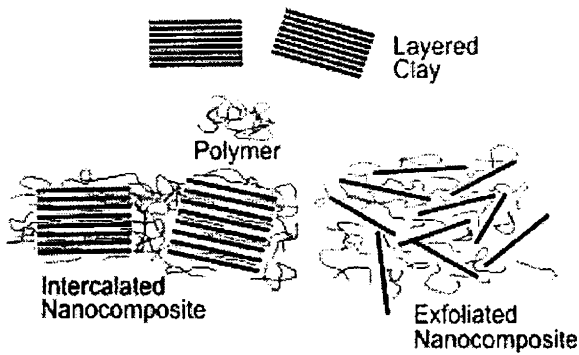
Figure 1.2: Formation of intercalated and exfoliated nanocomposites from layered silicates and polymers

Polymer nanocomposites consist of a polymeric material (e.g., thermoplastics, thermosets, or elastomers) with reinforcement of nanoparticles. Polymer could be incorporated either as the polymeric species itself or via the monomer, which is polymerized in situ to give the corresponding polymer nanocomposite. Most commonly used nano-particles include:

- Montmorillonite organoclays (MMT)

- Carbon nanofibers (CNFs)

- Polyhedral oligomeric silsesquioxane (POSS)

- Carbon nanotubes [multiwall (MWNTs), small-diameter (SDNTs), and single-wall (SWNTs)]

- Nanosilica (N-silica)

- Nano Aluminum oxide (Al_2O_3)

- Nano Titanium oxide (TiO_2)

- Nano Zinc oxide (ZnO) and

- Others

Thermosets and thermoplastics used as matrices for making polymer nanocomposites include:

- Nylons

- Polyolefin, e.g. polypropylene

- Polystyrene

- Ethylene-vinyl acetate (EVA) copolymer

- Epoxy resins

- Polyurethanes

- Polyimide

- Poly ethylene terephthalate (PET)

- Poly methyl methacrylate (PMMA) etc

There are two main challenges in developing nanocomposite materials after the desired polymer has been selected for the purpose. First, the choice of nanoparticles requires an interfacial interaction and/or compatibility with the polymer matrix. Second, the processing technique should address proper uniform dispersion and distribution of nanoparticles or nanoparticle aggregates within the polymer matrix.

Substantial fundamental research is still necessary to provide a basic understanding of these polymer nanocomposite materials to enable full exploitation of their nanoengineering potential. Despite the large number of combinations of matrices and potential reinforcing nanoelements with different chemistry, size, shape and properties, all PNCs share common features with regard to fabrication methodologies, processing, morphology characterization and fundamental physics [47].

The objective of PNC fabrication via exfoliation methodology is to uniformly disperse and distribute the inorganic filler, initially comprised of aggregates of the nanoparticles, within the polymer. The final PNC structure results from the transformation of the initially microscopic heterogeneous system to a nanoscopically homogenous system. In general, four approaches have been developed to fabricate PNCs via exfoliation - solution processing, mesophase mediated processing, in-situ polymerization and melt processing. Each methodology has advantages with respect to the processing steps necessitated by the desired final form of the PNC (powder, film, paste, fiber, bulk monolith). Substantial research efforts currently endeavor to address the fundamental challenge of providing general guidelines, including thermodynamic, kinetic and rheological considerations for morphology control via these fabrication processes [48, 49].

The key to any of these fabrication processes is the engineering of the polymer-nanoparticle interface. Surfactants are commonly used to facilitate this process. These surface modifiers mediate interlayer interactions by effectively lowering the interfacial free energy. Furthermore, they may serve to catalyze interfacial interactions, initiate

polymerizations, or serve as anchoring points for the matrix and thereby improve the strength of the interface between the polymer and inorganic filler. Developing an understanding of the characteristics of this interface region and its relationship to the PNC properties is a current research frontier in nanocomposites.

1.3.2 Advantages of Nanosized Additions

Nanomaterial additives can provide property advantages in comparison to both their conventional filler counterparts and base polymer [50].

Properties which have been shown to undergo substantial improvements include:

- Mechanical properties e.g. strength, modulus and dimensional stability

- Permeability to gases, water and hydrocarbons

- Thermal stability and heat distortion temperature

- Flame retardancy and reduced smoke emissions

- Chemical resistance

- Surface appearance

- Electrical conductivity

- Optical clarity in comparison to conventionally filled polymers

1.4   Applications of nanocomposites

The number of commercial applications of nanocomposites has been growing at a rapid rate. The key application areas include drug delivery systems, anti-corrosion barrier coatings, UV protection gels, lubricants and scratch free paints, fire retardant materials, scratch/abrasion resistant materials and superior strength fibers and films.

1.4.1 Industry applications

Nanocomposites promise new applications in the fabrication of mechanically-reinforced lightweight components, battery cathodes, nanowires, sensors and nonlinear optical devices.

a)   Producing batteries with higher power output - Researchers have developed a method to make anodes for lithium ion batteries from a composite formed with silicon nanospheres and carbon nanoparticles. The anodes made of the silicon-carbon nanocomposite make closer contact with the lithium electrolyte, which allows faster charging and discharging of power.

b)   Using nanocomposites to make flexible batteries- A nanocomposite of cellulose and carbon nanotubes can be used to make a conductive paper. When this conductive paper is soaked in an electrolyte, a flexible battery is formed.

c)   Thermoset nanocomposites result in improved dimensional /thermal stability, flame retardancy and chemical resistance

and have potential applications in marine industry and construction markets. These materials are eminently processable and can be shaped in conventional shaping steps, such as injection molding and extrusion processes. Shaped articles of a variety of types can be manufactured from such nanocomposite materials such as fibers, packaging materials and construction materials.

1.4.2 Food Packaging

The gaseous barrier property improvement that can result from incorporation of relatively small quantities of nanoclay materials into the polymer matrices has been substantial. The extent to which both the amount of clay incorporated in the polymer and the aspect ratio of the filler contributes to overall barrier performance has been studied. Such excellent barrier characteristics have resulted in considerable interest in nanoclay composites in food packaging applications, both flexible and rigid. Specific examples include packaging for processed meats, cheese, confectionery, cereals etc together with co-extrusion processes for the manufacture of beer and carbonated drinks bottles. The use of nanocomposite packaging would be expected to enhance considerably the shelf life of many types of food items.

Significant reductions in fuel transmission through polymers by incorporation of nanoclay filler makes use of these materials as both fuel tank and fuel line components for cars. Further interest for this type of application lies in the fact that, the reduced fuel transmission characteristics are accompanied by significant material cost reductions.

The presence of filler incorporation at nano-levels has significant effects on the transparency and haze characteristics of films. In comparison to conventionally filled polymers, nanoclay incorporation has been shown to significantly enhance transparency and reduce haze.

1.4.3 Environmental Protection

Significant reduction of water absorption in a polymer can be achieved by nanoclay incorporation. Similar effects can also be achieved with polyamide-based nanocomposites. Specifically, increasing aspect ratio diminishes substantially the amount of water absorbed, thus indicating the beneficial effects likely from nanoparticle incorporation compared to micr particle loading.

1.4.4 Flammability Reduction

Reduction in flammability behaviour can be achieved in polymers such as polypropylene with as little as 2% nanoclay loading. In particular, heat release rates, as obtained from cone calorimetry experiments, are found to diminish substantially by nanoclay incorporation.

1.4.5 Nanocomposites for UV-sheltering

Solar radiation spectrum comprises wavelengths of electromagnetic energy, which range between about 100 nm and 1 mm. This range is divided into three different regions, namely: 1) ultraviolet region (100-400 nm), 2) visible region (400-780 nm) and 3) infrared region (780 nm-1 mm). The ultraviolet region is arbitrarily divided into three bands, referred to as the UVA (315-400 nm), UVB (280-315 nm) and UVC (100-280 nm) bands.

UVC radiation from the sun does not reach the surface of the earth in high quantity. Thus, protection against UVC radiation is generally not a major concern, in contrast to the dangers posed by UVA and UVB radiations. UVB radiation is the principal cause of sunburn reactions and it is greatly effective in stimulating the tanning reaction in the skin. UVA radiation can also cause sunburns, but less compared to UVB radiation. Current data reveal that solar radiation containing UVA and UVB causes skin cancer, which presently accounts for 30-40 % of all new cancers each year [51]. UVA radiation has been shown to promote skin cancer by inhibiting enzymes that repair cells damaged by UVB radiation and also penetrates more deeply into the skin than UVB radiation and causes changes in blood vessels and premature aging of the skin, thus adding to the damage produced by UVB radiation [52]. Moreover, UV radiation perturbs profoundly the body's immune system. In addition to causing human damage, UV radiation is detrimental to buildings and it fades the color of paintings and natural fibers by photo-oxidative process [53].

During the past decades, the dosage of both UVB and UVA radiation has increased profoundly due to the adverse climate conditions and continuous ozone depletion. From 1998-99, the rate of photo injury due to hazardous UVB emission was about 12 % higher than that during the earlier years of the decade[54]. Consequently, a great deal of attention has been imparted upon the development of photo protective materials [55-59].

Currently, titania-based polymer hybrid thin films are utilized as transparent UV-sheltering materials. The current methods of preparation

make it possible to fabricate transparent materials only as thin films, and when higher thickness is required, materials become less transparent. The films, therefore, are always supported by a transparency sustaining substrate. However, they usually exhibit low mechanical strength and processability and the UV-sheltering effect will be inevitably diminished because of mechanical scratch. Furthermore, the low adhesion between the hybrid film and the substrate is always a critical problem.

Therefore, there is urgent need to develop transparent UV-sheltering materials suitable for applications such as UV-sheltering windows, contact lens, goggles, etc. Such materials can be realized by the proper incorporation of suitable UV absorbing nanomaterials into a transparent polymeric matrix.

1.4.6 Nanocomposites for Nonlinear Optical (NLO) applications

Nonlinear optical effects are applicable in many fields. In the field of optical information storage, frequency-doubling process can effect the conversion of near infrared laser light from the diode lasers into deep blue light. Since the size of a focused spot of light is inversely proportional to its wavelength, second harmonic generation (SHG) can increase the capacity of stored information on optical disks immensely. Using NLO related phenomena one can build devices such as frequency mixers that can act as new light sources or light modulators for controlling the phase or amplitude of a light beam. Optical switches, optical limiters (described in chapter 2) and numerous other devices can be realized for fast and efficient processing of the information content of data or images.

1.5 ZnO nanocrystals

Semiconductor nanocrystals have attracted much interest due to their fundamental importance in bridging the gap between bulk matter and molecular species [60, 61]. Wide band gap semiconductors exhibit inherent properties such as larger band gap, higher electron mobility and higher breakdown field strength. Therefore, they are suitable for high power, high temperature electronic devices and short wavelength optoelectronics. Wide gap II-VI compounds are characterized by the direct band gap with either zinc blend or wurtzite structures and large exciton binding energy. Among the wide band gap semiconductors, ZnO is attractive due to its remarkable optical properties and environmentally friendly nature. Zinc oxide is a direct wide band gap semiconductor with an energy gap of ~3.37 eV [62] and a large exciton binding energy of ~60 meV [63] at room temperature. These unique properties make ZnO a promising candidate for applications in optical and optoelectronic devices [64–67].

It is well known that low-dimensional structures have superior optical properties over bulk materials due to the quantum confinement effects. The possibility of tailoring the bulk material properties by varying the size or structure of the nanoscale particles makes them candidates for various important technological applications. Other favorable aspects of ZnO include its broad chemistry leading to many opportunities for wet chemical etching, low power threshold for optical pumping, radiation hardness and biocompatibility. ZnO is a versatile material exhibiting efficient blue-green emission, which can be utilized in field emission displays [68]. It is an efficient UV detector and emitter.

Solar cells made of ZnO are very popular. Its UV absorbing property has been utilized in UV protection films and cosmetic sunscreen lotions. Efficient UV lasing has been observed at room temperature from ZnO thin films and ZnO nanoclusters [69]. Because of high third order optical nonlinearity, ZnO finds application in the fabrication of efficient optical limiters for protection against high intensity laser radiation [70, 71]. Some of the key properties [72] of ZnO are shown in table 1.1. In the present work, ZnO nanoparticles are used to make ZnO/ polymer nanocomposites.

Table 1.1: Important characteristics of ZnO

Properties	Values
Eg (eV)	3.37 eV
Exciton binding energy	60 meV
Dielectric constant	3.7
Refractive index	2.008
Stable crystal structure	Wurtzite
Lattice parameters	a=3.25A° and c=5.12A°
Thermal conductivity	0.6-1.2 Wcm^{-1} K^{-1}
Thermal expansion coefficients	$\alpha_a = 4.31 \times 10^{-6}$ K^{-1} and $\alpha_c = 2.49 \times 10^{-6}$ K^{-1} at 300K
Specific heat capacity	Cp=40.3 J mol^{-1}K^{-1}

1.6 Conducting polymers

1.6.1 Introduction

Polymers are everywhere. The emergence of the synthetic polymer industry from the middle of the nineteenth century through to the rapid growth in the 1940s and 1950s has produced a range of polymers, which

provide acceptable alternatives to most traditional materials. A polymer is made up of many small molecules, which combine to form a single long or large molecule. The individual small molecules from which the polymer is formed are known as monomers (meaning, single part) and the process by which the monomer molecules are linked to form a big polymer molecule is called polymerization. The small molecules, which combine to form a big molecule, can be of one or more chemical compounds.

1.6.2 Conducting Polymers – an overview

Most organic polymers are electrically insulating. Since the first discovery in 1977 that chemical treatment with iodine converts electrically insulating polyacetylene into a highly conducting material with electrical conductivity above 10^4 Scm^{-1} [73], many electrically conducting polymers have been reported. Conducting polymers belong to a special class of polymers in which electrical conductivity can be tuned from insulating to metallic through proper doping [74, 75].

The electrically conducting polymers are able to transfer electrical charges to the same extent as an electrical conductor or a semiconductor. Due to their metal-like conductivity or semi conductivity and other fascinating properties, conducting polymers have played indispensable roles in specialized industrial applications in spite of their short history. However, the major aspect useful for most applications is not the metal-like electrical property itself, but the combination of electrical conductivity and polymeric properties such as flexibility, low density, and ease of structural modifications that suffice for many commercial applications.

Conducting polymers are easy to be synthesized through chemical or electrochemical processes, and their molecular chain structure can be modified conveniently by copolymerization or structural derivations. The conducting polymers, such as polypyrrole (PPy), polyaniline (PAni), polythiophene (PTh), etc all refer to intrinsic conducting polymers. Their main chains consist of alternative single and double bonds, which lead to broad π-electron conjugation. However, the conductivity of these pure conducting polymers are rather low ($<10^{-5}$ S cm^{-1}). In order to achieve much higher conductivity for these polymers, doping process is necessary. The concept of doping is the central theme, which distinguishes conducting polymers from all other conventional polymers [76].

The doping process corresponds to the oxidation or reduction of the polymer, with the concomitant incorporation of a counterion in order to preserve overall electrical neutrality. It is the charge introduced onto the polymer backbone, which imparts electrical conductivity. The change in the delocalized π system induced by doping not only increases the conductivity by many orders of magnitude (typically by a factor of 10^{10}) but also creates substantial alterations in the visible absorption spectrum of conducting polymers. These characteristics, are responsible for the potential of conducting polymers in a number of applications. Prof. Alan. J. Heeger, Prof. Alaqn. G. Macdiarmid and Prof. Hideki Shirakawa were awarded the Nobel Prize in the year 2000 for their pioneering contributions in conducting polymer research. Today thousands of laboratories all over the world are working in the field of conducting polymers and related areas.

1.7 Polymer crystallinity

When applied to polymers, the term 'crystalline' has a somewhat ambiguous usage. A synthetic polymer may be lightly described as crystalline if it contains regions of three-dimensional ordering on atomic (rather than macromolecular) length scales, usually arising from intramolecular folding and/or stacking of adjacent chains. Synthetic polymers may consist of both crystalline and amorphous regions. The degree of crystallinity may be expressed in terms of a weight fraction or volume fraction of crystalline material.

Polymer crystallinity is one of the important properties of all polymers since crystallinity influences many of its characteristics, including mechanical strength, opacity and thermal properties. While most of these manifestations of crystallinity can be measured, a direct measure of the degree of crystallinity provides a fundamental property from which these other physical properties can be predicted. Crystallinity measurement provides valuable information for both materials research and quality control in material processing [77-82]. Polymers exist both in crystalline and amorphous form. Crystallinity in polymers differs from that in low molecular weight compounds in that it is only partial. The polymer chains are not aligned with each other over their whole length, but only in small crystallite regions [83]. Figure 1.3 shows how the crystalline and amorphous regions can co-exist and how, long polymer chains running through them (semi crystalline) hold them together. Polymers that partially crystallize upon cooling from the melt state are called semi crystalline polymers. The degree of crystallization

(volume fraction of crystalline regions in a polymer) affects the optical, thermal, and mechanical properties of a polymer.
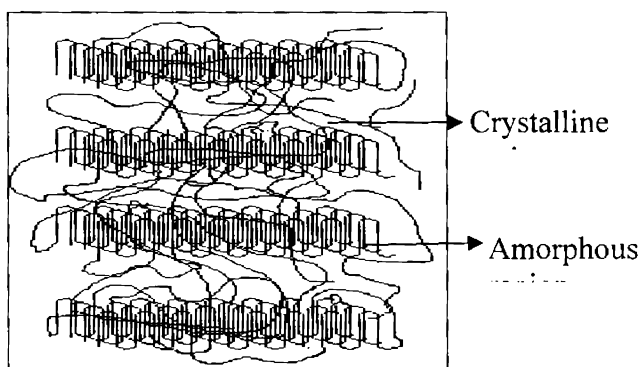
Figure 1.3: **Arrangement of polymer chains forming crystalline and amorphous regions in polymers**

Polymer crystals are never perfectly ordered, therefore they rarely experience sharp diffraction peaks like inorganic crystals. Polymers form ordered structures that are unlike the perfect crystals formed by atomic and molecular solids. Due to the constraints imposed by covalent intra-chain bonding, weak Van der Waals or hydrogen bonding inter-chain interactions and the large configuration space, i.e. large entropy of the flexible polymer chain, polymers form structures that are often semi crystalline and amorphous.

There are two broad types of polymer crystal structure, depending on the persistence length of the chains. Lamellae (Figure 1.4a), are formed by stiffer polymers and this is the commonly accepted crystal model for conjugated polymers. Fringed micelles (Figure 1.4b) are typically formed by very flexible polymers such as polyethylene. Both polymer systems show crystalline as well as amorphous regions.
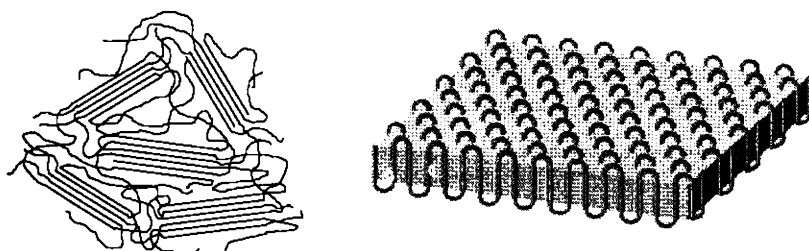
Figure 1.4: a) Stacked lamellae b) Fringed micelles.

Semi crystalline polymers have both crystalline and amorphous regions. Semi crystallinity is a desirable property for most plastics because they combine the strength of crystalline polymers with the flexibility of amorphous ones.

1.8 Polypyrrole

Among the conducting polymers, polypyrrole (PPy) has attracted great attention because of its high electrical conductivity and good environmental stability. PPy has been considered as the key material to many potential applications such as electrodes for rechargeable batteries and super capacitors, solid electrolytes for capacitors, as electromagnetic shielding materials, sensors, corrosion-protecting materials, actuators, and electro chromic devices, or membranes. The heteroaromatic and extended π-conjugated backbone structure of PPy provides it with chemical stability and electrical conductivity. However, the π-conjugated backbone structure is not sufficient to produce appreciable conductivity on its own. Partial charge extraction from PPy chain is also required and is achieved by a chemical or an electrochemical process referred to as doping. The conductivity of the neutral PPy can be remarkably changed from the insulating regime to the metallic one by doping. This is a very worthwhile

feature for applications, in which the electrical conductivity of a material must be controlled.

It has been reported that the electronic band structure of PPy can be changed with the doping level of the PPy chain [84, 85]. Neutral PPy, with the benzenoid structure shown in figure 1.5a, is categorized as an insulator and its proposed electronic energy diagram is shown in figure 1.6a. The band gap of neutral PPy is reported to be 3.16 eV, which is too wide for electrons to be transferred from the valence to the conduction band at room temperature. The PPy chain is however, simultaneously doped during polymerization [86]. Counter anions in the reaction medium are incorporated into the growing PPy chains to maintain the electrical neutrality of the polymer system. Upon extraction of a negative charge from a neutral segment of a PPy chain by the doping process, a local deformation to the quinoid structure occurs (Figure 1.5b), since it is favored energetically. In combination with the quinoid structure, the positive charge and the unpaired spin are referred to as a polaron (Figure 1.5b). Referring to figure 1.6b, the formation of a polaron induces two new intermediate states (bonding and ant bonding) within the band gap while the unpaired electron occupies the bonding (low energy) state, thus giving the polaron a spin of 1/2.

As oxidation continues further, another electron has to be removed from a PPy chain that already contains a polaron, resulting in the formation of a bipolaron which is energetically preferred to the formation of two polarons. A bipolaron is known to extend over about four pyrrole rings (Figure 1.5c). The bipolaron states lie further from the band edges (Figure 1.6c). The lower energy state of the bipolaron is

empty; thus, the species has a zero spin. As the degree of oxidation increases, the bipolaronic energy states overlap, resulting in the formation of narrow intermediate band structures (Figure 1.6d).
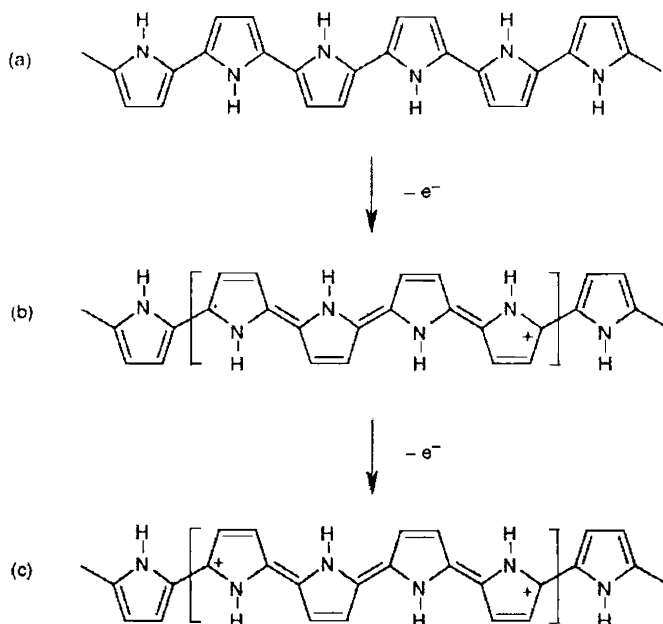
Figure 1.5: Electronic structures of (a) neutral PPy, (b) polaron in partially doped PPy and (c) bipolaron in fully doped PPy.

The energy diagram shown in figure 1.6d corresponds to a doped state of about 33-mol%, which is close to the maximum value found in electrochemically oxidized PPy. The typical doping level of PPy is in the range of 20 to 40 mol%. At this doping level, bipolarons are predominant in PPy with few polarons, and thus the charge carriers in the conducting PPy have zero-spin number.

The electrical conductivity of a material is proportional to the product of the concentration of charge carriers and their mobility. Even though the concentration of charge carriers in fully doped conducting

polymers, including PPy, is in the range of 10^{21} to $10^{23}/cm^3$, which is four to five orders of magnitudes higher than that of inorganic semiconductors, the electrical conductivities of most conducting polymers are merely in the same range as those of inorganic semiconductors. This indicates the relatively low mobility of carriers in conducting polymers, which results from the low degree of crystallinity and the presence of many types of defects. Therefore, if higher electrical conductivities are to be achieved in conducting polymers, including PPy, the mobility of charge carriers must be improved.

The overall mobility of charge carriers in conducting polymers depends on two components: intrachain mobility, which corresponds to charge transfer along the polymer chain; and interchain mobility, which involves the hopping or tunneling of the charge from a chain to neighboring chains [87]. When an electric field is applied to conducting PPy, the charge carriers (polarons and bipolarons) necessarily begin to move along the PPy chain by the rearrangement of double and single bonds in the PPy backbone since the interchain charge transport requires considerably more energy than intrachain conduction [87]. When the charge carriers reach any defect point in the chain or the end of the PPy chain itself, the carriers have to hop to neighboring chains to deliver charges. Therefore, the total conductivity of conducting PPy is dominated by the combination of intrachain and interchain components.
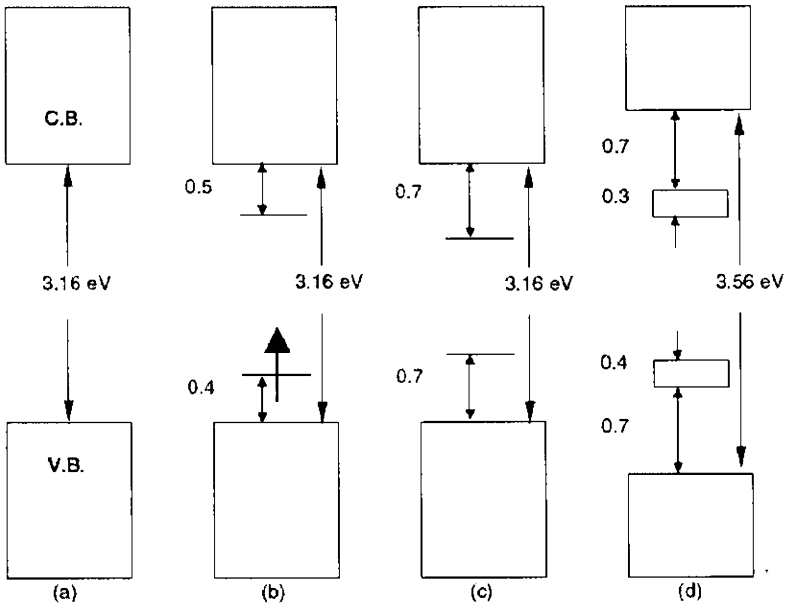
Figure 1.6: Electronic energy diagrams for (a) neutral PPy, (b) polaron dominated PPy, (c) bipolaron dominated PPy, and (d) fully doped PPy.

Interchain mobility of carriers in conducting polymers including PPy is strongly dependent upon the structural order. A high degree of structural order is usually achieved in the crystalline region in a conducting polymer, which can be produced by mechanical stretching. Nogami et al. found a partial crystalline structure in the stretched films of PPy doped with hexafluorophosphate [88]. The PPy film showed an extremely high electrical conductivity of 2×10^3 S cm^{-1} in the direction parallel to the stretch direction. However, when PPy was synthesized using other dopants, no crystalline structure was found, which indicates that the nature of the counter anion considerably influences the structural arrangement of PPy chains.

1.9 Soluble Polypyrrole

In the initial stages, conducting polymers were expected to possess properties of both common polymers (low density, flexibility, processibility, and low cost) and conductors or semiconductors. However, they tend to be insoluble and infusible since molecular interactions in conjugated polymers, composed of ring-based backbones are relatively stronger compared to the Vander Waals forces or hydrogen bonding between saturated polymers. The ionic interactions between doped regions on conducting polymer chains further increase the molecular interactions, making the conducting polymers even more intractable. As with most of the conducting polymers, PPy, polymerized either electrochemically or chemically, has been known to be insoluble and infusible due to the strong inter- or intramolecular interaction and cross linking.

Research has, therefore been focused on the development of new, soluble or fusible PPy. A major breakthrough has originated with the modification of the chemical structure of PPy by adding solubilizing substituents onto the pyrrole monomer unit. PPy derivatives containing alkyl or alkoxy substituents have been found to be soluble in chloroform, tetrahydrofuran and o-dichlorobenzene [89–91]. Since the bulky side groups reduce the molecular interactions between main chains and increase chain entropy, the substituted conducting polymers can be processed from the solution.

Before the synthesis of soluble PPy in 1995, general applications using PPy were limited due to its poor processibility in spite of some specific applications. However, a host of investigations have been

initiated on soluble PPy since Lee et al. [92] reported that soluble PPy in its doped state could be obtained by chemical polymerization in an aqueous medium with ammonium persulfate (APS) and dodecylbenzene sulfonic acid (DBSA) as oxidant and dopant source, respectively.

Soluble PPy can be prepared through a dedoping-redoping process. To start with, PPy is synthesized by chemical polymerization in an aqueous medium with ammonium persulfate (APS) and HCl as oxidant and dopant respectively. The obtained PPy powder is dedoped using ammonia solution and then redoped with CSA. This redoped sample is found to be soluble in m-cresol and NMP. Redoping can also be done using β-NSA and DBSA.

Polypyrrole finds potential applications as gas and ion sensors [93-97], as electronic or artificial tongue in food industry [98, 99], as electrochemical actuators [100-107], as electrodes for secondary batteries [108-115] and super capacitors [116-131]and in the fabrication of field effect transistors (FET) [132-135] and electromagnetic interference (EMI) shielding devices [136-143].

1.10 Importance of the materials selected for the present investigations

One of the objectives of the present work is to identify semiconductor/ polymer nanocomposite systems with characteristics ideal for realizing good quality optical devices, based on the linear and nonlinear optical properties of these systems. Considering the excellent optical characteristics of nano sized ZnO, it is chosen as the inorganic filler material in the polymer nanocomposites to be synthesized in the

present work. Taking into consideration, the advantageous optical properties and the excellent film forming properties of PS and PMMA, these polymers and the blend of PS and PMMA are chosen as the host polymer matrices for synthesizing the ZnO/polymer nanocomposites. The PS-PMMA blend is particularly chosen to investigate the effects of polymer blend host systems on the linear and nonlinear optical characteristics of ZnO/polymer nanocomposite systems.

Another prime objective of the present work is to realize an electrically conducting polymer with quite high degree of crystallinity. Polypyrrole, which is a highly pursued conducting polymer owing to its many advantageous electrical, optical and mechanical properties is chosen as the material to be investigated along these directions, taking into consideration its good environmental stability and film forming properties.

1.11 Objectives of the present investigations in a nutshell

- To synthesize ZnO nanoparticles using simple chemical methods without any surfactants, with the flexibility to control the particle size by varying the precursor concentrations.

- To synthesize successfully ZnO/polymer nanocomposites with homogeneous dispersity of the ZnO nanoparticles in the host polymer matrices, using PS,PMMA and PS-PMMA blend as the polymer matrices

- On the road to grow, good quality, homogeneous ZnO /polymer nanocomposite films on optically flat glass substrates and

investigate in detail the linear and nonlinear optical properties of these nanocomposite films, giving emphasis on the ZnO particle size dependence of these properties

- To identify the best ZnO/polymer nanocomposite film system with the ideal optical limiting and UV shielding characteristics.

- To realize polypyrrole films with exceptionally high degree of crystallinity adopting the doping-dedoping - redoping process and, to estimate quantitatively the extent of crystallinity.

References

[1]   Innocenzi P, Esposto MandMaddalena A, J Sol-Gel Sci Technol., 20:293 (2001).

[2]   L'u C, Cui Z and Yang B, Macromol Mater Eng., 288:717 (2003).

[3]   Hung CH and Whang WT, Macromol Chem Phys., 206:291 (2005).

[4]   Grasset F, Saito N and Li D, J Alloys Compd., 360:298 (2003).]

[5]   Joachin Piprek; "Semiconductor optoelectronic devices: Introduction to physics and simulation",Academic press, Elsevier Science-USA (2003)]

[6]   A Nakamura, Y L Lee, T Kataoka, and T Tokizaki; "Mesoscopic enhancement of optical nonlinearity in semiconducting quantum dots: CuCl and CuBr microcrystals" J. Lumin., 60–61, 376 (1994)]

[7]   Abdullah M, Lenggoro IW and Okuyama K, J Phys Chem B., 107:1957 (2003).

[8]   Hung CH and Whang WT, J Mater Chem., 15:267 (2005).

[9]   Khrenov V, Klapper M and M¨ullen K, Macromol Chem Phys., 206:95 (2005).

[10] Levine KL, Iroh JO and Kosel PB, Appl Surf Sci., 230:24 (2004).

[11]   Zheng J and Siegel RW, J Polym Sci B: Polym Phys., 41:1033 (2003).

[12]   Abdullah M and Morimoto T, Adv Funct Mater., 13:800 (2003).

[13]   Xiong HM and Zhao X, J Phys Chem B 105:10169 (2001).

[14]   Pron, A.; Rannou, P. Prog. Polym. Sci. 2001, 27, 135–190.

[15]   Lee JY, Kim DY, Kim CY (1995) Synthesis of soluble polypyrrole of the doped state in organic solvents. Synth Met 74:103

[16]   Li XG, Wang L, Huang MR, Lu Y, Zhu M, Menner A, Springer J (2001) Synthesis and characterization of pyrrole and anisidine copolymers. Polymer 42:6095

[17]   Li XG, Wei F, Huang MR, Xie YB (2007) Facile synthesis and intrinsic conductivity of novel pyrrole copolymer nanoparticles with inherent self-stability. J Phys Chem B 111:5829.

[18]   Meyyappan, M. <http://www.ipt.arc.nasa.gov/nanotechnology.html>, Feb 10 (2004)

[19]   Rodgers, P. (2006). "Nanoelectronics: Single file". Nature Nanotechnology. doi:10.1038/nnano.2006.5.)

[20]   C.Delure and M.Lanno, "Nanostructures", Springer, New Delhi (2004)

[21]   S.V.Gaponenko, "Optical properties of semiconductor nanocrystals", Cambridge Studies in Modern Optics; Cambridge University Press (1998).].

[22]   A.P. Alivisatos, Science 271, 933 (1996)

[23]   J.H.Davies, "The Physics of Low-Dimensional Semiconductors", Cambridge University Press, Cambridge (1998)

[24]   T. Yao and J. C. Woo; 'Physics and applications of semiconductor quantum structures" IOP publishing Bristol, Philadelphia (2001)

[25]   S Ogava, H Nagano and H Petek, Phys.Rev.Lett.88, 116801(2002)

[26] Abramowitz and Stegun," Handbook of Mathematical Functions", Dover Publications, USA (1972)

[27] C.B. Murray, D.J. North, and M.G. Bavendi; J.Am.Chem.Soc.115, 8706(1993)

[28] L.E.Brus., J.Phys.Chem, 90, 2555(1986)

[29] Van Dijken, E.A. Meulenkamp, D. Vanmaekelbergh, A.Meijerink, J. of Luminescence, 90,123 (2000)

[30] Ranjani Viswanatha, Sammer Sapra, B. Satpati, P.V. Sathyam, B.N.Dev,D.D.Sharma, J.Mater.Chem,14, 661(2004)].

[31] Massimiliano Di Ventra, Stphane Evoy and James R. Heflin, Jr."Introduction to Nanoscale Science and Technology", Kluwer academic Publishers, USA (2004).

[32] Xiong H. M, Wang Z. D, Liu D. P. Adv. Func. Mater. 2005, 15, 1751

[33] Coronado, E., Galan-Mascaros, J.R., Gomez-Garcia, C.J. and Laukhin, V., Nature 408, 447 (2000).

[34] Croce, F., Appetecchi, G.B., Persi, L. and Scrosati, B. Nature, 394, 456 (1998).

[35] Pinnavaia, T.J. Science, 220, 365 (1983).

[36] Wang, Y. and Herron, N. Science, 273, 632 (1996).

[37] Winiarz, J.G., Zhang, L.M., Lal, M., Friend, C.S. and Prasad, P.N. J. Am. Chem. Soc. 121, 5287 (1999).

[38] Sidorov, S.N. *et al.* J. Am. Chem. Soc. 123, 10502 (2001).

[39] Merkel, T.C. Freeman, B.D., Spontak, R.J., He, Z., Pinnau, I., Meakin, P. and Hill, A.J. Science, 296, 519 (2002).

[40] Joly, C., Smaihi, M., Porcar L. and Noble, R.D. Chem. Mater. 11, 2331 (1999).

[41] Hajji, P., David, L., Gerard, J.F., Pascault, J.P. and Vigier, G. J. Polym. Sci. 37, 3172 (1999).

[42] D. Suneel, D. Nageswra Rao, J.of Mechanical Engineering, 1, 75 (2008)

[43] M. Lieberthal and W.D. Kaplan, Materials Science and Engineering.A, 302, 83 (2001).

[44] X. Li, Y.Yang and X. Cheng, J.of Material Science, 39, 3211 (2004)

[45] E. Manias, Nature materials, 6, 9 (2007)

[46] Sangeeta Baksi, P R Basak & Soumitra Biswas (Nanocomposites – Technology trends & Application potential, http://www.tifac.org.in

[47] Dr. Richard A. Vaia Materials and Manufacturing Directorate Air Force Research Laboratory "Polymer nanocomposites open a new dimension for plastics and composites", The AMPTIAC Newsletter, Spring 2002 Volume 6, Number 1 17-24

[48] T. Lan, P.D. Kaviratna, and T.J. Pinnavaia, Chem. Mater., 7, 2144 (1995).

[49] T. Lan and T.J. Pinnavaia, Chem. Mater., 6, 2216 (1994).

[50] Professor J.N. Hay and S.J. Shaw; Source: Abstracted from "A Review of Nanocomposites 2000"

[51] Mitchnick, M. A., Gwozdz, G. T., Micale, F. J. US patent, 5,733, 531(1998).

[52] Hurwitz, S. The sun and sunscreen protection: recommendations for childen, Dermatol Surg. Oncol(1988).

[53] Masui, T.et al. J. Mat. Chem. 10, 353(2000).

[54] Dickerson, R. R. et al. Science 278, 827(1997).

[55] Disalvo, A. L., Mordas, C. J. PCT Int. Appl. WO2005042041(2005).

[56] Smith, T. W., McGrane, K. M. US patent 3,137,570(2003).

[57]   Giancaterina, S. et al. *Polymer* 43, 6397(2002).

[58]   Muela, A., Garcia-Bringas, J. M., Arana, I., Barcina, I. Microb. Ecol. 40, 336(2000).

[59]   Takama, M., Ishii, N., Wada, K. Fragrance Journal 26, 108(1998).

[60]   R. Rossetti, S. Nakahara, and L. E. Brus, J. Chem. Phys. 79, 1086 ~1983.

[61]   A. P. Alivisatos, J. Phys. Chem. 100, 13226 ~1996.

[62]   B.K. Meyer, H. Alves, D.M. Hofmann, W. Kriegseis, D. Forster, F. Bertram, J. Christen, A. Hoffmann, M. Straßburg, M. Dworzak, U. Haboeck, A.V. Rodina, Physica Status Solidi (b) 241(2), 231 (2004))

[63]   O. Madelung (ed.), Data in Science and Technology: Semiconductors (Springer, Berlin, 1992)

[64]   T.-H. Moon, M.-C. Jeong, W. Lee, J.-M. Myoung, Appl. Surf. Sci. 240(1–4), 280 (2005)

[65]   U. Ozgur, Y.I. Alivov, C. Liu, A. Teke, M.A. Reshchikov, S. Dogan, V. Avrutin, S.J. Cho, H. Morkoc, J. Appl. Phys. 98(4),41301 (2005)

[66]   S.J. Pearton, C.R. Abernathy, M.E. Overberg, G.T. Thaler, D.P. Norton, N. Theodoropoulou, A.F. Hebard, Y.D. Park, F. Ren, J. Kim, L.A. Boatner, J. Appl. Phys. 93(1), 1 (2003)

[67]   Tsukazaki, A. Ohtomo, T. Onuma, M. Ohtani, T. Makino, M. Sumiya, K. Ohtani, S.F. Chichibu, S. Fuke, Y. Segawa , H. Ohno, H. Koinuma, M. Kawasaki. Nat. Mater. 4(1) 42 (2005).

[68]   L Liao, J C Li, D F Wang, C Liu, C S Liu, Q.Fu and L X Fan; Nanotech.16, 985(2005)

[69]   H Cao, Y G Zhao, H C Ong, R P H Chang, Phys. Rev. B 59, 15107 (1999).

[70] Y.C. Gao, Y.X. Wang, Y.L. Ying, Y.L. Li, S.L. Qu, Opt. Commun. 223 (2003) 103.

[71] Y.L. Song, C. Zhang, G.P. Chen, G.Y. Fang, Y.X. Wang, X.Q. Xin, J. Opt. A 4 (2002) 199. of Effect of host and particle...)

[72] Chennupati Jagadish and Stephen Pearton," Zinc Oxide- Bulk, Thin films and Nano structures-Processing, Properties and Applications", Elsevier Ltd. UK (2006)

[73] Shirakawa, H., et al. 1977. Synthesis of electrically conducting organic polymers: Halogen derivatives of polyacetylene (CH)n. J Chem Soc Chem Commun 578].

[74] Bernhard Wessling,Chemical innovation31(2001)34

[75] Sajan D George,S Saravanan,M R Anantharaman,S Venkatachalam,P Radhakrishnan, V P N Nampoori,C P Vallabhan, Phys.RevB69 (2004) 235201].

[76] MacDiarmid, A.G. "Synthetic metals": A novel role for organic polymers (Nobel lecture). Angew. Chem. Int. Edit. 2001, *40*, 2581-2590

[77] L. E. Alexander, X-Ray Diffraction Methods in Polymer Science, Krieger Publishing Company, Malabar, FL, 1985.

[78] N. Kasai and M. Kakudo, X-Ray Diffraction by Macromolecules, Kodansha and Springer, Tokyo, 2005, 393–417.

[79] N. S. Murthy and H. Minor, General procedure for evaluating amorphous scattering and crystallinity from X-ray diffraction scans of semicrystalline polymers, Polymer 1990, 31, 996–1002.

[80] N. S. Murthy, H. Minor, M. K. Akkapeddi, and B. V. Buskirk, Characterization of polymer blends and alloys by constrained profile-analysis of X-ray diffraction scans, J. Appl. Polym. Sci. 1990, 41, 2265–2272.

[81] K. B. Schwartz, et al., Crystallinity and unit cell variations in linear high-density polyethylene, Adv. X-Ray Anal. 1995, 38, 495–502.

[82] N. S. Murthy and R. Barton Jr., Polymer industry, Industrial Applications of X-Ray Diffraction, edited by F. H. Chung and D. .K. Smith, Marcel Dekker, New York, 2000, 495–509.

[83] Raghavendra R Hegde, M G Kamath, Atul Dahiya, Polymer Crystallinity, www.utk.edu]

[84] Bre'das, J.L., et al. 1984. The role of mobile organic radicals and ions (solitons, polarons and bipolarons) in the transport properties of doped conjugated polymers. Synth Met 9:265.

[85] Bre'das, J.L., et al. 1984. Polarons and bipolarons in polypyrrole: Evolution of the band structure and optical spectrum upon doping. Phys Rev B 30:1023.

[86] Diaz, A.F., et al. 1981. Electrooxidation of aromatic oligomers and conducting polymers. Electroanal Chem 121:355.

[87] Mitchell, G.R., F.J. Davis, and C.H. Legge. 1988. The effect of dopant molecules on the molecular order of electrically-conducting films of polypyrrole. Synth Met 26:247.

[88] Nogami, Y., J. Pouget, and T. Ishiguro. 1994. Structure of highly conducting PF6_-doped polypyrrole.Synth Met 62:257.

[89] Kanazawa, K.K., et al. 1981. Electrical properties of pyrrole and its copolymers. Synth Met 4:119.

[90] Ezquerra, T., J. R_u_he, and G. Wegner. 1988. Hopping conduction in 3,4-cycloalkylpolypyrrole perchlorates: A model study of conductivity in polymers. Chem Phys Lett 144:194.

[91] R_u_he, J., T. Ezquerra, and G. Wegner. 1989. New conducting polymers from 3-alkylpyrroles. Synth Met 28:C177.

[92] Lee, J.Y., D.Y. Kim, and C.Y. Kim. 1995. Synthesis of soluble polypyrrole of the doped state in organic solvents. Synth Met 74:103

[93]   Selampinar, F., et al. 1995. A conducting composite of polypyrrole *a*. As a gas sensor. Synth Met 68:109.

[94]   Lin, C.W., B.J. Hwang, and C.R. Lee. 1998. Methanol sensors based evanescent wave sensor to monitor the deposition rate of thin films. Thin Solid Films 325 (1–2):139.

[95]   Suri, K., et al. 2002. Gas and humidity sensors based on iron oxide–polypyrrole nanocomposites. Sensor Actuat B Chem 81:277.

[96]   Diab, N., and W. Schuhmann. 2001. Electropolymerized manganese porphyrin=polypyrrole films as catalytic surfaces for the oxidation of nitric oxide. Electrochim Acta 47 (1–2):265.

[97]   Michalska, A., A. Hulanicki, and A. Lewenstam. 1997. All-solid-state potentiometric sensors for potassium and sodium based on poly(pyrrole) solid contact. Microchem J 57:59.

[98]   Riul, A., et al. 2002. Artificial taste sensor: Efficient combination of sensors made from langmuir–blodgett films of conducting polymers and a ruthenium complex and self-assembled films of an azobenzene-containing polymer. Langmuir 18:239.

[99]   Riul, A., Jr., et al. 2003. An electronic tongue using polypyrrole and polyaniline. Synth Met 132:109.

[100] Baughman, R.H. 1996. Conducting polymer artificial muscles. Synth Met 78:339.

[101] Hutchison, A.S., et al. 2000. Development of polypyrrole-based electromechanical actuators. Synth Met 113:121.

[102] Madden, J.D., et al. 2000. Fast contracting polypyrrole actuators. Synth Met 113:185.

[103] Smela, E., and N. Gadegaard. 1999. Surprising volume change in PPy(DBS): An atomic force microscopy study. Adv Mater 11:953.

[104] Okuzaki, H., and T. Kunugi. 1997. Adsorption-induced chemomechanical behavior of polypyrrole films. J Appl Polym Sci 64:383.

[105] Okuzaki, H., and T. Kunugi. 1996. Adsorption-induced bending of polypyrrole films and its application to a chemomechanical rotor. J Polym Sci Pol Phys 34:1747.

[106] Okuzaki, H., T. Kuwabara, and T. Kunugi. 1997. A polypyrrole rotor driven by sorption of water vapour. Polymer 38:5491.

[107] Okuzaki, H., and K. Funasaka. 2000. Electro-responsive polypyrrole film based on reversible sorption of water vapor. Synth Met 108:127.

[108] Watanabe, M., H. Shirai, and T. Hirai. 2002. Wrinkled polypyrrole electrode for electroactive polymer actuators. J Appl Phys 92:4631.

[109] Otero, T.F., and I. Cantero. 1999. Conducting polymers as positive electrodes in rechargeable lithium-ion batteries. J Power Sources 81:838.

[110] Otero, T.F., I. Cantero, and H. Grande. 1999. Solvent effects on the charge storage ability in polypyrrole. Electrochim Acta 44:2053.

[111] Kuwabata, S., S. Masui, and H. Yoneyama. 1999. Charge-discharge properties of composites of $LiMn_2O_4$ and polypyrrole as positive electrode materials for 4 V class of rechargeable Li batteries. Electrochim Acta 44:4593.

[112] Kuwabata, S., et al. 2000. Charge-discharge properties of chemically prepared composites of V_2O_5 and polypyrrole as positive electrode materials in rechargeable Li batteries. Electrochim Acta 46:91.

[113] Kuwabata, S., et al. 2000. Charge-discharge properties of composites of polypyrrole and vanadium oxide powder. Macromol Symp 156:213.

[114] Osaka, T., et al. 1997. Performances of lithium=gel electrolyte=polypyrrole secondary batteries. J Power Sources 68:392.

[115] Veeraraghavan, B., et al. 2002. Study of polypyrrole graphite composite as anode material for secondary lithium-ion batteries. J Power Sources 109:377.

[116] Satoh, M., et al. 1995. Characterization of a tantalum capacitor fabricated with a conducting polypyrrole as a counter electrode. Synth Met 71:2259.

[117] Larmat, F., J.R. Reynolds, and Y.J. Qiu. 1996. Polypyrrole as a solid electrolyte for tantalum capacitors. Synth Met 79:229.

[118] Yamamoto, H., et al. 1999. Solid electrolytic capacitors using an aluminum alloy electrode and conducting polymers. Synth Met 104:38.

[119] Krings, L.H.M., et al. 1993. Application of polypyrrole as counterelectrode in electrolytic capacitors. Synth Met 54:453.

[120] Kudoh, Y., et al. 1991. An aluminum solid electrolytic capacitor with an Electroconducting polymer electrolyte. Synth Met 41–43:1133.

[121] Kudoh, Y., et al. 1996. Covering anodized aluminum with electropolymerized polypyrrole via manganese oxide layer and application to solid electrolytic capacitor. J Power Source 60:157.

[122] Satoh, M., et al. 1994. Highly conducting polypyrrole prepared from homogeneous mixtures of pyrrole-oxidizing agent and its applications to solid tantalum capacitors. Synth Met 65:39.

[123] Tsai, M.L., P.J. Chen, and J.S. Do. 2004. Preparation and characterization of Ppy-Al$_2$O$_3$-Al used as a solid-state capacitor. J Power Sources 133:302.

[124] Sung, J.H., S.J. Kim, and K.H. Lee. 2003. Fabrication of microcapacitors using conducting polymer microelectrodes. J Power Sources 124:343.

[125] Niu, C., et al. 1997. High power electrochemical capacitors based on carbon nanotube electrodes. Appl Phys Lett 70:1480.

[126] Frackowiak, E.A., et al. 2000. Supercapacitor electrodes from multiwalled carbon nanotubes. Appl Phys Lett 77:2421

[127] Frackowiak, E.B., and F. Guin. 2001. Carbon materials for the electrochemical storage of energy in capacitors. Carbon 39:937.

[128] Frackowiak, E., et al. 1999. Electrochemical storage of lithium multiwalled carbon nanotubes. Carbon 37:61.

[129] Hughes, M., et al. 2002. Electrochemical capacitance of a nanoporous composite of carbon nanotubes and polypyrrole. Chem Mater 14:1610.

[130] Jurewicz, K., et al. 2001. Supercapacitors from nanotubes-polypyrrole composites. Chem Phys Lett 347:36.

[131] Frackowiak, E., et al. 2001. Nanotubular materials for supercapacitors. J Power Sources 97:822.

[132] Lee, M.S., S.B. Lee, and J.Y. Lee. 2003. All-polymer FET based on simple photolithographic micropatterning of electrically conducting polymer. Mol Cryst Liq Cryst 405:171.

[133] Kou, C.T., and T.R. Liou. 1996. Characterization of metal-oxide-semiconductor field-effect transistor (MOSFET) for polypyrrole and poly(N-alkylpyrrole)s prepared by electrochemical synthesis. Synth Met 82:167.

[134] Lee, M.S., et al. 2005. Flexible all-polymer field effect transistors with optical transparency using electrically conducting polymers. Thin Solid Films 477:169.

[135] MacDiarmid, A.G. 2001. "Synthetic metals": A novel role for organic polymers. Curr Appl Phys 1:269.

[136] Gregory, R.V., W.C. Kimbrell, and H.H. Kuhn. 1989. Application and processing conductive textiles. Synth Met 28:823.

[137] Olmedo, L., P. Hourquebie, and F. Jousse. 1993. Microwave absorbing materials based on conducting polymers. Adv Mater 5:373.

[138] Kim, M.S., et al. 2002. PET fabric=polypyrrole composite with high electrical conductivity for EMI shielding. Synth Met 126:233.

[139] J.R. Reynolds, Ly Hiep, F. Selampinar, P.J. Kinlen, Polym. Prepr (Am. Chem. Soc., Div. Polym. Chem.) 40 (1) (1999)

[140] W.K. Lu, R.A. Elsenbaumer, Annu. Tech. Conf. Soc. Plast. Eng. 56 (2) (1998) 1276. .

[141] K. Fraoua, S. Aeiyach, J. Aubard, M. Delamar, P.C. Lacaze, C.A. Ferreira, J. Adhes. Sci. Technol. 13 (4) (1999) 517.

[142] T. Ito, P. Buehlmann, Y. Umezawa, Anal. Chem. 71 (9) (1999) 1699.

[143] C.R. Martin, W. Liang, V. Menon, R. Parthasarathy, A. Parthasarathy, Synth. Met. 55–57 (1993) 3766.

.....ෂාශ.....

Experimental Techniques and Theory

This chapter gives a brief description of the synthesis methods of ZnO nanoparticles, ZnO/Polymer nanocomposite films and polypyrrole films. An account of the fundamental theories of the various experimental tools and their implementation, for the characterization of the materials under investigation in the present studies is also included in this section.

2.1   Introduction

Modern technologies continuously need new materials with special combination of properties. The identification of ideal materials for specific applications has much to do with the choice of the most appropriate material synthesis routes. In the case of nanostructured materials, a deep insight into the growth processes is a prerequisite for the understanding of all basic properties. The most important information to be obtained from growth analysis concerns the particle size, the particle size distribution, structure and the interface configuration of the nanomaterials.

2.2   Synthesis of nanomaterials

There are many methods for the synthesis of nanostructured materials, which can be classified into two broad areas which are

1.   Physical methods
2.   Chemical methods

2.2.1 Physical methods

Several physical methods are currently in use for the synthesis and commercial production of nanostructured materials [1]. These methods include inert-gas evaporation technique [2], sputtering, mechanical milling etc.

2.2.2 Chemical methods

Chemistry has played a major role in developing new materials with novel and technologically important properties. The main advantage of chemical synthesis is its versatility in designing and

synthesizing new materials that can be refined into a final product. The superiority of chemical processes over other methods is good chemical homogeneity, as chemical synthesis offers mixing at the molecular level. A basic understanding of the principles of crystal chemistry, thermodynamics and phase equilibrium, and reaction kinetics is important to take advantage of the many benefits that chemical processing has to offer.

Solution chemistry is sometimes used to prepare the precursor, which is subsequently converted to the nanophase particles by chemical reactions [3]. Precipitation of a solid from a solution is a common technique for the synthesis of fine particles. The general procedure involves reactions in the aqueous or non-aqueous solutions containing the soluble or suspended salts. Once the solution becomes supersaturated with the product, the precipitate is formed by either homogeneous or heterogeneous nucleation. The formation of a stable material with or without the presence of a foreign species is referred to as heterogeneous or homogeneous nucleation. The growth of the nuclei after formation usually proceeds by diffusion, in which case concentration gradients and reaction temperatures are very important in determining the growth rate of particles, to form the mono dispersed particles. For the formation of un-agglomerated particles with a very narrow size distribution, all the nuclei must be formed at nearly the same time and the subsequent growth must occur without further nucleation or agglomeration of particles.

Nano structured materials can also be prepared by other chemical methods such as chemical vapour deposition (CVD), hydrothermal method, sol-gel method, co-precipitation method etc.

2.2.3 Synthesis of ZnO nanoparticles for the present studies

In the present work, ZnO nanoparticles have been prepared using wet chemical method. Generally, this method comprises three steps. First step is the preparation of an alcohol-based solution. The second step is the addition of a metal oxide precursor to the alcohol-based solution to form the reaction mixture. The third step is the reaction of this mixture to form the nanosized metal oxide particles. Here the alcohol based solution is prepared using KOH in methanol and the metal oxide precursor used is zinc acetate dehydrate [Zn $(CH_3COO)_2 . 2H_2O$].

In the present work, ZnO nanoparticles were synthesized as follows. Initially, potassium hydroxide (0.1M) was dissolved in 200 ml methanol. This solution was heated to 60^0 C under reflux and stirring. To this solution, zinc acetate dehydrate (0.1M) was added. This mixture was kept for two hours under the same conditions during which, precipitation was observed to start. After stirring, the system was cooled to 20^0C. The precipitate was filtered and washed with hexane and isopropyl alcohol. The filtrate was dried in an oven at 60^0C for five hours.

ZnO nanoparticles were also synthesized at room temperature using a simple method. Zinc acetate (0.1 mol I^{-1}) was dissolved in 100 ml of methanol with magnetic stirring and then potassium hydroxide (KOH) was added. The mixture was stirred for about 2 hours and then washed and filtered. The filtrate was dried in an oven at 50^0 C for 5–6 hours. The white powder obtained was detected to be pure, nanosized ZnO.

2.3   Synthesis of Nanocomposites

Nanocomposites can be obtained by two different approaches namely in-situ and ex-situ techniques. In in-situ methods, nanoparticles are generated inside the host material matrix by decomposition or chemical reduction of a metallic precursor dissolved in the host material. In the ex-situ approach, nanoparticles are first produced by soft chemistry routes and then dispersed into host material matrices. Usually the preparative scheme allows the growth of nanoparticles whose surface can be passivated by monolayers of suitable agents like n- alkanethiol molecules. Surface passivation has an important role, since it inhibits aggregation of nanoparticles and avoids surface oxidation or contamination phenomenon [4]. Methods generally adopted for processing nanocomposites are mechanical alloying, sol-gel synthesis, and thermal spray synthesis.

In the present study, ZnO/polymer nanocomposites were prepared by a simple mixing procedure. Appropriate amount of ZnO nanoparticles was mixed with the polymer solution in toluene. The resulting mixture, after stirring and ultrasonication was used to prepare thin films of the ZnO/polymer nanocomposite on glass substrates using spin coating technique (Spin 150). Film thickness was recorded using a Dektak 6M Stylus Profiler working in the nanometer and micrometer ranges. Polystyrene (PS), Polymethyl methacrylate (PMMA) and PS-PMMA blend were used as the polymer matrices for the preparation of the ZnO/polymer nanocomposites.

2.4 Synthesis of conducting polymers and conducting polymer films

2.4.1 Synthesis of conducting polymers

Conducting polymers in general can be synthesized by chemical or electrochemical oxidation of the corresponding monomers [5]. Chemical oxidation involves mixing monomer and oxidant in solution, and for synthesizing polymers like polyaniline (PAni), an acid medium is necessary to ensure that the resulting product is a linear structured polymer. The most widely used oxidants are ammonium persulfate, ferrum chloride, hydrogen peroxide, potassium dichromate and cerium sulfate. Both aqueous and organic media are used as the solvents. For electrochemical synthesis, galvanostatic, potentiostatic, cyclic voltammetry and other potentiodynamic approaches can be employed. For all these approaches, a three-electrode system composed of a working electrode, a counter electrode and a reference electrode is the best choice to get optimum results.

Many conducting polymers such as poly (phenylene vinylene), poly (phenylene ethynylene) and their derivatives are usually synthesized through other chemical routes, rather than oxidation polymerization. That is because their backbones consist of aromatic rings along with C-C double or triple bonds. These reactions include Wittig reaction [6], Heck reaction [7] and Gilch polymerization [8] . Polythiophene and its derivatives can be synthesized via coupling reactions [9]. These chemical routes are specialized synthetic procedures capable of delivering regular structured conducting polymers, or well-defined copolymers.

2.4.2 Preparation of conducting polymer films

Various techniques have been developed to realize good quality films of conducting polymers on various types of substrates. The film deposition techniques include, electrochemical deposition [10-12], dip coating [13-16], spin coating [17, 18], solution casting, Langmuir-Blodgett (LB) technique, Layer-by-layer (LBL) self-assembly technique [19, 20], thermal evaporation [21], vapor deposition polymerization [22], drop coating [23, 24] etc.

In the present work, polymer thin films were deposited on flat glass substrates using solution casting and spin coating techniques. Usually, in solution casting, the sample solution is spread on a substrate uniformly and the solvent is allowed to evaporate and subsequently, a thin film is formed. Spin coating is a simple method for depositing films from solutions. In this process, the sample solution is spread on a rotating substrate. After evaporation of solvent, a thin film is formed. Repeating the above process is feasible, which can control the thickness of the film.

2.5 Methods for the synthesis of polypyrrole

Polypyrrole (PPy) can be synthesized by either chemical or electrochemical oxidation of pyrrole monomer. In the present work, chemical oxidative polymerization method is used to synthesize PPy samples. In the chemical oxidation method, an oxidizing agent such as lead dioxide, quinones, ferric chloride or persulfates is added to the pyrrole monomer and the dopant dissolved in a suitable solvent, resulting in the precipitation of doped PPy powder. The precipitate

obtained is filtered, washed and dried. This is one of the easiest methods adopted for synthesizing conducting polymers in bulk form. In general, the electrical conductivity of chemically prepared PPy is slightly lower than that of PPy films prepared electrochemically. Nevertheless,· the chemical oxidation method is suitable for commercial mass production of PPy and can be adopted to synthesize processible PPy, since the method has much greater feasibility to control the molecular weight and structural features of the resulting polymer than the electrochemical oxidation method [25–27]. It is well known that various properties such as electrical conductivity, stability, and morphology of synthesized PPy strongly depend on various reaction conditions such as the types and concentrations of oxidant and dopant, polymerization temperature and time, stoichiometry, and solvent. Following are the modified chemical polymerization techniques to improve some of the properties of polypyrrole.

(a)   Chemical Polymerization with Surfactants

To improve conductivity, stability or solubility in organic solvents, various kinds of surfactants have been used as additives in the chemical polymerization of pyrrole [28–32].

(b)   Chemical Polymerization with Sulfonic Acid Dopants

It has been reported that the type of sulfonic acid used as a dopant in chemical polymerization shows considerable effect on the properties of the resulting PPy such as morphology, electrical conductivity, and solubility [33].

(c) **In Situ Polymerization of PPy on Polymer Latex**

To improve the poor processibility of PPy, micrometer-sized PPy-coated polystyrene (PS) latexes have been synthesized by in situ deposition process [34, 35]. It is reported that if the PPy layer is sufficiently thin, it can lie inside the steric stabilizer layer and the coated latexes can maintain reasonable stability.

(d) **In Situ Polymerization of PPy on Substrates**

Highly transparent, electro active, and conductive poly [(3,4-alkylenedioxy)pyrrole-2,5-diyl] thin films have been prepared by in situ chemical polymerization [36-39]. The process possesses a significant advantage, as environmentally harmful organic solvents are not required since coatings can be obtained directly on the substrate.

(e) **Interfacial and Supercritical Fluid Polymerization**

It is reported that thin PPy films can be synthesized by chemical polymerization at the interface of chloroform solution of pyrrole and aqueous solution of $(NH_4)_2S_2O_8$ [40, 41]. There are several conditions for the solvents to be used for interfacial polymerization of pyrrole. The oxidant and monomer should be soluble in different solvents for the reaction to occur only at the interface.

(f) **Plasma Polymerization**

Plasma polymerization has been recognized as an important process to obtain thin films of conductive polymer, which are formed by reactions in gas phase without any chemical oxidants [42]. The chemical structure of plasma-polymerized PPy is

different from that obtained by conventional chemical or electrochemical polymerization processes because of fragment formation, trapped radicals, and a higher degree of branching and crosslinking [43-46].

(f) Copolymerization

Even though PPy can be of practical application in a variety of fields, its poor processibility and mechanical properties have been obstacles. To improve the processibility and mechanical properties, various types of PPy copolymers have been synthesized with many conventional or conducting polymers. PPy has been copolymerized electrochemically with thiophene to improve its disadvantageous properties such as sensitivity to oxygen [47], resulting in copolymer films with much less porosity than PPy films. There are different modified methods of copolymerization [48-55] that result in improved properties.

2.5.1 Synthesis of PPy for the present studies

Chemical oxidative polymerization,[56], a common method to synthesize conducting polymers in bulk form has been employed in the present work for the synthesis of polypyrrole. The monomer pyrrole was dissolved in the dopant acid (HCl) solution. The oxidant, ammonium persulfate (APS) dissolved in water was added drop wise to the mixture with continuous stirring for 4-5 hours. The precipitate obtained was filtered, washed and dried. This is one of the easiest methods adopted for synthesizing conducting polymers in bulk form.

2.5.2 Synthesis of PPy films

For the deposition of polypyrrole films on glass substrates, solution casting and spin coating methods have been used in the present work. First of all, HCl doped PPy was synthesized using APS as oxidant. The doped polypyrrole was dedoped using ammonia solution and then redoped with camphor sulphonic acid (CSA). Solution cast films were prepared by dissolving definite amounts of the redoped polymer samples, in selected organic solvents. The mixture was stirred for several hours. The resulting solution was poured onto ultrasonically cleaned glass substrates to cast films and the films were dried in an oven. Commonly used solvents are m-cresol, N-methyl pyrrolidinone (NMP), P-cresol, cyclohexanol and xylene [57-59].M-cresol is preferred over the rest because of its better solvation properties. Also the polymer- solvent interactions are stronger for m-cresol solution compared to others [57, 60]. The solubility of conducting polymers in organic solvents still remains a difficult task, the main reason being the rigid polymer back bone. The <pi> conjugation imparts stiffness to the polymer back bone which makes the polymer intractable. The <pi> electron delocalization leads to large electronic polarizability, giving rise to interchain attraction. This favors polymer aggregation rather than solvation. Also the rigidity of the polymer back bone thus formed creates unfavourable entropy for solution. The polymer chains complexed with ionic dopants also contain hydrophobic organic segments. It is very difficult to find solvents capable of solvating both hydrophilic and hydrophobic segments [57]. However, polymer nanostructures are found to be soluble in common organic solvents.

2.6   Characterization Tools

2.6.1 Structural characterization tools

It is very important to determine the size, structure and surface morphology of the different types of samples synthesized in the present work. A variety of techniques can be used for this purpose, and the details are given in the following sections.

2.6.1 (a) X-ray diffraction

X-ray diffraction (XRD) yields the atomic structure of materials and is based on the elastic scattering of X-rays from the electron clouds of the individual atoms in the system. Diffraction occurs as X-rays interact with a regular structure whose repeat distance is about the same as the X-ray wavelength.

Powder diffraction is a technique used to characterize the crystallographic structure, crystallite size (grain size), and preferred orientation in polycrystalline or powdered solid samples. This technique is commonly used to identify unknown substances, by comparing diffraction data against a database maintained by the International Centre for Diffraction Data. It may also be used to characterize heterogeneous solid mixtures to determine relative abundance of crystalline compounds and, can provide structural information on unknown materials. Powder diffraction is also a common method for determining strains in crystalline materials. The effect of the finite crystallite sizes is seen as a broadening of the peaks in the X-ray diffraction pattern and is explained by the Debye Scherrer Equation [61].

(i)   Fundamental principles of X-ray powder diffraction

Max von Laue, in 1912, discovered that crystalline substances act as three-dimensional diffraction gratings for X-ray wavelengths. X-ray diffraction is now a common technique for the study of crystal structures and atomic spacing. X-ray diffraction is based on constructive interference of monochromatic X-rays diffracted from a crystalline sample. A cathode ray tube, filtered to produce monochromatic radiation, collimated to concentrate, and directed toward the sample, generates X-rays. The interaction of the incident X-rays with the crystal lattice of the sample produces constructive interference (and a diffracted ray) when conditions satisfy Bragg's law,
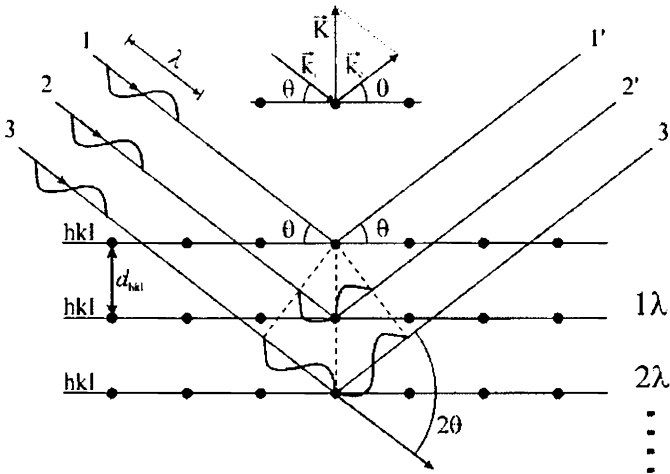
Figure 2.1: Bragg's diffraction phenomenon

$$n\lambda = 2d \sin \theta, \quad \text{---} \quad (2.1)$$

where n is the order of diffraction, λ is the wavelength of the X-rays, d is the spacing between consecutive parallel planes and θ is the glancing angle (or the complement of the angle of incidence) [62].

The average grain size of the sample can be calculated using the Scherrer's formula [61]

$$d = \frac{0.9\lambda}{\beta Cos\theta}$$ -------------------------------- (2.2)

where, λ is the wavelength of the X-rays and β is the full width at half maximum intensity in radians. The lattice parameters for different crystallographic systems can be calculated from the following equations using the (hkl) parameters and the interplanar spacing d.

Cubic system

$$\frac{1}{d^2} = \left(\frac{h^2 + k^2 + l^2}{a^2} \right)$$ -------------------------- (2.3)

Tetragonal system

$$\frac{1}{d^2} = \left(\frac{h^2 + k^2}{a^2} \right) + \frac{l^2}{c^2}$$ -------------------------- (2.4)

Hexagonal system

$$\frac{1}{d^2} = \frac{4}{3}\left(\frac{h^2 + hk + k^2}{a^2} \right) + \frac{l^2}{c^2}$$ ------------------ (2.5)

(ii) X-ray powder diffraction instrumentation

X-ray diffractometers consist of three basic elements, which are, the X-ray tube, the sample holder, and the X-ray detector. X-rays are generated in a cathode ray tube by heating a filament to produce electrons, and then accelerating the electrons toward a target by applying a voltage, and subsequently bombarding the target material with the accelerated electrons. When electrons have sufficient energy to dislodge inner shell electrons of the target material, characteristic X-ray spectra are produced. The specific wavelengths are characteristic of the target material. Filtering, by foils or crystal monochromaters, is required to

produce monochromatic X-rays needed for diffraction. These X-rays are collimated and directed onto the sample. The sample and detector are rotated and the intensity of the reflected X-rays is recorded. When the geometry of the incident X-rays impinging the sample satisfies the Bragg Equation, constructive interference occurs and a peak in intensity occurs. The detector records and processes the X-ray signal and converts the signal to a count rate, which is output to a device such as a printer or computer monitor.
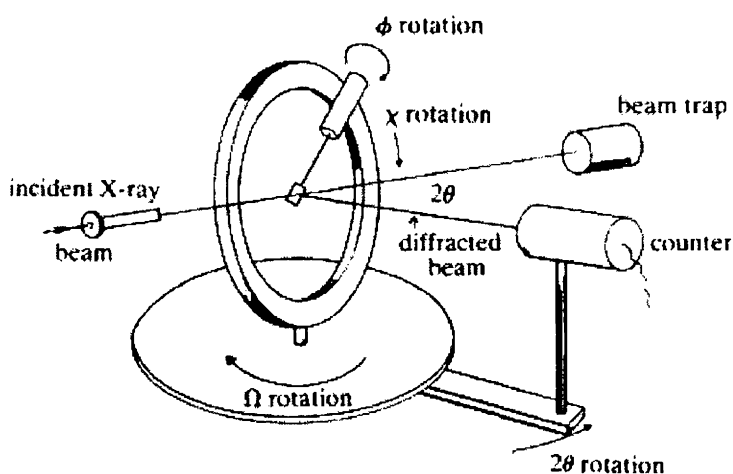
Figure 2.2: XRD experimental set up

XRD experiments in the present studies are done using Rigaku automated X-ray diffractometer. The filtered Cu-Kα radiation (λ =1.5414A°) with nickel filter is used for recording the diffraction pattern. The accelerating potential applied to the X ray tube is 30 kV and the tube current is 20 mA. A given substance always produces a characteristic diffraction pattern, irrespective of it being in the pure state or as a constituent of the mixture state. This fact is the basis for the diffraction method of chemical analysis. Compared to ordinary chemical

analysis, the diffraction method has the additional advantages that it is usually much faster, requires only very small quantity of sample and is non-destructive [61, 63]

(iii) Applications

X-ray powder diffraction is most widely used for the identification of unknown crystalline materials (e.g. minerals, inorganic compounds etc). Identification of unknown solids is critical to studies in geology, environmental science, material science, engineering and biology.

Other applications include:

- Characterization of crystalline materials

- Identification of fine-grained minerals such as clays and mixed layer clays that are difficult to observe optically

- Determination of unit cell dimensions

- Assessment of sample purity

- Measurement of percentage crystallinity

2.6.1(b) Fourier Transform InfraRed Spectroscopy

Fourier Transform Infrared, (FT-IR) spectroscopy is an important and popular tool for structural elucidation and compound identification. In infrared spectroscopy, IR radiation is passed through a sample. Part of the infrared radiation is absorbed by the sample and part of it is transmitted. The resulting spectrum represents the molecular absorption and transmission creating a molecular fingerprint of the sample. Like a fingerprint, no two unique molecular structures produce the same infrared spectrum. This makes infrared spectroscopy quite useful for

several types of analysis [64-67]

The term *Fourier transform infrared spectroscopy* originates from the fact that a Fourier transform (a mathematical algorithm) is required to convert the raw data into the actual spectrum. Figure 2.3 depicts a schematic diagram of FT-IR spectrometer.
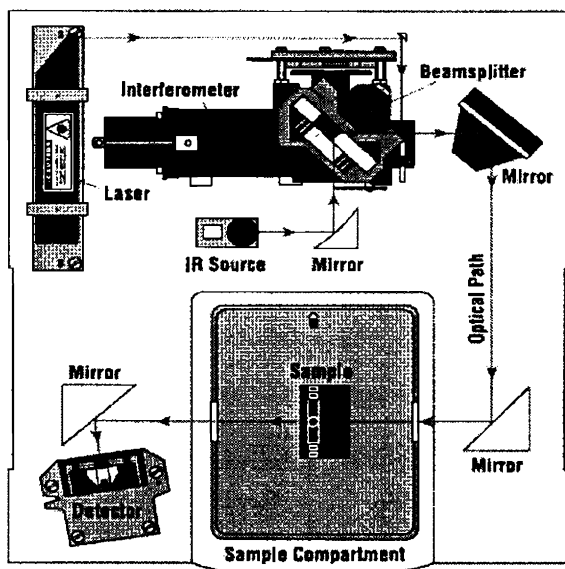
Figure 2.3: Schematic diagram of FTIR spectrometer

The basic optical component of Fourier transform spectrometers is the Michelson interferometer. Light from an infrared source-a heated element or a glow bar-is collimated and directed to a beam splitter. An ideal beam splitter creates two separate optical paths by reflecting 50% of the incident light and transmitting the remaining 50%.In the near and middle infrared regions, germanium deposited on a KBr substrate is used as the beam splitter. In one of the paths, the beam is reflected back to the beam splitter by a fixed position mirror, where it is partially transmitted

to the source and partially reflected to the detector. In the other leg of the interferometer, the beam is reflected by a movable mirror that is translated back and forth (typically a few millimeters) while maintained parallel to itself. The beam from the movable mirror is also returned to the beam splitter where it too, is partially reflected back to the source and partially transmitted to the detector. Although the light from the source is incoherent, when it is split into two components by the beam splitter, the components are coherent and can produce interference phenomenon when the beams are combined. The resulting signal is called an interferogram, which has the unique property, that every data point (a function of the moving mirror position) which makes up the signal has information about every infrared frequency, which comes from the source. In order to get the frequency spectrum (a plot of the intensity at each individual frequency), the measured interferogram signal is interpreted (by decoding) using Fourier transformation. This transformation is performed by the computer, which then presents the desired spectral information for analysis.

There are two main advantages for a FT spectrometer compared to a scanning (dispersive) spectrometer.[68, 69]

1. The multiplex or Fellgett's advantage: This arises from the fact that information from all wavelengths is collected simultaneously. It results in a higher signal-to-noise ratio for a given scan-time or a shorter scan-time for a given resolution.

2. The throughput or Jacquinot's advantage: This results from the fact that, in a dispersive instrument, the monochromator has entrance

and exit slits which restrict the amount of light that passes through it. The interferometer throughput is determined only by the diameter of the collimated beam coming from the source.

In the present study, Fourier transform infrared (FT-IR) spectra of the samples were obtained with AVTAR 370 DTGS   FT-IR spectrophotometer in the wave number range $500 - 4000$ cm^{-1}.

2.6.1(c) Raman Spectroscopy

Raman spectroscopy is a powerful technique used to study vibrational, rotational, and other low-frequency modes in a system [70]. It relies on inelastic scattering, or Raman scattering, of monochromatic light, usually from a laser in the visible, near infrared, or near ultraviolet range. The laser light interacts with molecular vibrations, phonons or other excitations in the system, resulting in the energy of the laser photons being shifted up or down. The shift in energy gives information about the phonon modes in the system.

Theory:

Raman spectroscopy differs from the infrared spectroscopy by an indirect coupling of high-frequency radiation, such as visible light, with vibrations of chemical bonds. Raman spectrum is very sensitive to the lengths, strengths and arrangements of chemical bonds in a material, but less sensitive to the chemical composition. When the incident photon interacts with the chemical bond, the chemical bond is excited to a higher energy state. Most of the energy would be re-radiated at the same frequency as that of the incident exciting light, which is known as the Rayleigh scattering. A small portion of the energy is transferred and

results in exciting the vibrational modes, and this Raman process is called Stokes scattering. The subsequent re-radiation has a frequency lower (smaller wave number) than that of the incident exciting light. The vibrational energy is deducted by measuring the difference between the frequency of the Raman line and the Rayleigh line. Existing exciting vibrations, e.g. through thermal activation, can also couple with and add their energies to the incident beam, which is called anti-Stokes scattering. The resulting Raman lines appear at higher frequencies or larger wave numbers. The Stokes and anti-Stokes scattering spectra are mirror images on opposite sides of the Rayleigh line. However, Stokes scattering spectra are mostly used, since they are less temperature sensitive. The Raman effect is extremely weak and, hence, intense monochromatic continuous gas lasers are used as the exciting light sources. It should be noted that Raman spectroscopy is more a structural characterization technique than a chemical analysis.
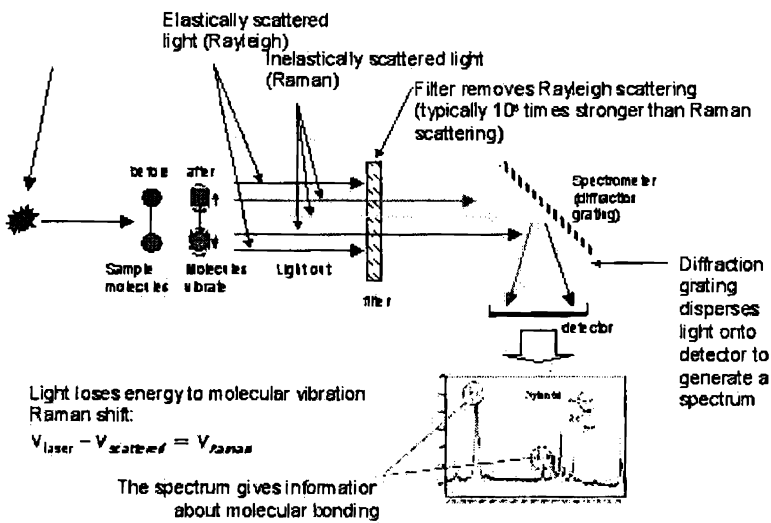
Figure 2.4: Principle of Raman Spectroscopy
(newton.ex.ac.uk)
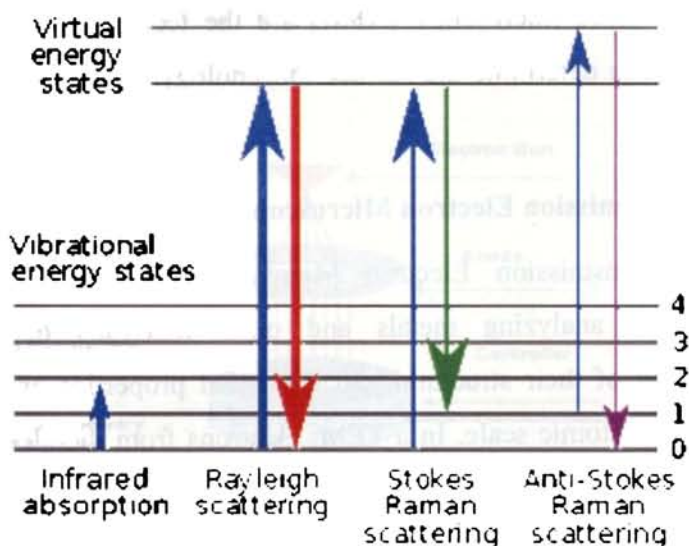
Figure 2.5 Energy Level Diagram Depicting Raman Scattering

Raman spectroscopy can be used to detect both organic and inorganic species. It is free from charging effects which is a disadvantage for electron and ion beam techniques. It is sensitive to strain, allowing it to be used for detecting stress in a semiconductor material or device. The major semiconductor applications of Raman spectroscopy include the identification of structural defects, alloy fluctuations, interfaces and heterojunctions [71].

In the present work, Raman spectroscopic studies have been carried out, using a Confocal Micro Raman Spectrometer, HORIBA JOBINYVON (Lab RAM HR), employing a 633 nm He-Ne laser.

2.6.2 Morphological studies

Transmission Electron Microscopy (TEM), Field Emission Scanning Electron Microscopy, Scanning Electron Microscopy (SEM)

and Atomic force microscopy (AFM) are the techniques used in the present work to determine the surface morphology and the particle size of the samples.

2.6.2(a) Transmission Electron Microscopy

The Transmission Electron Microscopy (TEM) is an ideal technique for analyzing metals and other materials to gain an understanding of their structural and elemental properties on the sub-micrometer to atomic scale. In a TEM, electrons from the electron gun are accelerated from 100 kV to 400 kV and are focused onto the specimen by a combined lens system [72-75].

The sample is kept very thin for effective transmission and is placed on a copper grid. The transmitted and forward scattered electrons produce a diffraction pattern in the back focal plane of the lens and a magnified image on the image plane of the lens. Either of it is projected onto a fluorescent screen for photographing or electronic recording. Formation of diffraction pattern helps to study the structural details. Schematic diagram of a Transmission Electron Microscope is given in figure 2.6.

There are mainly three imaging techniques-bright field, dark field and high resolution imaging [73].Contrast depends on diffraction and scattering of electrons. Transmitted electrons give rise to bright field image and specific diffracted beam, to the dark field image Contrast depends on the intensity of electrons transmitted through the sample that pass through the imaging lens. Heavier elements lead to greater scattering of electron beam. So, intensity of transmitted electrons is

reduced. Contrast comes about by phase contrast, mass contrast, thickness contrast and diffraction contrast.

Electrons are produced with an electron gun, similar to the one in a television.

The electrons are then accelerated through the Anode plate and focused with the Magnetic Lens.

Both crystallographic information and surface topographic information can be viewed.

Specimens must be very thin, on the order of 0.1 micrometers.

Electron Gun

Anode

Computer Control

Controller

Specimen

Stage

Diffraction Information

Image Information

Monitor Viewer

Parallel Detector

Figure 2.6: Schematic diagram of transmission electron microscope

High resolution TEM (HRTEM) is used to obtain information on the atomic scale and is particularly used in the interface analysis. Here a number of different diffracted beams are combined together to give an interference image. In the present study TEM micrographs have been taken using JEOL 3010 instrument with a UHR pole piece

2.6.2(b) Scanning electron microscopy

Scanning electron microscopy (SEM) and Energy dispersive X-ray spectroscopy (EDS) measurements are performed using a Joel Model

JSM 6390LV scanning electron microscope. The schematic diagram of a scanning Electron Microscope is given in figure 2.7.
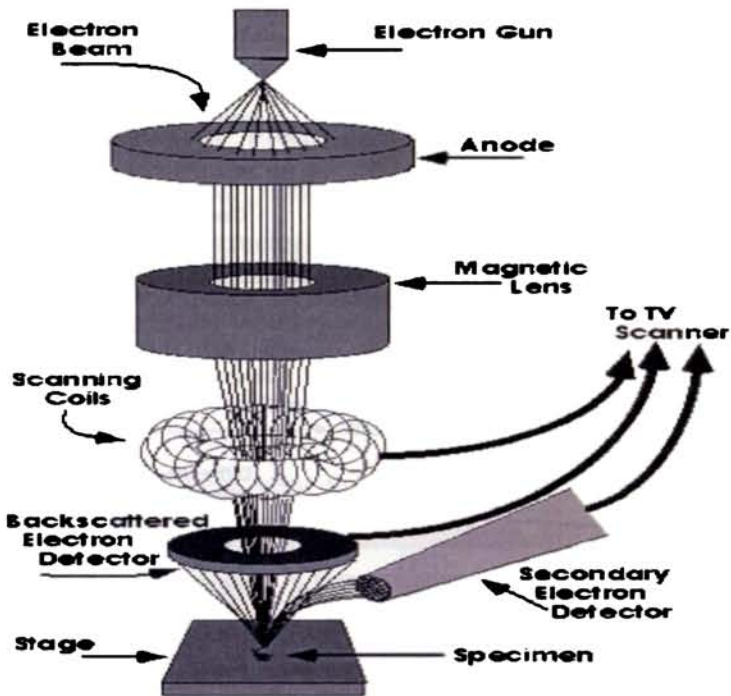
Figure 2.7: Schematic diagram of a scanning electron microscope

Scanning Electron Microscopy is similar to optical microscopy. But here electrons are used instead of photons. Electrons of energy 10-30 keV impinge on the sample. Secondary electrons, back scattered electrons, auger electrons and X-ray photons are produced. Secondary electrons form the SEM image. Back scattered electrons also form an image [76]. Absorbed electrons are measured as electron beam induced current.
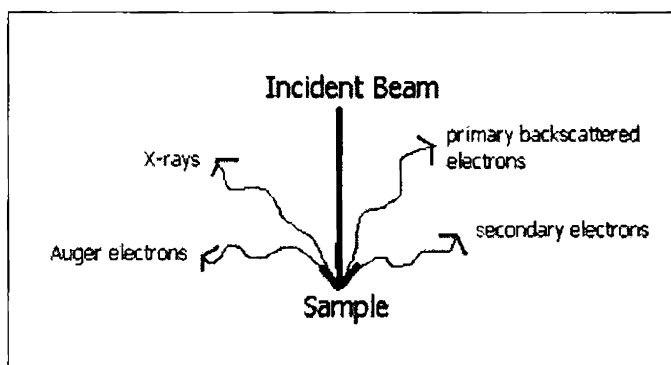
Figure 2.8: Production of secondary electrons

The secondary electrons are detected and amplified. The image of the specimen is mapped onto a CRT screen. There should be one to one correspondence between each point on the specimen and each point on the screen. Magnification is defined as the ratio of the length of CRT display to length of sample scan. Using SEM, magnification of the order of 10^6 can be achieved which is impossible through optical microscope. Large magnification is possible because electrons have smaller wavelengths and depth of field produced is large. Contrast is an important parameter for SEM imaging. For flat, uniform samples, there is no contrast. But for samples composed of materials with different atomic numbers, contrast is observed. Contrast is observed mainly due to back scattered electrons because back scattering coefficient is a strong function of atomic number than secondary electron emission coefficient. Other factors affecting contrast are sample surface; surface topography and local electric fields. Secondary electrons are emitted from the top 10nm of the sample surface. When the sample is tilted through an angle θ from the normal beam direction, electron beam path inside the sample increases by 1/cos θ.

$$\text{Contrast C=tan } \theta \text{ d}\theta \text{ --- (2.6)}$$

Sample stage is an important parameter. It should allow sufficient tilt and rotation for the sample to be viewed in all directions. In SEM, the detector collects even those electrons moving away from it, unlike an optical microscope [64].

Energy Dispersive X-ray Spectroscopy (EDS) is an analytical capability that can be coupled with several applications including SEM, TEM and STEM. EDS, when combined with these imaging tools, can provide elemental analysis on areas as small as nanometers in diameter. The impact of the electron beam on the sample produces x-rays that are characteristic of the elements present on the sample. EDS can be used to determine the elemental composition of individual points or to map out the lateral distribution of elements from the imaged area.

2.6.2(c) Field Emission Scanning Electron Microscopy

Field Emission SEM (FESEM) is a microscope that works with electrons (particles with a negative charge) instead of light. These electrons are liberated by a field emission source. Electrons according to a zigzag pattern scan the object. FESEM is used to visualize very small topographic details on the surface or entire or fractioned objects. Researchers in biology, chemistry and physics apply this technique to observe structures that may be as small as 1 nm. This technique gives 3 to 6 times better resolution than conventional SEM.

Electrons are liberated from a field emission source and accelerated in a high electrical field gradient. Within the high vacuum column these so-called primary electrons are focused and deflected by

electronic lenses to produce a narrow scan beam that bombards the object. As a result, secondary electrons are emitted from each spot on the object. The angle and velocity of these secondary electrons relates to the surface structure of the object. A detector catches the secondary electrons and an image of the sample surface is constructed by comparing the intensity of these secondary electrons to the scanning primary electron beam. Finally, the image can be seen on a monitor or to a digital image that can be saved and processed further [77].
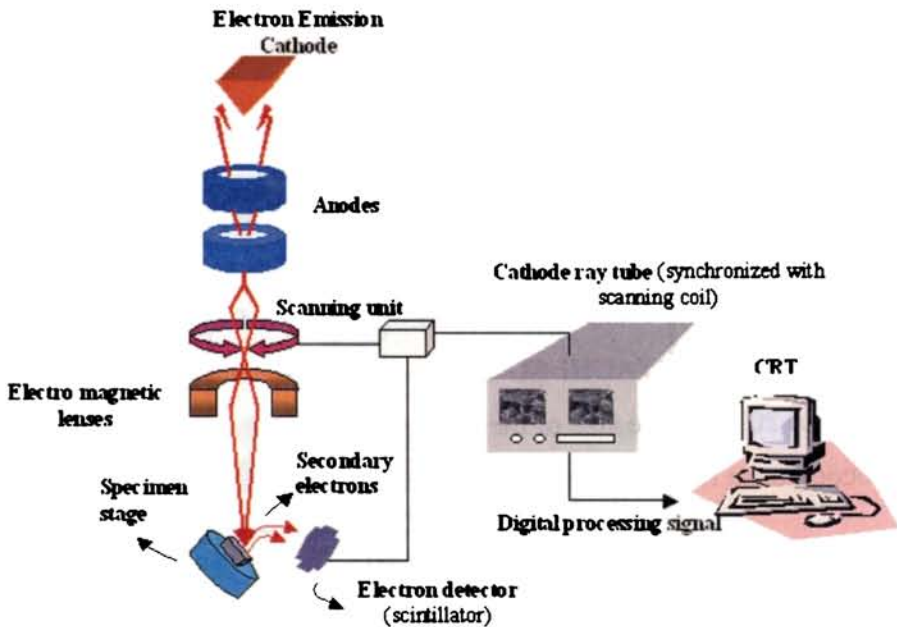
Figure 2.9: Schematic diagram for FESEM analysis

(infohost.nmt.edu)

i) ***Advantages***

- Smaller-area contamination spots can be examined at electron accelerating voltages compatible with Energy Dispersive X-ray Spectroscopy. ii) Reduced penetration of low kinetic

energy electrons probes closer to the immediate material surface. iii) High quality, low voltage images are obtained with negligible electrical charging of samples (Accelerating voltages range from 0.5 to 30 kV). iv) Need for placing conducting coatings on insulating materials is virtually eliminated.

ii) *Applications*

- Semiconductor device cross section analyses for gate widths, gate oxides, film thicknesses, and construction details

- Advanced coating thickness and structure uniformity determination

- Small contamination feature geometry and elemental composition measurement

In this study, Field Emission SEM images of the samples were obtained using a HITACHI SU 6600 Microscope with an accelerating voltage of 20 kV. The size of the ZnO nanoparticles and surfaces of the nanocomposite films have been studied using FESEM.

2.6.2(d) Atomic Force Microscopy (AFM)

Atomic force microscopy is a powerful tool allowing a variety of surfaces to be imaged and characterized at the atomic level. The atomic force microscope (AFM) was also invented by Binning et al. in 1986. While the scanning tunneling microscope (STM) measures the tunneling current (conducting surface), the AFM measures the forces acting between a fine tip and a sample. The tip is attached to the free end of a cantilever and is brought very close to a surface. Attractive or repulsive

forces resulting from interactions between the tip and the surface will cause a positive or negative bending of the cantilever. The cantilever bending or deflection is usually detected by a laser beam focused on the free end of the cantilever and is reflected into a photodiode. AFM cantilevers and tips are usually made of silicon or silicon nitride. Figure 1 shows the basic concept of AFM.
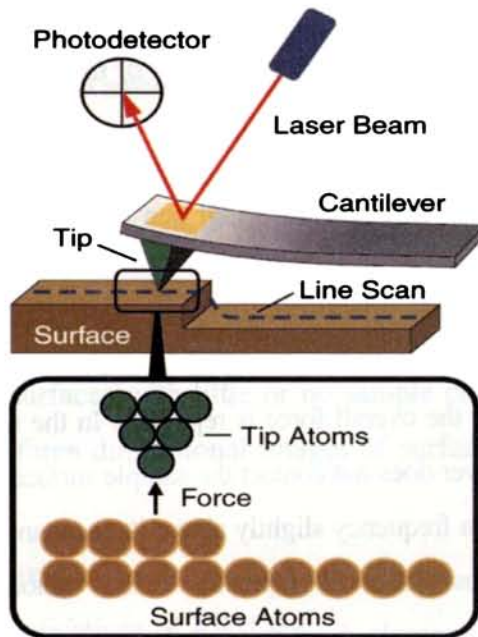
Figure 2.10: Principle of AFM.

If the tip was scanned at a constant height, a risk would exist that the tip collides with the surface, causing damage. Hence, in most cases a feedback mechanism is employed to adjust the tip-to-sample distance to maintain a constant force between the tip and the sample. Traditionally, the sample is mounted on a piezoelectric tube that can move the sample in the z direction for maintaining a constant force, and

the *x* and *y* directions for scanning the sample. Alternatively a 'tripod' configuration of three piezo crystals may be employed, with each responsible for scanning in the x, y and z directions. This eliminates some of the distortion effects seen with a tube scanner. In newer designs, the tip is mounted on a vertical piezo scanner while the sample is being scanned in X and Y using another piezo block. The resulting map of the area $z = f(x, y)$ represents the topography of the sample.

The AFM can be operated in a number of modes, depending on the application. In general, possible imaging modes are divided into static (also called *contact*) modes and a variety of dynamic (non-contact or "tapping") modes where the cantilever is vibrated.

In the static mode operation, the static tip deflection is used as a feedback signal. Thus static mode AFM is almost always operated in contact mode where the overall force is repulsive. In the non-contact mode, the tip of the cantilever does not contact the sample surface. The cantilever is instead oscillated at a frequency slightly above its resonant frequency where the amplitude of oscillation is typically a few nanometers (<10 nm). Measuring the tip-to-sample distance at each (x, y) data point allows the scanning software to construct a topographic image of the sample surface [78]. In tapping mode-AFM the cantilever is oscillating close to its resonance frequency.

An electronic feedback loop ensures that the oscillation amplitude remains constant, such that a constant tip-sample interaction is maintained during scanning. For a good phase contrast, larger tip forces are of advantage, while minimization of this force reduces the contact

area and facilitates high-resolution imaging. So in applications it is necessary to choose the right values matching the objectives. Silicon probes are used primarily for Tapping Mode applications [79].

i)   *Advantages*

This technique is involved in many fields of nanoscience and nanotechnology. The remarkable feature of STM and AFM instruments is their ability to examine samples not only in an ultrahigh vacuum but also at ambient conditions or even in liquids [80].

One of the advantages of AFM is that it can image the non-conducting surfaces, and therefore it is very suitable for biological systems.

The AFM is capable of measuring nanometer scale images of insulating surfaces with little or no sample preparation as well as measuring three dimensional images of surfaces and studying the topography.

ii)   *Applications*

Some possible applications of AFM are:

- Substrate roughness analysis.

- Step formation in thin film epitaxial deposition.

- Pin-holes formation or other defects in oxides growth.

- Grain size analysis.

- Phase mode is very sensitive to variations in material properties, including surface stiffness, elasticity and adhesion.

- Obtaining information of what is happening under indentation at very small loads.

- By in situ AFM analysis with changes in temperature one can study changes in the structure.

In the present work, AFM images of the composite films have been obtained with Park XE-100 Atomic Force Microscope

2.6.3 Optical characterization tools

The optical properties of the samples investigated in the present work are studied using tools such as optical absorption spectroscopy, Diffuse Reflectance Spectroscopy (DRS) and Photoluminescence s (PL).

2.6.3(a) Linear Optical absorption spectroscopy

An optical absorption spectrum provides information on the wavelength of electromagnetic radiation that can be absorbed by the samples under study. This is determined by varying the wavelength and recording the intensity of the transmitted beam. When light is absorbed, the energy of absorbed photons is used to excite a transition between electronic levels, usually starting from the electronic ground state. The position of higher energies can be derived from the absorption spectrum [81]. In addition, it can be used to determine the band gap of the material [82]. When an incident light beam reaches a medium, a part of the beam will be reflected by the medium, a part of the beam will be transmitted through the medium and rest of the beam will be absorbed. Absorption of photons results in the transition of electrons from the lower energy level to the higher energy levels. The absorption ability of a material is measured by its absorption coefficient.

If one assumes a parabolic band structure for the material, the absorption coefficient and band gap can be related by the expression

$$\alpha = (A/h\upsilon)(h\upsilon - E_g)^r, \text{---------------------------------} (2.7)$$

where E_g is the band gap, α is the absorption coefficient corresponding to the frequency υ and A is the parameter which depends upon the transition probability. The constant r depends upon the nature of electronic transition. For direct allowed transitions r=1/2, for indirect allowed transitions r=2, for forbidden indirect transitions r=3 and for forbidden direct transitions r=3/2.

The absorption coefficient can be deduced from the absorption or transmission spectra using the relation

$$I = I_0 \exp(-\alpha t) \text{---} (2.8)$$

where I is the transmitted intensity and I_0 is the intensity of the incident light and t is the thickness of the sample. The band gap energy can be determined by extrapolating the linear portion in the $(\alpha h\upsilon)^2$ versus $h\upsilon$ plot to the abscissa in the case of direct allowed transitions. The absorption coefficient is a function of frequency.

In the present study, the optical absorption of the samples is recorded using JASCO V-570 spectrophotometer, having a Deuterium lamp (190-350 nm) and a halogen lamp (330-2500 nm) as sources. The optical system used was a single monochromator. The spectrometer has two detectors - 1.Photo Multiplier Tube (PMT) 2.Lead sulphide (PbS) Photoconduction cell. The instrument has a resolution of 0.1 nm in the UV/Visible region and 0.5 nm in the NIR region.
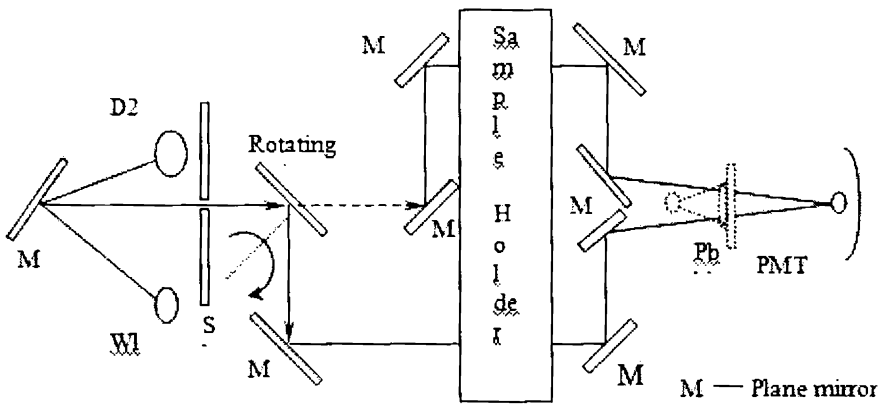
Figure 2.11: UV-Vis-NIR spectrophotometer for optical measurements

2.6.3(b) Diffuse Reflectance Spectroscopy (DRS)

Optical measurements using DRS technique are used to determine the band gap energy as well as the degree of reflectance of powder samples. The optical band gap Eg of powder samples is estimated from the UV-Vis diffuse reflectance spectroscopic (UV-Vis DRS) studies, using JASCO V-570 spectrophotometer, in the wavelength range from 190 nm to 1200 nm, in the present work. The samples for this study are used in the form of powder and pure $BaSO_4$ is used as the reference. Diffuse Reflectance Spectroscopy (DRS), also sometimes known as Elastic Scattering Spectroscopy, is a non-invasive technique that uses the interaction of light with the medium. Reflection and scattering produce a characteristic reflectance spectrum, providing information about the structure and composition of the medium. The light from a broadband source is launched into a fiber-optic bundle, the end of which constitutes a reflectance probe. Light leaves the probe and enters the medium under investigation. After the processes of scattering and absorption, light that leaves the medium is collected by another fiber, and directed into a

spectrometer. This is interfaced to a computer, which controls the data acquisition and displays the collected spectrum. The spectrum may then be further processed to determine the characteristics of the medium. Figure 2.12 demonstrates the working of a DRS system. In the case of polycrystalline powder samples, absorption spectra cannot be recorded. Even if light is not absorbed by the sample, it will be scattered and the intensity of the transmitted beam will be close to zero. For such samples a DRS is recorded. Poly- crystalline MgO or $BaSO_4$ powder is used as reference. Both MgO and $BaSO_4$ are perfectly white in the wavelength range 190nm to 1200 nm and the light will be scattered and not absorbed. If the sample absorbs part of the light, intensity of the reflected and scattered light will be reduced and will be lower than the intensity reflected by the reference. Reflection spectra can be used to determine the position of the absorption bands.
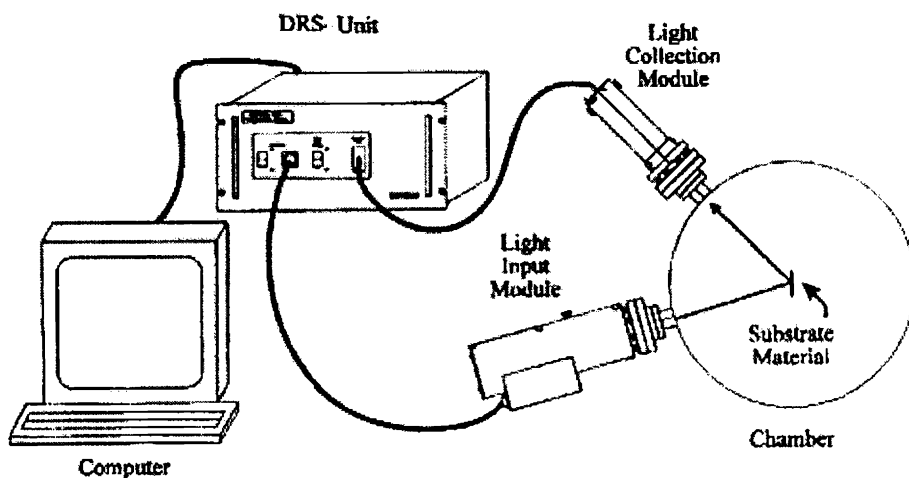
Figure 2.12: Basic components for recording diffuse reflectance spectrum

The intensity of the reflected light depends on the scattering coefficient's' and the absorption coefficient 'k'. The reflectance data can

be converted to absorbance by Kubelka-Munk equation [83]. Kubelka-Munk equation is

$$\text{Log } [(1-r_\alpha) 2 / 2r_\alpha] = \text{Log } k - \text{Log } s \text{ ------------------ (2.9)}$$

where $r_\alpha = R_\alpha$ (sample) $/R_\alpha$ (standard).

Here the standard used is $BaSO_4$. R_α (standard) is taken as unity. R_α(sample) is the diffuse reflectance of the sample ($R = I_{sam}/I_{ref}$).

Equation implies,

$$F(R) = (1-R)^2 /2R = k/s \text{ ----------------------------------(2.10)}$$

The band gap is estimated from the plot of $[(k/s). h\upsilon]^2$ versus $h\upsilon$ where $h\upsilon$ is the photon energy. By extrapolating the linear portion of the curve to meet at $h\upsilon=0$, the band gap can be found out. In the present study the band gap of ZnO samples is calculated from the plot of percentage of reflectance (%R) versus the energy in electron volt (eV).

2.6.3(c) Photoluminescence (PL)

Photoluminescence spectroscopy is a contact-less, non-destructive method of probing the electronic structure of materials. Light is directed onto a sample, where it is absorbed and imparts excess energy into the material in a process called photo-excitation. One of the ways through which this excess energy can be dissipated by the sample is through the emission of light, or luminescence. In the case of photo-excitation, this luminescence is called photoluminescence. Photo-excitation causes electrons within the material to move into permissible excited states. When these electrons return to their equilibrium states, the excess energy

is released and may include the emission of light (a radiative process) or may not (a nonradiative process). The energy of the emitted light (photoluminescence) relates to the difference in energy levels between the two electron states involved in the transition between the excited state and the equilibrium state. The quantity of the emitted light is related to the relative contribution of the radiative process. The intensity and spectral content of this photoluminescence give a direct measure of various important material properties. The excitation energy and intensity are chosen to probe different regions and excitation concentrations in the sample [84]. PL investigations can be used to characterize a variety of material parameters. Features of the emission spectrum can be used to identify surface, interface, uniformity and impurity levels and to gauge alloy disorder and interface roughness. The intensity of the PL signal provides information on the quality of surfaces and interfaces.

Luminescence is a process, which involves at least two steps: the excitation of the electronic system of the material and the subsequent emission of photons. Figure 2.13 given below illustrates the configuration co-ordinate diagram of luminescence process. These steps may or may not be separated by intermediate processes. Excitation may be achieved by bombardment with photons (photoluminescence), with electrons (cathodoluminescence), or with other particles. Luminescence can also be induced as the result of a chemical reaction (chemiluminescence) or by the application of an electric field (electroluminescence). When light of sufficient energy is incident on a material, photons are absorbed and electronic excitations are created. Eventually, these excitations relax and the electrons return to the ground state. If radiative relaxation occurs, the

emitted light is called PL. This light can be collected and analyzed to yield a wealth of information about the photo-excited material. The PL intensity gives a measure of the relative rates of radiative and non-radiative recombination.
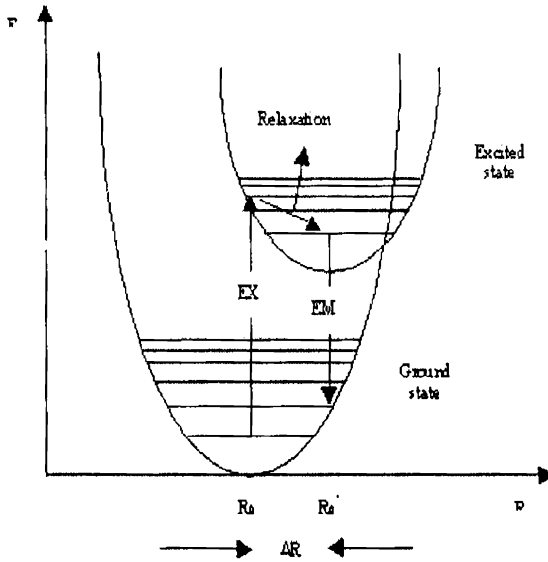
Figure 2.13: Configuration coordinate diagram illustrating luminescence process

Uses of photoluminescence studies

i) *Band gap determination*

The most common radiative transition in semiconductors is between states in the valence band and conduction band, with the energy difference being known as the band gap. Band gap determination is particularly useful when working with new compound semiconductors.

ii) *Impurity levels and defect detection*

Radiative transitions in semiconductors involve localized defect levels. The PL energy associated with these levels can be used to

identify specific defects and the intensity of PL emission can be used to determine the concentration.46

ii) Recombination mechanism

The return to the equilibrium also known as the "recombination" can involve both radiative and non-radiative processes. The intensity of PL emission and its dependence on the level of photo excitation and temperature are directly related to the dominant recombination processes.

Analysis of PL spectrum helps to understand the underlying physics of recombination mechanism.

iv) Material quality

In general, non-radiative processes are associated with localized defect levels, whose presence is detrimental to material quality and subsequent device performance. Material quality can be assessed by a qualitative analysis of radiative recombination.

2.7 Nonlinear optical properties

Non-linear optics is essentially concerned with the study of phenomenon that results from field-induced modifications in the optical properties of materials. Measurements using conventional light sources give a polarization P that is linearly dependent on electric field strength E.

$$P(t) = \varepsilon_0 \, \chi^{(1)} \, E(t) \text{ --- (2.11)}$$

where ε_0 is the permittivity of free space and $\chi^{(1)}$ is linear susceptibility. But, at very high intensities of light such as that provided by pulsed lasers, the dielectric polarization P(t) responds nonlinearly to the electric field E(t) of the light and is given by

$$P(t) = \varepsilon_0[\chi^{(1)} E(t) + \chi^{(2)} E^2(t) + \chi^{(3)} E^3(t) + \ldots\ldots\ldots] \text{------ (2.12)}$$

$$P_i = \varepsilon_0 \left[\sum_j \chi_{ij}^{(1)} E_j + \sum_{jk} \chi_{ijk}^{(2)} E_j E_k + \sum_{jkl} \chi_{ijkl}^{(3)} E_j E_k E_l + \cdots \right] \text{-------(2.12b)}$$

where terms are summed over repeated indices.

Here $\chi^{(2)}$ and $\chi^{(3)}$ are called second order and third order susceptibilities respectively. In the nonlinear regime, a number of interesting phenomena like second harmonic generation, third harmonic generation, optical limiting etc emerge that are absent in linear regime. Many of these nonlinear effects have important scientific and technological significance. The magnitude and response of third order nonlinear susceptibility is one of the important parameters of nonlinear materials and several techniques exist for measuring these parameters.

Optical nonlinearity in semiconductor nanocrystals is important, because it becomes considerably large compared to the bulk material. Studies on optical nonlinearity and related dynamics are desirable for the development of new materials for applications in ultrafast optical devices [85]. Nonlinear optical responses have also been studied for a long time in relation to the photonic device application and the laser operation. In particular, the third order nonlinear processes are of special importance because they belong to the nonlinearity, which is the lowest-order nonlinear effect in majority of the materials. When the energy of the incident light is tuned to the exciton level, the nonlinearity arises from the enhancement of exciton oscillator strength. Recently, relations between the $\chi^{(3)}$ nonlinearity and the interaction between the excitons are investigated theoretically and reported [86]. In the nano regime, quantum confinement effects produce exciton resonances that are

sharper than the corresponding ones in bulk semiconductors and these results in large optical nonlinearities.

2.7.1 Nonlinear absorption

Nonlinear absorption refers to the change in transmittance of a material as a function of intensity or fluence. At sufficiently high intensities, the probability of a material absorbing more than one photon before relaxing to the ground state can be greatly enhanced. In addition, population redistribution induced by intense laser fields leads to interesting counter plays of stimulated emission and absorption, complicated energy transitions in complex molecular systems and the generation of free carriers in solids. These phenomena are manifested optically in a reduced (saturable) or increased (reverse saturable) absorption [87].

2.7.1(a) Two photon absorption (TPA)

Two-photon absorption involves a transition from the ground state of a system to a higher-lying state by the simultaneous absorption of two photons from an incident radiation field or fields. TPA spectroscopy compliments linear absorption spectroscopy in studying the excited states of systems [87]. Figure 2.14 shows the schematic representation of TPA. The intermediate state is not real and hence the system must absorb two photons simultaneously. This makes the process sensitive to the instantaneous optical intensity.
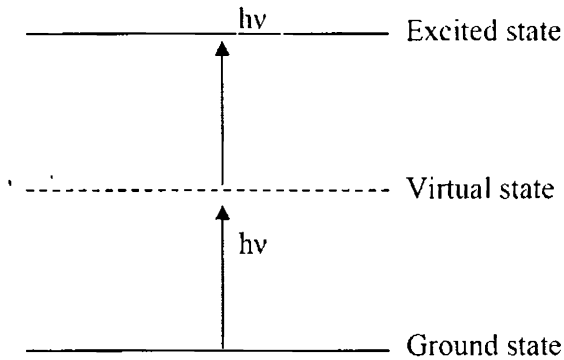
Fig.2.14: Schematic diagram of two-photon absorption

The nonlinear absorption in this case is proportional to the square of the instantaneous intensity and is given by

$$\frac{dI}{dz} = -\alpha I - \beta I^2$$

---(2.13)

where α is the linear absorption coefficient and β is the two photon absorption coefficient.

2.7.1(b) Multiphoton absorption

Multiphoton absorption refers to the simultaneous absorption of n photons from a single beam or multiple beams. The absorption of (n+1) photons from a single optical beam is given by

$$\frac{dI}{dz} = -\left(\alpha + \gamma^{(n+1)} I^n\right) I$$

------------------------------(2.14)

where $\gamma^{(n+1)}$ is the (n+1) photon absorption coefficient.

2.7.1(c) Excited state absorption (ESA)

In systems such as polyatomic molecules and semiconductors, there is a high density of states near the state involved in the excitation

[87]. The excited electron can rapidly make a transition to one of these states before it eventually make transitions back to the ground state. There are also a number of higher lying states that may be radiatively coupled to these intermediate states, and for which the energy differences are in near-resonance with the incident photon energy. Therefore, before the photon relaxes to the ground state, it may experience absorption that promotes it to a higher-lying state. This process is called excited state absorption.

2.7.1(d) Saturable absorption (SA)

When the absorption cross-section from excited state is smaller than that from the ground state, the transmission of the system will be increased when the system is pumped with high intensity laser beam. This process is called saturable absorption.

2.7.1(e) Reverse saturable absorption (RSA)

When the absorption cross-section from excited state is larger than that from the ground state, the transmission of the system will be less under intense laser fields. This process is called reverse saturable absorption.

2.7.1(f) Free carrier absorption (FCA)

In semiconductors, the absorption of a photon with energy greater than the band gap will promote an electron to the conduction band, where it is a free carrier and can contribute current flow when a field is applied. The excited electron will rapidly thermalize and relax to the bottom of the conduction band. From there it will recombine with an excited hole in the valence band after a characteristic recombination

time. However, at sufficiently high intensities, it can, with high probability, absorb another photon while it is still in the conduction band. This process is called free carrier absorption.

2.7.1(g) Two photon induced free carrier absorption

When two-photon absorption is particularly strong in a material, it can lead to significant population of a two photon allowed state. If a semiconductor is exposed to light of photon energies greater than the half of *Eg*, both bound electronic and free carrier nonlinearity occur simultaneously. Thus, two photon induced free carrier absorption is the dominant mechanism in semiconductors.

In general, induced absorption can occur due to a variety of processes. However, the dominant mechanism is decided by factors such as duration of the excitation pulse, lifetimes of excited singlet and triplet states and intersystem crossing time, crossing yield, etc. TPA is an irradiance dependent process whereas ESA is fluence dependent. This means that the same fluence for two different pulse widths will give the same nonlinear absorption if the mechanism is ESA. By measuring the nonlinear absorption for various pulse durations, it is possible to confirm whether ESA or TPA dominates in contributing to the induced absorption. As a rule, transmittance change ΔT at fixed pulse energy will be independent of pulse width if the mechanism is ESA but will depend on pulse width if it is TPA.

2.7.2 Nonlinear refraction (NLR)

Nonlinear index of refraction is the change in refractive index or the spatial distribution of the refractive index of a medium, due to the

presence of optical waves, and has generated significant and technological interest. It has been utilized for a variety of applications such as nonlinear spectroscopy, correcting optical distortions, optical switching, optical 'logic gates, optical data processing, optical communications, optical limiting, passive laser mode-locking, wave guide switches and modulators. The general dependence of the NLR on intensity is given by [87]

$$n(r,t) = n_0(r,t) + \Delta n[I(r,t)] \text{------------------------(2.15)}$$

This equation indicates that the change in the refractive index, Δn over its value at low intensities, n_0, has a functional dependence on intensity, $I(r,t)$. Several physical mechanisms that contribute to the NLR include electronic polarization; Raman induced Kerr effect, molecular orientation effects, electrostriction, population redistribution, thermal contributions, cascaded second order effects and photorefractive effect.

2.7.3 Applications of NLO

Nonlinear optical effects are applicable in many fields. Examples of nonlinear optical phenomena that are potentially useful are the ability to alter the frequency or colur of light, to amplify one source of light with another and switch it or alter its transmission characteristics through a medium, depending on its intensity. In the field of optical information storage, frequency-doubling process can effect the conversion of near infrared laser light from diode lasers into deep blue light. Since the size of a focused spot of light is inversely proportional to its wavelength, second harmonic generation (SHG) can increase the

capacity of stored information on optical disks immensely. Using related phenomena, one can build devices such as frequency mixers that can act as new light sources or as amplification schemes, light modulators for controlling the phase or amplitude of a light beam, optical switches, optical logic, optical information storage, optical limiters and numerous ways of processing the information content of data or images.

2.7.4 Optical limiting

Optical limiting refers to a decrease in the optical transmittance of a material with an increase in incident light intensity [88]. It generally occurs when the optical transmission of a system decreases with increasing input intensity. An ideal optical limiter is a device that exhibits linear transmittance below a threshold and clamps the output to a constant value above it [89] as shown in figure 2.15. The threshold of limiting is defined as the fluence at which the transmissions decreases to a half of the value at low input fluence [90]. The demand for protection and eyes and various types of optical sensors from laser beam pulses has resulted in search for optical limiting devices that has the property of being transparent at the low intensity of light but non-transparent towards high intensity of light.
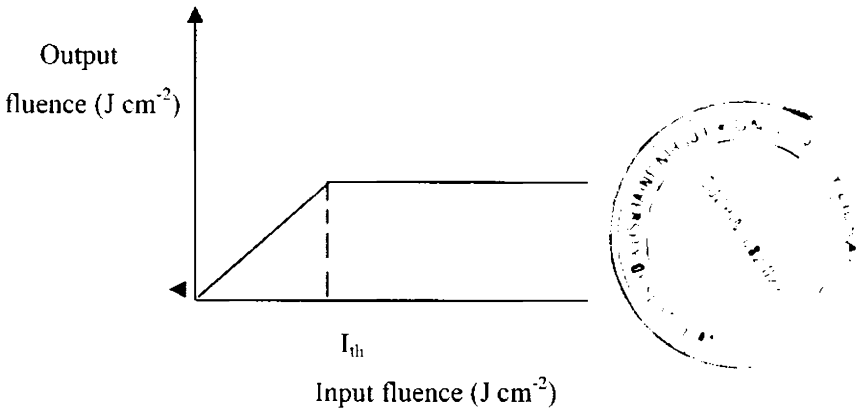
Figure 2.15: An ideal optical limiter characteristic curve

Optical limiters must have properties such as high linear transmission throughout the detector bandwidth and good resistance to laser induced damage stability over time. One can achieve this behavior or more of the non-linear optical mechanisms such as excited state absorptions (ESA), reverse saturable absorption (RSA), free carrier absorption (FCA), two photon absorption (TPA), thermal defocusing, thermal scattering and nonlinear refraction. The optical, limiting performance will be enhanced by coupling two or more of the nonlinear optical mechanisms [88].

2.8 Measurement techniques for NLO characterization

Some of the characterization methods for studying materials exhibiting NLO properties are z- scan, degenerate four wave mixing, three wave mixing, optical Kerr effect, ellipse rotation, interferometric methods, beam self bending, higher harmonic generation, two photon fluorescence, photo thermal and photo acoustic techniques and beam distortion measurements [87]. Z-scan technique has been employed in

investigating the NLO properties of ZnO nanocomposite samples of the present investigations.

2.8.1 Z-scan technique

Z-scan is a single beam technique developed by Sheik Bahae to measure the magnitude of nonlinear absorption as well as the sign and magnitude of nonlinear refraction [91, 92]. The technique is based on the principle of spatial beam distortion, but offers simplicity as well as high sensitivity comparable to interferometric methods. When a high irradiance laser beam propagates through any nonlinear material, photo induced refractive index variations may lead to self-focusing of the beam. The propagation of laser beam inside such a material and the ensuing self-refraction can be studied using the Z-scan technique. It enables one to determine the third order nonlinear properties of solids, ordinary liquids, and liquid crystals.
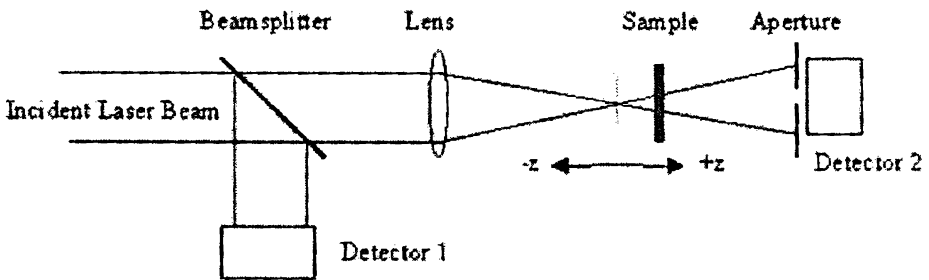
Figure 2.16: Schematic representation of the experimental setup for Z-scan technique

The experimental set up for single beam Z-scan technique is given in figure 2.16.In the single beam configuration, the transmittance of the sample is measured, as the sample is moved along the propagation direction

of a focused Gaussian beam. A laser beam propagating through a nonlinear medium will experience both amplitude and phase variations. If transmitted light is measured through an aperture placed in the far field with respect to focal region, the technique is called closed aperture Z-scan [91-92]. In this case, the transmitted light is sensitive to both nonlinear absorption and nonlinear refraction. In a closed aperture Z-scan experiment, phase distortion suffered by the beam while propagating through the nonlinear medium is converted into corresponding amplitude variations. On the other hand, if transmitted light is measured without an aperture, the mode of measurement is referred to as open aperture Z-scan [92]. In this case, the throughput is sensitive only to nonlinear absorption. Closed and open aperture Z-scan graphs are always normalized to linear transmittance i.e., transmittance at large values of $|z|$.

Closed and open aperture Z-scan methods yield the real part and imaginary part of nonlinear susceptibility $\chi^{(3)}$ respectively. Usually closed aperture Z-scan data is divided by open aperture data to cancel the effect of nonlinear absorption contained in the closed aperture measurements [92]. The new graph, called divided Z-scan, contains information on nonlinear refraction alone.

In a Z-scan measurement, it is assumed that the sample thickness is much less than Rayleigh's range z_0 (diffraction length of the beam), defined as $z_0 = k\omega_0^2 / 2$ where k is the wave vector and ω_0 is the beam waist radius given by $\omega_0 = f \lambda/D$ where f is the focal length of the lens used, λ is the wavelength of the source and D is the beam radius at the lens. Z-scan technique is highly sensitive to the profile of the beam and to the thickness of the sample. Any deviation from Gaussian profile of

the beam and from thin sample approximation will give rise to erroneous results. For ensuring that the beam profile does not vary appreciably inside the sample, the sample thickness should always be kept less than the Rayleigh's range. The sensitivity of the Z-scan method is used to monitor nonlinear refraction at low irradiance levels, where a third order nonlinearity attributed to n_2 caused by bound electrons can be observed. At higher irradiance levels the refraction caused by two photon absorption induced free charge carriers becomes significant. Thus the electronic Kerr effect will be dominant at low irradiance levels whereas TPA induced FCA will be dominant at high irradiance levels [93].

2.8.1(a)Open aperture Z-scan

Open aperture Z-scan technique is employed to measure nonlinear absorption in the sample. If nonlinear absorption such as two photon absorption is present, it is manifested in the measurements as a transmission minimum at the focal point41. On the other hand, if the sample is a saturable absorber, transmission increases with increase in incident intensity and results in a transmission maximum at the focal region [94]. Brief description of the theory described by Sheik Bahae et al. is given below [92].

Theory of open aperture Z-scan technique

In the case of an open aperture Z-scan, the transmitted light measured by the detector is sensitive only to intensity variations. Hence, phase variations of the beam are not taken into consideration. The intensity dependent nonlinear absorption $\alpha(I)$ can be written in terms of

linear absorption coefficient α and the nonlinear absorption coefficient β as

$$\alpha(I) = \alpha + \beta I \quad \text{---(2.16)}$$

The irradiance distribution at the exit surface of the sample can be written as

$$I_r(z,r,t) = \frac{I(z,r,t)e^{-\alpha l}}{1+q(z,r,t)} \quad \text{------------------------------(2.17)}$$

where $\quad q(z, r, t) = \beta I(z, r, t) L_{eff} \quad$ ------------------------------(2.18)

L_{eff} is the effective length and is given in terms of the length of the sample (l) by the relation

$$L_{eff} = \frac{(1-e^{-\alpha l})}{\alpha} \quad \text{------------------------------------- (2.19)}$$

The total transmitted power P (z, t) is obtained by integrating equation (2.11) over z and r and is given by

$$P(z,t) = P_i(t)e^{-\alpha l}\frac{\ln[1+q_0(z,t)]}{q_0(z,t)} \quad \text{--------------------(2.20)}$$

where $P_i(t)$ and $q_0(z, t)$ are given by

$$P_i(t) = \frac{\pi \omega_0^2 I_0(t)}{2} \quad \text{---------------------------------(2.21)}$$

$$q_0(z,t) = \frac{\beta I_0(t)L_{eff}\, z_0^2}{z^2 + z_0^2} \quad \text{------------------------------------(2.22)}$$

For a pulse of Gaussian temporal profile, equation (2.14) can be integrated to give the transmission as

$$T(z) = \frac{1}{q_0 \sqrt{\pi}} \int_{-\infty}^{\infty} \ln(1 + q_0 e^{-t^2}) dt$$

----------------------(2.23)

If $|q_0| < 1$, equation (1.17) can be simplified as

$$T(z, S = 1) = \sum_{m=0}^{\infty} \frac{[-q_0(z, 0)]^m}{(m + 1)^{\frac{3}{2}}}$$

----------------------------(2.24)

where m is an integer. Once an open aperture Z-scan is performed, the parameter q_0 can be obtained by fitting the experimental results to equation (2.17). Then the nonlinear absorption coefficient b can be unambiguously deduced using equation (2.12). The imaginary part of third order susceptibility $\chi^{(3)}$ determines the strength of the nonlinear absorption. The following relation relates the nonlinear absorption coefficient to Im χ (3) as

$$\operatorname{Im}(\chi^{(3)}) = \frac{\varepsilon_0 n_0^2 c^2 \beta}{\omega} \quad (m^2 V^{-2}) = \frac{n_0^2 c^2 \beta}{240\pi^2 \omega} \quad (esu)$$

----------(2.25)

where n_0 is the linear refractive index, ε_o e is the permittivity of free space and c the velocity of light in vacuum.

2.8.1(b) Closed aperture Z-scan

The basis of closed aperture Z-scan is the self-refraction and self phase modulation effects. The technique relies on the transmittance measurement of a nonlinear medium through a finite aperture in the far

field as a function of the sample position z with respect to the focal plane using a single Gaussian beam in tight focus geometry.

Consider, for instance, a material with a negative nonlinear refraction and thickness smaller than the diffraction length ($k\omega_0^2$ /2) of the focused beam being positioned at various points along the z-axis. This assumption implies that the sample acts as a thin lens of variable focal length due to the change in refractive index at each position ($n = n_0 + n_2 I$).

Suppose that the sample is kept at a distance far away from the focus (-z).

The irradiance is low and there is negligible nonlinear refraction. Hence the transmittance characteristics are linear. As the sample is moved close to the focus, the beam irradiance increases, which leads to self-lensing in the sample. A negative self-lensing prior to focus will tend to collimate the beam, causing a beam narrowing at the aperture, which results in an increase in the measured transmittance. As the scan in z direction continues and passes the focal plane, the sample, which acts as a negative lens, increases the defocusing effect thus increasing the beam divergence, leading to beam broadening at the aperture. Hence, the transmittance decreases. Thus, there is a null as the sample crosses the focal plane (z_0). The Z-scan is completed as the sample is moved away from focus (+z) such that the transmittance becomes linear since the irradiance is again low. A prefocal transmittance maxima (peak) followed by a post focal transmittance minima (valley) is the Z-scan signature of negative refraction nonlinearity.
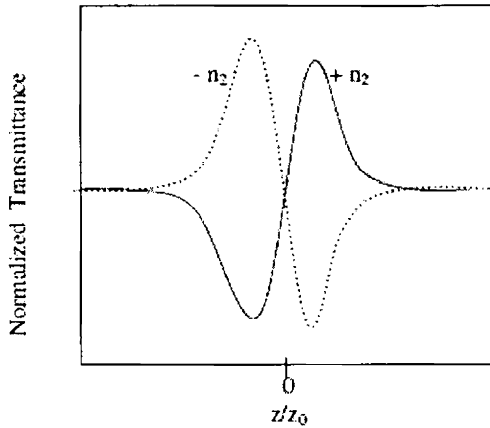
Figure 2. 17: Typical closed aperture z-scan curves of samples having positive (solid line) and negative (dashed line) nonlinearity.

The curves for closed Z-scan in the case of positive nonlinearity and negative nonlinearity show opposite effects as depicted in figure 2.17. This is the case of purely refractive nonlinearity where nonlinear absorption is absent. In the presence of multiphoton absorption, there is a suppression of the peak and enhancement of the valley, whereas the opposite effect occurs if there is a saturation of absorption [92].

Theory of closed aperture Z-scan technique

In a cubic nonlinear medium the index of refraction (n) is expressed in terms of nonlinear indices n_2 (m^2/W) through

$$n = n_0 + n_2 \, |E|^2 = n_0 + n_2 \, I \text{ ------------------------------(2.26)}$$

where n_0 is the linear index of refraction, E is the peak electric field, n_2 the intensity dependent refractive index and I denotes the irradiance of the laser beam within the sample. Assume a TEM_{00} beam of waist radius w_0 travelling in the +z direction. E can be written as [92]

$$E(z,r,t) = E_0(t)\frac{w_0}{w(z)}\exp\left[-\frac{r^2}{w^2(z)} - \frac{ikr^2}{2R(z)}e^{i\varphi(z,t)}\right]$$

-------(2.27)

where $w^2(z) = w_0^2(1 + z^2/z_0^2)$ is the beam radius, $R(z) = z(1 + z^2/z_0^2)$ is the radius of curvature of the wave front at z, $z_0 = k\omega_0^2/2$ is the diffraction length of the beam and $k = 2\pi/\lambda$ is the wave vector. $E_0(t)$ denotes the radiation electric field at the focus and contains the temporal envelope of the laser pulse. The term $e^{i\varphi(z,t)}$ contains all the radially uniform phase variations. For calculating the radial phase variations $\Delta\varphi(r)$, the slowly varying envelope approximation (SVEA) is used and all other phase changes that are uniform in r are ignored. For L<< $z_0/\Delta\varphi(0)$, where L is the sample length, the amplitude $\sqrt{I}$ and the phase φ of the electric field as a function of z' are now governed in the SVEA by a pair of simple equations

$$\frac{d\Delta\phi}{dz} = \Delta n(I)k$$

--(2.28)

and

$$\frac{dI}{dz} = -\alpha(I)I$$

--(2.29)

where z' is the propagation depth in the sample and α(I) in general includes linear and nonlinear absorption terms. In the case of cubic nonlinearity and negligible nonlinear absorption, equation (2.22) and equation (2.23) can be solved to get the phase shift Δφ at the exit of the sample and is given by

with

$$\Delta\phi(z,r,t)=\Delta\phi(z,t)\exp\left[-\frac{2r^2}{w^2(z)}\right]$$
-----------------(2.30)

$$\Delta\phi(z,t)=\frac{\Delta\phi_0(t)}{\left[1+\frac{z^2}{z_0^2}\right]}$$
-----------------(2.31)

where $\Delta\phi_0(t)$ is the on axis phase shift at the focus which is defined as

$$\Delta\phi_0(t)=k\Delta n_0(t)L_{eff}=\frac{2\pi}{\lambda}n_2I_0(t)L_{eff}$$
-----------------(2.32)

where $I_0(t)$ is the on axis irradiance at focus (i.e. at z=0). The complex electric field exiting the sample E_e now contains the nonlinear phase distribution

$$E_e(z,r,t)=E(z,r,t)e^{-\frac{\alpha l}{2}}e^{i\Delta\phi(z,r,t)}$$
-----------------(2.33)

By virtue of Huygen's principle and making use of Gaussian decomposition method [GD] one can show that

$$e^{i\Delta\phi(z,r,t)}=\sum_{m=0}^{\infty}\frac{[i\Delta\phi_0(z,r,t)]^m}{m!}e^{-2mr^2/w^2(z)}$$
-----------------(2.34)

Each Gaussian beam can be simply propagated to the aperture plane and it will be resumed to reconstruct the beam. After including the initial beam curvature for the focused beam, the resultant electric field pattern at the aperture is

$$E_a(r,t) = E(z, r = 0, t) e^{-\alpha l/2}$$

$$\times \sum_{m=0}^{\infty} \frac{\left[i\Delta\phi_0(z,t) \right]^m}{m!} \frac{w_{m0}}{w_m} \exp\left[-\frac{r^2}{w_m^2} - \frac{ikr^2}{2R_m} + i\theta_m \right] \quad \ldots/(2.35)$$

Defining d as the propagation distance in free space from the sample to the aperture plane and

g=1+ d/R (z), the remaining parameters in equation (2.29) are expressed as

$$w^2_{mo} = \frac{w^2(z)}{(2m+1)} \qquad d_m = \frac{kw_{mo}^2}{2} \qquad \theta_m = \tan^{-1}\left[\frac{d/d_m}{g} \right]$$

$$w_m^2 = w_{mo}^2 \left[g^2 + \frac{d^2}{d_{mo}^2} \right] \qquad \text{and} \quad R_m = d\left[1 - \frac{g}{g^2 + d^2/d_m^2} \right]^{-1}$$

The on-axis electric field at the aperture plane can be obtained by putting r=0 in equation (1.29). In the limit of small nonlinear phase change ($[\Delta\varphi_0 \ll 1]$) and small aperture, only two terms in the sum in equation (2.29) need to be retained. The normalized Z-scan transmittance can be written as

$$T(z, \Delta\phi_0) = \frac{\left| E_a(z, r = 0, \Delta\phi_0) \right|^2}{\left| E_a(z, r = 0, \Delta\phi_0 = 0) \right|^2} \quad \text{-----------------------(2.36)}$$

$$= \frac{\left| (g + id/d_0)^{-1} + i\Delta\phi_0 (g + id/d_1)^{-1} \right|^2}{\left| (g + id/d_0)^{-1} \right|^2}$$

The far field condition d>>z_0 can give a geometry-independent normalized transmittance as

$$T\left(z, \Delta\phi_0\right) = 1 - \frac{4\Delta\phi_0 x}{\left(x^2 + 9\right)\left(x^2 + 1\right)}$$

-------------------------(2.37)

wherw x = z/z_0.

For a cubic nonlinearity, the peak and valley of the Z-scan transmittance can be calculated by solving the equation

$$\frac{dT\left(z, \Delta\phi_0\right)}{dz} = 0$$

--(2.38)

Solution to this equation (2.32) yields the peak-valley separation as

$$\Delta Z_{p-v} = 1.7\,z_0$$ ---(2.39)

Then the peak-valley transmittance change is

$$\Delta T_{p-v} = 0.406\,\Delta\phi_0$$ --(2.40)

Numerical calculations show that this relation is accurate to 0.5% for $|\Delta\phi_0| \leq \pi$. For large aperture, this equation is modified within a ±2% accuracy and is given by

$$\Delta T_{p,v} \approx 0.406\left(1 - S\right)^{0.25}\left|\Delta\phi_0\right|$$ -------------------------------(2.41)

for $|\Delta\phi_0 \leq \pi\,|$

where S is the linear transmittance of the far field aperture. From the closed aperture z-scan fit, $\Delta\phi_0$ can be obtained. Then the nonlinear refractive index n_2 can be determined using equation (2.26) and is given by

$$n_2 \quad (m^2/W) = \frac{\lambda}{2\pi I_0 L_{eff}} \Delta\phi_0$$

-------------------------------(2.42)

$$n_2 \quad (esu) = \frac{cn_0}{40\pi} \frac{\lambda}{2\pi I_0 L_{eff}} \Delta\phi_0$$

The n_2 is related to $Re(\chi^{(3)})$ by the relation

$$Re(\chi^{(3)}) = \frac{n_0 n_2 \, (esu)}{3\pi}$$

---(2.43)

From the real and imaginary parts of $\chi^{(3)}$, the modulus of third order nonlinear susceptibility can be found out.

$$\left|\chi^{(3)}\right| = \sqrt{\left[Re\left(\chi^{(3)}\right)\right]^2 + \left[Im\left(\chi^{(3)}\right)\right]^2}$$

---------------------(2.44)

The magnitude of $\chi^{(3)}$ is significantly affected by the molecular orientation and it determines the strength of nonlinearity of the material.

2.8.1(c) Merits and demerits of Z-scan technique

This technique has several advantages, some of which are

1. Simplicity of the technique as well as simplicity of interpretation

2. Simultaneous measurement of both sign and magnitude of nonlinearity

3. Possibility of isolating the refractive and absorptive parts of nonlinearity

4. High sensitivity, capable of resolving a phase distortion of $\lambda/300$

5. Close similarity between Z-scan and the optical limiting geometry

Some of the disadvantages include,

1. Stringent requirement of high quality Gaussian TEM_{00} beam for absolute measurements

2. Beam walk-off due to sample imperfections, tilt, or distortions

3. Not suitable for measurements of off diagonal elements of the susceptibility tensor, except when a second non-degenerate frequency beam is employed

4. The determination of the nonlinear coefficients depend on the temporal and spatial profiles, power or energy content and stability of the laser source

2.9   Thermo gravimetric analysis

Thermo gravimetric analysis or thermal gravimetric analysis (TGA) is a type of testing performed on samples that determines changes in weight in relation to change in temperature. Such analysis relies on a high degree of precision in three measurements: weight, temperature, and temperature change. A derivative weight loss curve can identify the point where weight loss is most apparent. Again, interpretation is limited without further modifications and deconvolution of the overlapping peaks may be required [95].

Materials analyzed by TGA include polymers, plastics, composites, laminates, adhesives, food, coatings, pharmaceuticals, organic materials, rubber, petroleum, chemicals, explosives and   samples.TGA is commonly employed in research and testing to determine characteristics of materials such as polymers, to determine degradation temperatures, absorbed moisture content of materials, the level of inorganic and organic

components in materials, decomposition points of explosives, and solvent residues. It is also often used to estimate the corrosion kinetics in high temperature oxidation

2.9.1 Theory

Thermo gravimetric analysis is used primarily for determining thermal stability of polymers. The most widely used TGA method is based on continuous measurement of weight on a sensitive balance (called a *thermo balance*) as sample temperature is increased in air or in an inert atmosphere. This is referred to as *non-isothermal TGA*. Data are recorded as a thermo gram of weight versus temperature. Weight loss may arise from evaporation of residual moisture or solvent, but at higher temperatures, it results from polymer decomposition. Besides providing information on thermal stability, TGA may be used to characterize polymers through loss of a known entity, such as HCl from poly (vinyl chloride). Thus weight loss can be correlated with percentage of vinyl chloride in a copolymer. TGA is also useful for determining volatilities of plasticizers and other additives. Thermal stability studies are the major applications of TGA, however [96].

A variation of the method is to record weight loss with time at a constant temperature. This method called *isothermal TGA* is less commonly used than non-isothermal TGA. Modern TGA instruments allow thermo grams to be recorded on microgram quantities of material. Some instruments are designed to record and process DSC and TGA data simultaneously, and may also be adapted for gas chromatographic and/or mass spectrometric analysis of effluent degradation products.

When used in combination with FTIR, TGA/FTIR is capable of detailed FTIR analysis of evolved gases produced from the TGA.

2.9.2 Applications

Applications of the TG/DTA instrument are compositional analysis, decomposition temperature studies, oil volatility measurements, flammability studies, heat of transition analysis, thermal stability analysis, oxidative stability analysis, transition temperature detection etc.

Figure 2.18: Photograph of TGA experimental set up

Advantages

- Sample is held isothermal until transition completed – thus excellent resolution of overlapping transitions

- Permits careful control of reaction environment

- Available on all TA Instruments TGA's

Disadvantages

- May require several scans to optimize run conditions

- Inappropriate parameter choices may produce artifacts

The TGA measurements in the present study are done using Perkin Elmer, Diamond TG/DTA instrument in the temperature range, (Ambient to 1200°C) at heating rate 10 K/min in nitrogen atmosphere.

2.10 Differential scanning calorimetry

Differential Scanning Calorimetry (DSC) measures the temperature and heat flow associated with transitions in materials as a function of time and temperature in controlled atmosphere. These measurements provide quantitative and qualitative information about physical and chemical changes that involve endothermic or exothermic processes, or changes in heat capacity. The technique was developed by E.S. Watson and M.J. O'Neill in 1960 [97,98], and introduced commercially at the 1963 Pittsburgh Conference on Analytical Chemistry and Applied Spectroscopy.

In DSC, both the sample and reference are maintained at nearly the same temperature throughout the experiment. Generally, the temperature program for a DSC analysis is designed such that the sample holder temperature increases linearly as a function of time. The reference sample should have a well-defined heat capacity over the range of temperatures to be scanned.
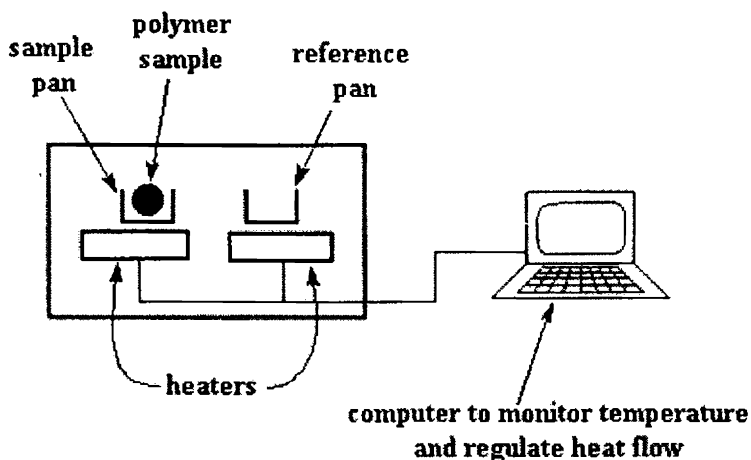
Figure 2.19: Schematic representation of the experimental setup for DSC

Differential scanning calorimetry can be used to measure a number of characteristic properties of a sample. Using this technique it is possible to observe fusion and crystallization events as well as glass transition T_g. DSC can also be used to study oxidation, as well as other chemical reactions [99-102].

Features of a DSC curve
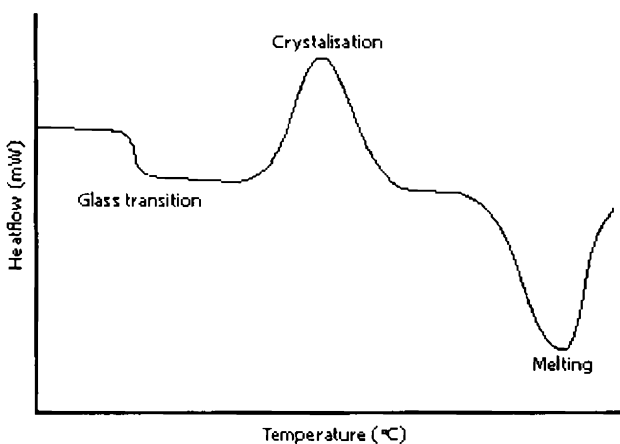
Figure 2.20: A schematic DSC curve demonstrating the appearance of several common phenomena

Glass transitions may occur as the temperature of an amorphous solid is increased. These transitions appear as a step in the baseline of the recorded DSC signal. This is due to the sample undergoing a change in heat capacity and no formal phase change occurs [99, 101]. As the temperature increases, an amorphous solid will become less viscous. At some point the molecules may obtain enough freedom of motion to spontaneously arrange themselves into a crystalline form. This is known as the crystallization temperature (T_c). This transition from amorphous solid to crystalline solid is an exothermic process, and results in a peak in the DSC signal. As the temperature increases, the sample eventually reaches its melting temperature (T_m). The melting process results in an endothermic peak in the DSC curve. The ability to determine transition temperatures and enthalpies makes DSC a valuable tool in producing phase diagrams for various chemical systems [99].

DSC provides a rapid method for determining polymer crystallinity based on the heat required to melt the polymer. Polymer crystallinity can be determined with DSC by quantifying the heat associated with melting (fusion) of the polymer. This heat is reported as Percent Crystallinity by normalizing the observed heat of fusion to that of a 100 % crystalline sample of the same polymer. As authentic samples of 100 % crystalline polymer are rare, literature values are often used for this value [103,104]

Polymer crystallinity can also be determined with DSC using the following method.

Let the heat of crystallization be H_C, and the total heat given off during melting be H_T,

$$H = (H_T - H_C) \text{ Joules, } \text{---}(2.45)$$

where H is the heat given off by that part of polymer, which is already in crystalline state. By dividing H by Hc_1 (specific heat of melting), where Hc_1 is the amount of heat given off when 1gram of polymer is melted, the total amount of polymer that is crystalline below T_C, the crystallization temperature, is obtained.

$$H/Hc_1 = \text{Joules / Joules per gram} = \text{Mc grams } \text{-----}(2.46)$$

The percentage of crystallinity in the polymer sample is

$$(M_C/M_t) \times 100 = \% \text{ crystallinity in the sample } \text{---------}(2.47)$$

where, Mt is the total mass of sample taken.

In the present study, Differential scanning calorimetry (DSC) has been carried out on a Mettler Toledo DSC 822e instrument. This measures the difference between the heat flows from the sample and reference sides of a sensor as a function of temperature or time

2.12 D.C electrical conductivity

The four-point, or Kelvin, probe method is the most common way to measure a semiconductor material's resistivity. Two of the probes are used to source current and the other two probes are used to measure voltage. Using four probes eliminates measurement errors due to the probe resistance, the spreading resistance under each probe, and the

contact resistance between each metal probe and the semiconductor material [105]. This technique involves bringing four equally spaced probes into contact with the material of unknown resistance. The probe array is usually placed at the center of the material, as shown in figure 2.21.
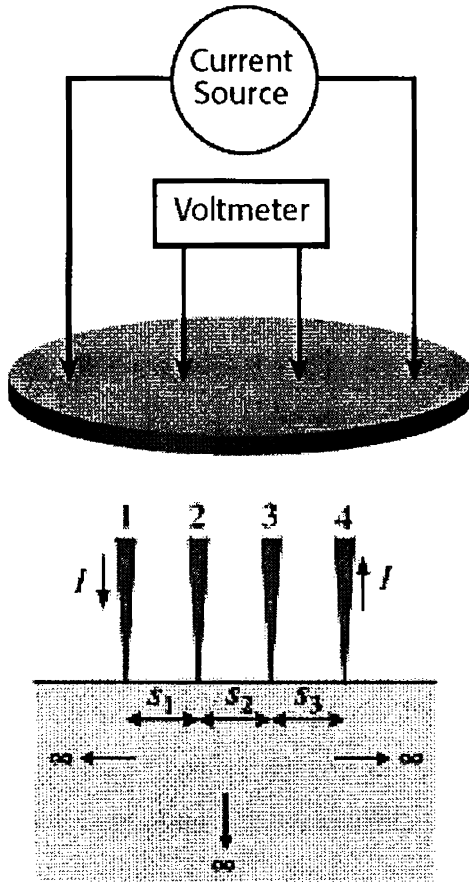
Figure 2.21: Four-Point Collinear Probe Resistivity Method
(Keithley Instruments, Inc.)

Theory

Let I be the current entering through probe1 and leaving through probe4.The potential V at a distance r from an electrode in a material of resistivity ρ is given by,

$$V = \frac{\rho I}{2\pi r} \quad \text{--(2.48)}$$

For probes resting in a semi-infinite medium, with current entering probe 1 and leaving probe 4, the voltage V_0, measured with respect to zero reference potential becomes,

$$V_0 = \frac{\rho I}{2\pi} \left(\frac{1}{r_1} - \frac{1}{r_4} \right) \quad \text{-----------------------------} \ (2.49)$$

where r_1 and r_4 are the distances from the probes 1 and 4 respectively. The minus sign accounts for current leaving through probe4.For probe spacing s_1, s_2 and s_3, the voltage at probe 2 is,

$$V_2 = \frac{\rho I}{2\pi} \left(\frac{1}{s_1} - \frac{1}{s_2 + s_3} \right) \quad \text{------------------------------------}(2.50)$$

and at probe 3 is

$$V_3 = \frac{\rho I}{2\pi} \left(\frac{1}{s_1 + s_2} - \frac{1}{s_3} \right) \quad \text{-----------------------------}(2.51)$$

The total measured voltage $V = V_2 - V_3$ becomes

$$V = \frac{\rho I}{2\pi} \left[\left(\frac{1}{s1} - \frac{1}{s_2 + s_3} \right) - \left(\frac{1}{s_1 + s_2} - \frac{1}{s_3} \right) \right] \quad \text{------------}(2.52)$$

The resistivity ρ is given by,

$$\rho = \frac{2\pi V}{I} \left[\left(\frac{1}{s1} - \frac{1}{s_2 + s_3} \right) - \left(\frac{1}{s_1 + s_2} - \frac{1}{s_3} \right) \right]^{-1}, \quad \text{--------}(2.53)$$

usually expressed in ohm.cm, with V measured in volts, I in amperes, and s in cm. The current is usually such that the resulting voltage is

approximately 10mV.For most four-point probes, the probe spacings are equal. With s= s_1=s_2= s_3, the equation becomes,

$$\rho = \frac{2\pi s V}{I}$$ --- (2.54)

Smaller probe spacings allows measurements closer to wafer edges.

Semiconductor wafers are not semi-infinite in extent in either the lateral or vertical dimension. So, the equation for resistivity must be corrected for finite geometries.

For an arbitrarily shaped sample, the resistivity is given by,

$$\rho = 2\pi s F \left(\frac{V}{I}\right)$$ -- (2.55)

Conductivity, $\sigma = \frac{1}{\rho}$

$$= \frac{I}{2\pi s F V}$$ ---(2.56)

where F is a correction factor that depends on the sample geometry. F corrects for probe location near sample edges, for sample thickness, sample diameter, probe placement and sample temperature.

For collinear or in-line probes with equal probe spacing s, the correction factor F is a product of three separate correction factors F_1, F_2 and F_3.

I.e.,   F= F1×F2 ×F_3 ---(2.57)

F_1 corrects for sample thickness F_2 corrects for lateral sample dimensions, and F_3 corrects for placement of probes relative to sample edges.

Sample thickness must be corrected for most measurements since semi-conducting wafers are not infinitely thick. Their thickness is usually approximately the probe spacing, or less, introducing the correction factor [106],

$$F_{11} = \frac{t/s}{2\ln\{[\sinh(t/s)]/[\sinh(t/2s)]\}} \quad \text{------------------(2.58)}$$

This is for a non-conducting bottom surface, where t is the wafer or layer thickness.

For a conducting bottom surface, the correction factor becomes

$$F_{12} = \frac{t/s}{2\ln\{[\cosh(t/s)]/[\cosh(t/2s)]\}} \quad \text{------------------(2.59)}$$

Conducting bottom surfaces are difficult to achieve. For most four-point probe measurements are made with insulating bottom boundaries. For thin samples,

$$F_{11} = \frac{t/s}{2\ln(2)}. \quad \text{------------------------------------(2.60)}$$

Conventional four probe measurements are suitable for moderate or low resistivity materials, while minority carrier injection and sample loading by the voltmeter limit the accuracy of measurement for the case of high resistivity samples.

References

[1]   A K Bandyopadhyay "nanomateials" New Age International (P) Ltd
       (2007)

[2]   K.E. Gonsalves, S.P.Rangarajan, J. Wang ed Hari Singh Nalwa,
       "Nanostructure Materials and Nanotechnology", Academic Press (2002).

[3]   Li,Yuntao,Sue,Hung-jue, Nishimura, Riichi, Miyatake, Nubuo," Process
       for preparing nanosized metal oxide particles-patent 7482382 (2009)

[4]   Valmikanathan P. Onbattuvelli, "Synthesis and Characterization of
       Palladium/Polycarbonate   Nanocomposites",   thesis,   Oregon   State
       University (2007).

[5]   Shi, G.Q.; Jin, S.; Xue, G.; Li, C. A conducting polymer film stronger
       than aluminum. Science, 1995, 267, 994-996.].

[6]   Yang, Z.; Hu, B.; Karasz, F.E. Polymer Electroluminescence Using Ac
       or Reverse Dc Biasing. Macromolecules, 1995, 28, 6151-6154.

[7]   Jung, S.H.; Kim, H.K.; Kim, S.H.; Kim, Y.H.; Jeoung, S.C.; Kim, D.
       Palladium-catalyzed direct synthesis, photophysical properties, and
       tunable   electroluminescence   of   novel   silicon-based   alternating
       copolymers. Macromolecules, 2000, 33, 9277-9288.

[8]   Gilch, H.G.; Wheelwright, W.L. Polymerization of ?-halogenated p-
       xylenes with base. J. Polym. Sci. A 1966, 4, 1337-1349.

[9]   McCullough, R.D. The chemistry of conducting polythiophenes. Adv.
       Mater. 1998, 10, 93-116.]

[10]   The classification of film preparation method, and for film preparation of
       PAni, also see Ref 5. [5. Nicolas-Debarnot, D.; Poncin-Epaillard, F.
       Polyaniline as a new sensitive layer for gas sensors. Anal. Chim. Acta,
       2003, 475, 1-15.]

[11]   Lu, G.W.; Qu, L.T.; Shi, G.Q. Electrochemical fabrication of neuron-
       type networks based on crystalline oligopyrene nanosheets. Electrochim.
       Acta, 2005, 51, 340-346.

[12] Reemts, J.; Parisi, J.; Schlettwein, D. Electrochemical growth of gas-sensitive polyaniline thin films across an insulating gap. Thin Solid Films, 2004, 466, 320-325.

[13] McGovern, S.T.; Spinks, G.M.; Wallace, G.G. Micro-humidity sensors based on a processable polyaniline blend. Sens. Actuators B, 2005, 107, 657-665.

[14] Cho, J.H.; Yu, J.B.; Kim, J.S.; Sohn, S.O.; Lee, D.D.; Huh, J.S. Sensing behaviors of polypyrrole sensor under humidity condition. Sens. Actuators B 2005, 108, 389-392.

[15] Brady, S.; Lau, K.T.; Megill, W.; Wallace, G.G.; Diamond, D. The development and characterisation of conducting polymeric-based sensing devices. Synth. Met. 2005, 154, 25-28.

[16] Silverstein, M.S.; Tai, H.W.; Sergienko, A.; Lumelsky, Y.L.; Pavlovsky, S. PolyHIPE: IPNs, hybrids, nanoscale porosity, silica monoliths and ICP-based sensors. Polymer, 2005, 46, 6682- 6694.

[17] Prasad, G.K.; Radhakrishnan, T.P.; Kumar, D.S.; Krishna, M.G. Ammonia sensing characteristics of thin film based on polyelectrolyte templated polyaniline. Sens. Actuators B, 2005, 106, 626-631.

[18] Tongpool, R.; Yoriya, S. Kinetics of nitrogen dioxide exposure in lead phthalocyanine sensors. Thin Solid Films, 2005, 477, 148-152.

[19] Ram, M.K.; Yavuz, O.; Lahsangah, V.; Aldissi, M. CO gas sensing from ultrathin nano-composite conducting polymer film. Sens. Actuators B 2005, 106, 750-757.

[20] Nohria, R.; Khillan, R.K.; Su, Y.; Dikshit, R.; Lvov, Y.; Varahramyan, K. Humidity sensor based on ultrathin polyaniline film deposited using layer-by-layer nano-assembly. Sens. Actuators B 2006, 114, 218-222.

[21] Agbor, N.E.; Petty, M.C.; Monkman, A.P. Polyaniline Thin-Films for Gas-Sensing. Sens. Actuators B, 1995, 28, 173-179.

[22] Stussi, E.; Cella, S.; Serra, G.; Venier, G.S. Fabrication of conducting polymer patterns for gas sensing by a dry technique. Mater. Sci. Eng. C-Biomimetic Mater. Sens. Syst. 1996, 4, 27-33.

[23] Ruangchuay, L.; Sirivat, A.; Schwank, J. Selective conductivity response of polypyrrole-based sensor on flammable chemicals. React. Funct. Polym. 2004, 61, 11-22.

[24] Sandberg, H.G.O.; Backlund, T.G.; Osterbacka, R.; Jussila, S.; Makela, T.; Stubb, H. Applications of an all-polymer solution-processed high-performance, transistor. Synth. Met. 2005, 155, 662-665.

[25] Roncali, J., et al. 1987. Effects of steric factors on the electrosynthesis and properties of conducting poly(3-alkylthiophenes). J Phys Chem 91:6706.

[26] Angelopoulos, M., et al. 1988. Polyaniline: Solutions, films and oxidation state. Mol Cryst Liq Cryst 160:151.

[27] Lee, J.Y., D.Y. Kim, and C.Y. Kim. 1995. Synthesis of soluble polypyrrole of the doped state in organic solvents. Synth Met 74:103.

[28] Stejskal, J., M. Omastova´ , and S. Fedorova. 2003. Polyaniline and polypyrrole prepared in the presence of surfactants: A comparative conductivity study. Polymer 44:1353.

[29] Omastova´ , M., M. Trchova´ , and J. Kova´rˇova´ . 2005. Synthesis and structural study of polypyrroles prepared in the presence of surfactants. Synth Met 138:447.

[30] Kudoh, Y. 1996. Properties of polypyrrole prepared by chemical polymerization using aqueous solution containing Fe2(SO4)3 and anionic surfactant. Synth Met 79:17.

[31] Kudoh, Y., K. Akami, and Y. Matsuya. 1998. Properties of chemically prepared polypyrrole with an aqueous solution containing Fe2(SO4)3, a sulfonic surfactant and a phenol derivative. Synth Met 95:191.

[32] Omastova´ , M., J. Pionteck, and M. Trchova´ . 2003. Properties and morphology of polypyrrole containing a surfactant. Synth Met 135:447.

[33] Shen, Y., and M. Wan. 1998. In situ doping polymerization of pyrrole with sulfonic acid as a dopant. Synth Met 96:127.

[34] Lascelles, S.F., and S.P. Armes. 1997. Synthesis and characterization of micrometre-sized, polypyrrole- coated polystyrene latexes. J Mater Chem 7:1339.

[35] Lascelles, S.F., et al. 1997. Surface characterization of micrometre-sized, polypyrrole-coated polystyrene latexes: Verification of a 'core-shell' morphology. J Mater Chem 7:1349.

[36] Sonmez, G., P. Schottland, and K.K. Zong. 2001. Highly transmissive and conductive poly[(3,4- alkylenedioxy) pyrrole-2,5-diyl] (PXDOP) films prepared by air or transition metal catalyzed chemical oxidation. J Mater Chem 11:289.

[37] Thomas, C.A., K. Zong, and P. Schottland. 2000. Poly (3,4-alkylenedioxypyrrole) s as highly stable aqueous-compatible conducting polymers with biomedical implications. Adv Mater 12:222.

[38] Wang, P.C., Z. Huang, and A. MacDiarmid. 1999. Critical dependency of the conductivity of polypyrrole and polyaniline films on the hydrophobicity-hydrophilicity of the substrate surface. Synth Met 101:852.

[39] Wang, P.C., and A.G. MacDiarmid. 2001. Dependency of properties of in situ deposited polypyrrole films on dopant anion and substrate surface. Synth Met 119:367.

[40] Lu, Y., et al. 1998. Thin polypyrrole films prepared by chemical oxidative polymerization. J Appl Polym Sci 70:2169.

[41] Fu, Y., et al. 1997. Synthesis of conductive polypyrrole=polyurethane foams via a supercritical fluid process. Macromolecules 30:7611.

[42] John, R.K. and Kumar, D.S. 2002. Structural, electrical, and optical studies of plasma polymerized and iodine-doped polypyrrole. J Appl Polym Sci 83:1856.

[43] Wang, J.G., K.G. Neoh, and E.T. Kang. 2004. Comparative study of chemically synthesized and plasma polymerized pyrrole and thiophene thin films. Thin Solid Films 446:205.

[44] Hosono, K., I. Matsubara, and N. Murayama. 2003. Structure and properties of plasma polymerized and 4-ethylbenzenesulfonic acid-doped polypyrrole films. Thin Solid Films 441:72.

[45] Morales, J., M.G. Olayo, and G.J. Cruz. 2002. Plasma polymerization of random polyaniline– polypyrrole–iodine copolymers. J Appl Polym Sci 85:52.

[46] Nastase, F., D. Mihaiescu, and C. Nastase. 2005. Plasma polymerized ferrocene-pyrrole copolymer films. Composites Part A Appl Sci Manuf 36:503.

[47] Cha, S.K. 1997. Electropolymerization rate of polythiophene= polypyrrole composite polymer with some dopant ions. J Polym Sci Part B Polym Phys 35:165.

[48] Simmons, M.R., P.A. Chaloner, and S.P. Armes. 1998. Synthesis and characterization of colloidal polypyrrole particles using reactive polymeric stabilizers. Langmuir 14:611.

[49] McCarthy, G.P., et al. 1997. Synthesis and characterization of carboxylic acid-functionalized polypyrrole-silica microparticles using a 3-substituted pyrrole comonomer. Langmuir 13: 3686.

[50] Li, X.G., L.X. Wang, and M.R. Huang. 2001. Synthesis and characterization of pyrrole and m-toluidine copolymers. Synth Met 123:443.

[51] Li, X.G., L.X., Wang, and M.R. Huang. 2001. Synthesis and characterization of pyrrole and anisidine copolymers. Polym Plast Technol 42:6095.

[52] Fusalba, F., and D. Belanger. 1999. Electropolymerization of polypyrrole and polyaniline– polypyrrole from organic acidic medium. J Phys Chem B 103:9044.

[53] Sari, B., and M. Talu. 1998. Electrochemical copolymerization of pyrrole and aniline. Synth Met 94:221.

[54] Li, X.G., M.R. Huang, and M.F. Zhu. 2004. Synthesis and nitrosation of processible copolymer from pyrrole and ethylaniline. Polym Plast Technol 45:385.

[55] Kalaycioglu, E., et al. 1998. Synthesis of conducting H-type polysiloxane–polypyrrole blocks copolymers. Synth Met 97:7.}

[56] M Amrithesh,S Aravind, S Jayalekshmi ,R S Jayasree , J.Alloys Compd 458(2008)532

[57] Terje A Skotheim,L Ronald, Elsenbaumer, John R Reynolds, Handbook of Conducting Polymers, Marcel Dekker,INC,New York,1998

[58] Y Long,Z Chen,N Wang,J Li,M Wan,PhysicaB344(2004)82

[59] P Juvin,M Hasik,J Fraysse,J Planes,A Pron,l K Bajer, J. Appl. Polym. Sci 74 (1999) 471

[60] D L Wise,G E Wnek,D J Trantalo,T M Cooper,J D Gresser,Electrical and optical polymer systems Fundamentals, Methods and Applications,Marcel Dekker INC, New York,1998(chapter10)

[61] B.D.Cullity and S.R. Stock," Elements of X-Ray Diffraction", Third edition, New Jersey, Prentice Hall (2001)

[62] C. Kittel," Introduction to solid State Physics", Seventh edition,Wiley Eastern Ltd, New Delhi (1996)

[63] M.J. Buerger, "X-Ray Crystallography", John Wiley and sons, NewYork (1962).

[64] Dieter K. Schroder. Semiconductor material and device characterization. John Wiley 3rd Ed., 2005.

[65] J B Pendry, Low Energy Electron Diffraction, Academic press, New York, 1974

[66] K Heinz, Progr.Surf.Sci.27 (1988)239

[67] B F Lewis J Grunthaner, A Madhukar, T C Lee, R Fernandez, J.Vac.Sci.Technol.B3 (Sep/Oct1985)1317

[68] Banwell, C.N.; McCash, E.M. (1994). Fundamentals of Molecular Spectroscopy, (4th ed.). McGraw-Hill. ISBN 0-07-707976-0.

[69] Robert White (1990). Chromatography/Fourier transform infrared spectroscopy and its applications, Marcel Dekker. ISBN 0824781910.

[70] Gardiner, D.J. (1989). Practical Raman spectroscopy. Springer-Verlag. ISBN 978-0387502540).

[71] R Young Ward Scire, Rev.Sci.Instrum.43 (1972)999

[72] M V Heimendahl, Electron Microscopy of Materials, Academic Press, New York, 1980

[73] D B Williams B Carter, Transmission Electron Microscopy, Plenum, NY, 1996

[74] D C Joy, A D Romig, Jr., J I Goldstein (Eds), Principles of Analytical Electron Microscopy, Plenum Press, New York, 1986

[75] W R Runyan, T J Shaffner, Semiconductor Measurements and Instrumentation, McGraw Hill, New York, 1998

[76] V E Cosslet,Advances in Optical and Electron Microscopy(R Barer and V E Cosslet (Eds)), Academic Press,London,1988,p215-267

[77] Goldstein, G. I.; Newbury, D. E.; Echlin, P.; Joy, D. C.; Fiori, C.; Lifshin, E. (1981). Scanning electron microscopy and x-ray microanalysis, New York: Plenum Press. ISBN 030640768X.

[78] Giessibl, Franz J. (2003). "Advances in atomic force microscopy". Reviews of Modern Physics 75: 949. doi:10.1103/RevModPhys.75.949..

[79] Geisse, Nicholas A. (July-August 2009). "AFM and Combined Optical Techniques". Materials Today 12 (7-8): 40–45. doi:10.1016/S1369-7021(09)70201-9. Retrieved 4 November 2011.

[80] Arantxa Vilalta-Clemente and Kathrin Gloystein, Principles of Atomic Force Microscopy, Physics of Advanced Materials Winter School 2008 (1-10)

[81] D.R.Viji, "Luminescence of solids", Plenum Press, NewYork (1998)

[82] A.L. Fahrenbruch and R.H.Bube," Fundamentals of solar cells", Academic Press, NewYork (1983)

[83] Kubelka, P.; Munk, F. Ein Beitrag zur Optik der Farbanstriche.Z. Tech. Phys. 1931, 12, 593–620.

[84] T.H.Gfroerer," Photoluminescence in Analysis of Surfaces andInterfaces", JohnWiley & Sons Ltd, Chichester (2000)

[85] Hari Singh Nalwa and Seizo Miyata; "Nonlinear optics of organic molecules and polymers", CRC press (1997)

[86] T Yao and J C Woo; "Physics and applications of semiconductor quantum structures" IOP publishing Bristol and Philadelphia (2001)

[87] Richard L Sutherland; "Handbook of nonlinear optics", Second edn, CRC press (2003)

[88] Kazen Jamshidi, Ghaleshy and Nastaran Mansour, J. Phys. D; Appl. Phys., 40 (2007) 366

[89] D. T Nguyen, N. H. Kwong, R. Norwood and N. Peyghambarian, "Optical Limiting in Bragg-Spaced Semiconductor Quantum Wells", Conference on Lasers and Electro-Optics/Quantum Electronics and Laser Science Conference and Photonic Applications Systems Technologies, OSA Technical Digest (Optical Society of America, 2008) JWA18.

[90] Sandeep Banerjee, G. Ravindra Kumar, Pradeep Mathur and P Sekar, Chem. Commun., 6 (1997) 299.

[91] M S Bahae, A A Said and E W van Stryland; "High-sensitivity, single-beam n2 measurements", Opt Lett, 14, 955 (1989)

[92] M S Bahae, A A Said, T H Wei, D J Hagan and E W Van Stryland; "Sensitive measurement of optical nonlinearities using a single beam", IEEE J. Quantum Electron. 14, 760 (1990)

[93] Said A A, Bahae M S, Hagan D J, Wei T H, Wang J, Young J and Van Stryland E W; "Determination of bound-electronic and free-carrier nonlinearities in ZnSe, GaAs, CdTe, and ZnTe" JOSA B; 9, 405 (1992)

[94] Aniruddha Paul, Prasun Kumar Mandal and Anunay Samanta; "How transparent are the imidazolium ionic liquids? A case study with 1-methyl-3-butylimidazolium hexafluorophosphate, [bmim][PF6] ", Chem. Phys. Lett. 402, 375 (2005)

[95] M.E. Brown, Introduction to Thermal Analysis, Kluwer Academic Publisher ,London, 2001.

[96] G.W.Ewing , Analytical Instrumentation Handbook, Marcel Dekker Inc, New York, 1990.

[97] U.S. Patent 3,263,484

[98] Wunderlich, B. (1990). Thermal Analysis. New York: Academic Press. pp. 137–140. ISBN 0127656057.

[99] Dean, John A. (1995). The Analytical Chemistry Handbook. New York: McGraw Hill, Inc.. pp. 15.1–15.5. ISBN 0070161976.

[100] Pungor, Erno (1995). A Practical Guide to Instrumental Analysis. Florida: Boca Raton. pp. 181–191.

[101] Skoog, Douglas A., F. James Holler and Timothy Nieman (1998). Principles of Instrumental Analysis (5 ed.). New York. pp. 805–808. ISBN 0030020786.

[102] M. J. O'Neill (1964). "The Analysis of a Temperature-Controlled Scanning Calorimeter.". Anal. Chem. 36: 1238–1245. doi:10.1021/ ac60213a020

[103] B. Wunderlich, Thermal Analysis, Academic Press, 1990, pp. 417-431

[104] TN 48, "Polymer Heats of Fusion", TA Instruments, New Castle, DE.

[105] Schroder Dieter K., Semiconductor Material and Device Characterization, 2nd Edition, (John Wiley &Sons, New York, 1998)

[106] J Albers, H L Berkowitz, J.Electrochem.Soc.132 (1985)2453

.....୫ଓଓ.....

Chapter **3**

Optical properties of highly transparent, thermally stable, spin coated Zinc Oxide (ZnO)/Polystyrene (PS) nanocomposite films

This chapter deals with the interesting optical properties of zinc oxide/polystyrene (ZnO/PS) nanocomposite films prepared by simple mixing followed by film deposition, using spin coating technique. Spin coating is an advantageous technique where one can control the film thickness by suitably adjusting the viscosity of the solution and the spinning speed and get homogeneous films with thickness around a few hundreds of nanometers. These aspects have provided the motivation for the present work where emphasis is given to investigating the optical properties of ZnO/PS nanocomposite films obtained by spin coating and analyzing the effects of each component of the composite (ZnO/PS) on the properties of the other. The nanocomposite films are found to be highly transparent throughout the visible region and the thermal stability is better compared to polystyrene. The optical absorption of the composite films in the UV region is quite high and this aspect highlights the prospects of applications of these films in UV shielding. The polystyrene matrix brings about considerable surface modification of ZnO nanoparticles, resulting in the reduction of defect states within ZnO and facilitating sharp, near band edge photoluminescence (PL) emission.

3.1 Introduction

Recently much attention has been given to studies on the organic/inorganic nanocomposite materials which exhibit a host of interesting optical and electrical properties. Combination of organic and inorganic materials results in the formation of composites which inherit the properties of both organic and inorganic components, thus creating scope for extensive applications in many areas of science and technology. Furthermore, improvements of many of the properties are achieved at very low loadings, compared to micron-sized fillers [1]. Among the many inorganic materials, ZnO is specifically interesting, owing to its direct band gap (E_g =3.37 eV), large room temperature exciton binding energy (60 meV) [2] and the variety of application fields such as solar cells [3], gas sensors [4,5], varistors [6], acoustic and luminescent devices etc [7-9]. Another advantage is that ZnO can be synthesized through wet chemistry, which offers a potential viable route to achieve uniform dispersion in polymer matrices through simple mixing. As the size decreases the semiconductor nanocrystals can have mechanical, optical, electrical and thermal properties quite different from the bulk [10]. It is believed that the unique characteristics of the nanocomposites may also give rise to new opportunities for developing functional polymer/semiconductor nanocomposites [11].

Polystyrene - an amorphous, optically clear thermoplastic material, which is flexible as thin films, is chosen as the host matrix because of its ideal properties for investigating the optical properties of the ZnO/PS nanocomposite. Polystyrene (PS) is in solid (glassy) state at room temperature but flows if heated above its glass transition temperature

and becomes solid again when cooled. Introduction of ZnO filler into polymeric matrices can in general, modify the optical, electrical and mechanical properties of the polymers [12-14]. In the present study, ZnO/PS nanocomposite samples have been prepared by mixing ZnO powder well in PS solution using ultrasonification. Highly transparent thin films of this composite are then obtained by spin coating technique. Though there are a few reports on the synthesis and various properties of ZnO/PS nanocomposites [15, 16], there are no detailed studies on the optical characterization of ZnO/PS nanocomposite films prepared by spin coating technique. The present work is an attempt to investigate in detail the optical absorption and photoluminescence in these spin coated nanocomposite films and see how the presence of each component (ZnO/PS) in the nanocomposite is influencing the properties of the other.

3.2 Synthesis of ZnO nanoparticles

The method used for the synthesis of nanostructured ZnO is the chemical method. Generally, this method comprises of three steps. The first step is the preparation of an alcohol-based solution. The second step is the addition of a metal oxide precursor to the alcohol-based solution to form the reaction mixture. The third step is the reaction of this mixture to form the nanosized metal oxide particles. In the present work, the alcohol based solution is prepared using KOH in methanol and the metal oxide precursor used is zinc acetate dehydrate [Zn (CH3COO) 2. 2H2O].

To start with, potassium hydroxide (0.1M) was dissolved in 200 ml methanol. This solution was heated to 60^0 C under reflux and

stirring. To this solution zinc acetate dehydrate (0.1M) was added. This mixture was kept for two hours under the same conditions, during which precipitation was observed to start. After stirring, the mixture was cooled to 20^0C. The precipitate was filtered and washed with hexane and isopropyl alcohol. The filtrate was dried in an oven at 60^0C for five hours. The white powder obtained was detected to be pure, nanosized (10 nm) ZnO and used to prepare the ZnO/PS nanocomposite.

3.3 Synthesis of Zinc oxide/PS Nanocomposite

For the preparation of ZnO/PS, 1gm of PS was dissolved in 10ml of toluene to obtain a 10% w/v solution after one hour of stirring. The ZnO/PS nanocomposite solution was prepared by adding ZnO powder into PS solution and the mixture was stirred for one hour and then sonicated for five minutes. This solution was used to prepare thin films by spin coating on ultrasonically cleaned and optically flat glass substrates (Spin 150). Films with three different weight percentages of ZnO (5, 10 and 20%) were prepared. For reference, PS films were also prepared by spin coating, using the solution of PS in toluene.

3.4 Characterization

3.4.1 Structural analysis

It is very important to do the structural characterization of the ZnO nanoparticles and the ZnO/PS nanocomposite samples prepared in the present work, as the initial and fundamental characterization. X-Ray diffraction (XRD) is widely used for identification and characterization of nanoparticles. Width and shape of the obtained XRD patterns are characteristic of crystallite size and micro strain. Line profile analysis of

XRD data is often used for the determination of crystallite size distribution. Field emission scanning electron microscopy (FESEM), Energy dispersive spectroscopy (EDS) and Fourier transform infrared spectroscopy (FT-IR) are also used for the structural characterization of the samples.

3.4.1(a) X-Ray Diffraction (XRD) analysis

X-Ray diffraction is widely used for identification and characterization of nanoparticles. In the present work, XRD patterns were taken on a Rigaku X-ray Diffractometer with Cu-Kα (1.5418 A°) radiation operating at 30 kV and 20 mA. Scanning was carried out in the 2θ range from 10–70 °. and the powder samples were scanned at a scan speed of 5° per minute and the film samples, at a scan speed of 2° per minute.

The XRD pattern of ZnO depicted in figure 3.1 shows the diffraction peaks corresponding to (100), (002), (101), (102), (110), (103), and (112) planes which indicate the hexagonal structure of ZnO. The broadening of the XRD peaks indicates the formation of nanosized particles in the prepared sample The average particle size is determined from the X-ray line broadening using the Scherrer equation, $\beta = k\lambda/d\cos\theta$, where β is the full width at half maximum (fwhm) in radians of the diffraction peak, λ is the X-ray wavelength, k is a constant (0.89), θ is the Bragg angle of the peak and d is the average particle size.
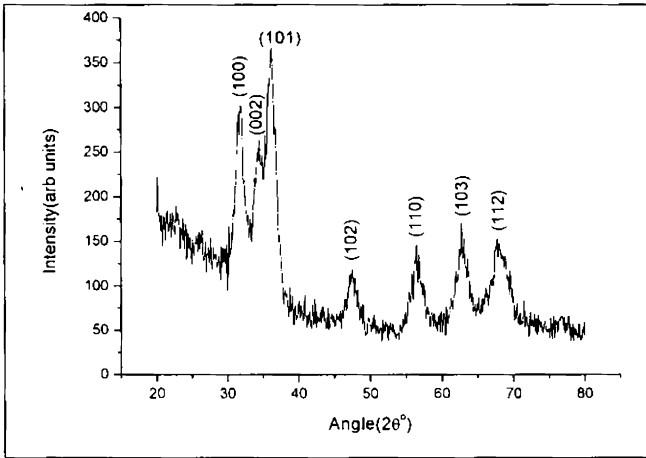
Figure 3.1: XRD pattern of ZnO powder prepared at 60°C (10 nm size)

The XRD patterns of PS and ZnO/PS nanocomposite films are shown in figure 3.2.The patterns show a broad, noncrystalline peak of PS and more intense and crystalline diffraction peaks of ZnO. The presence of ZnO produces neither new peaks nor peak shifts with respect to PS which indicates that nano ZnO filled PS composites consist of two-phase structures.
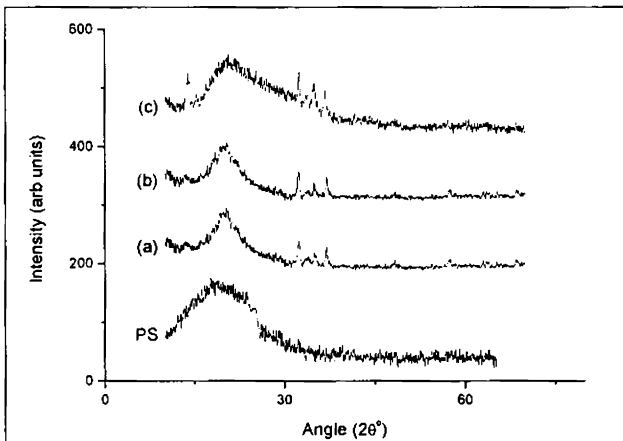
Figure 3.2: XRD patterns of PS and ZnO/PS nanocomposite films
(a, b, and c- correspond to XRD patterns of ZnO/PS composite films with 5, 10,and 20 wt% of ZnO , respectively).

3.4.1(b) Field emission scanning electron microscopy (FESEM)

Field emission scanning electron microscopy (FESEM) is a versatile tool used for diversified ranges of applications, especially in the field of nanomaterials. In the present work, FESEM images were obtained using a HITACHI SU 6600 Microscope with an accelerating voltage of 20 kV. The surfaces of the ZnO nanoparticles and ZnO/PS nanocomposite films were studied using FESEM. FESEM images of ZnO nanoparticles and ZnO/PS nanocomposite film with 10 wt% ZnO are shown in figure 3.3. ZnO nanoparticles (average size, 10 nm) are found to be homogeneously dispersed in the PS matrix. The efficiency of nanoparticles in improving the properties of the polymer material is primarily determined by the degree of dispersion in the matrix. These nanostructured ZnO in the polymer can change the thermal and optical properties of the composite. The size of the ZnO nanoparticles in the PS matrix corresponds to that of primary particles, except for a very few agglomerates. The energy dispersive spectrum (EDS) of the nanoparticles and composites were obtained with JEOL Model JSM - 6390LV scanning microscope. The EDS data clearly indicates the presence of ZnO in the PS matrix (Figure 3.3b).

(a)

(b)

(c)

(d)
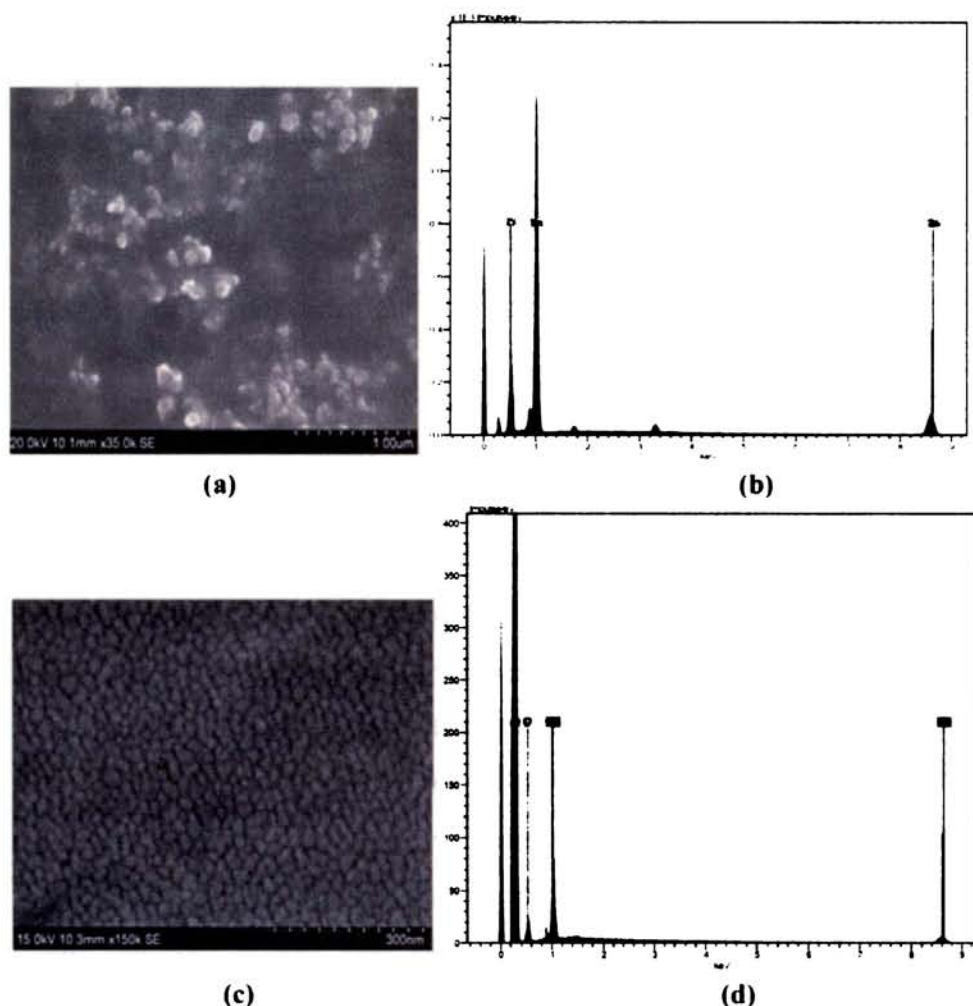
Figure 3.3: **FESEM images of (a) ZnO nanoparticles (c) ZnO/PS nanocomposite film with 10 wt % of ZnO; (b) and (d) correspond to the EDS patterns of ZnO nanoparticles and ZnO/PS nanocomposite.**

3.4.1(c) FT IR analysis

Fourier transform infrared (FT-IR) spectra of the samples were obtained with AVTAR 370 DTGS FTIR spectrophotometer in the wave number range 400–4000 cm $^{-1}$. Figure 3.4 shows the FT-IR spectra of ZnO,

PS, and ZnO/PS nanocomposite. The spectrum of the nanocomposite exhibits the characteristic absorption bands corresponding to polymeric groups and ZnO. In the spectrum of ZnO, the bands observed at 424, 453, and 527 cm^{-1} are assigned to Zn-O vibrations [17-19] out of which the bands at 453 and 527 cm^{-1} are present in the ZnO/PS composite spectrum confirming the presence of ZnO in the composite. The three bands centered at 1338, 1412, and 1572 cm^{-1} observed in the ZnO spectrum are attributed to the stretching vibrations of C =O, C = C, and C-H groups in acetate species. The characteristic vibration bands of aromatic C = C of styrene units are observed at 1452, 1493, and 1601 cm^{-1} in the spectra of PS and ZnO/PS but the relative intensity of these peaks in ZnO/PS has slightly changed. The peaks due to the adsorbed acetate species cannot be clearly distinguished in the ZnO/PS spectra. This could be due to the presence of the PS matrix in which the ZnO nanoparticles are dispersed. The PS matrix can bring about considerable surface modification of the ZnO nanoparticles by eliminating most of the adsorbed species on the surface. That is why the peaks due to the adsorbed species on the surface are not clearly seen in the spectrum of the composite. The changes in the relative intensities of the bands in the region 1500 cm^{-1} in the composite can be due to the minute presence of adsorbed species on the surface of the ZnO nanocrystals. The bands centered at 2924 and 2850 cm^{-1}observed in PS and ZnO/PS spectra are assigned to the asymmetric and symmetric stretching vibrations of -CH$_2$, respectively. The absorption bands corresponding to aromatic C-H stretching are observed in the range 2900-3200 cm^{-1}. The characteristic bands of PS and ZnO are both observed in the ZnO/PS spectrum, which confirms that ZnO is well dispersed in the PS matrix.
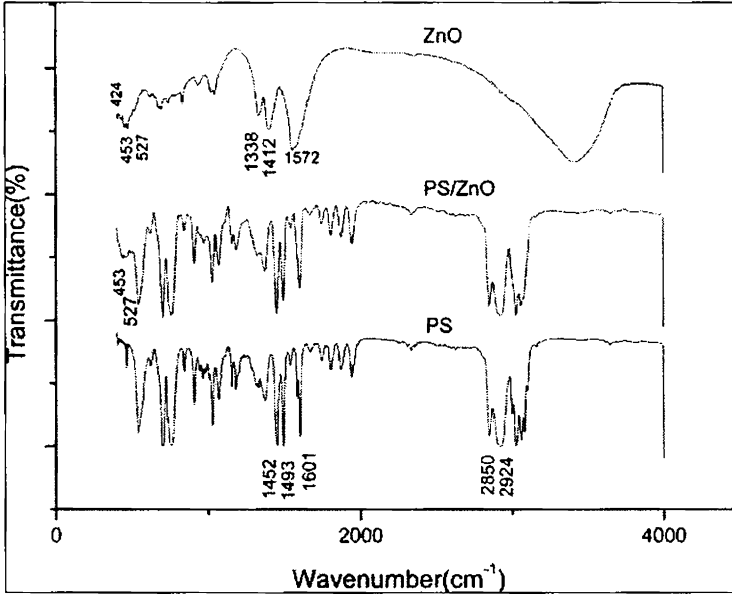
Figure 3.4: FT-IR spectra of ZnO, PS and ZnO/PS nanocomposite

3.4.2 Thermal analysis using TGA

Thermo gravimetric analysis (TGA) of the nanocomposite samples was carried out on a Diamond TG/DTA instrument. Samples were heated to $800^{\circ}C$ at a scan rate of $10^{\circ}C$ per minute in nitrogen atmosphere. Thermo gravimetric analysis (TGA) determines the weight changes of a sample upon heating. The TGA curves of PS and ZnO/PS nanocomposite are shown in figure 3.5 and the TGA data is summarized in table 3.1. The presence of the nanosized ZnO increases the degradation temperature of the polymer composite. The degradation onset temperature (T_{onset}) of ZnO/PS composite, measured as the temperature required for % degradation is higher than that of pure PS beyond 10% degradation. $T_{0.1}$, $T_{0.3}$ . . . $T_{0.9}$ denote the temperatures for 10%, 30%...90% degradation in weight, respectively (Table 3.1). The composite is more thermally stable compared to PS.
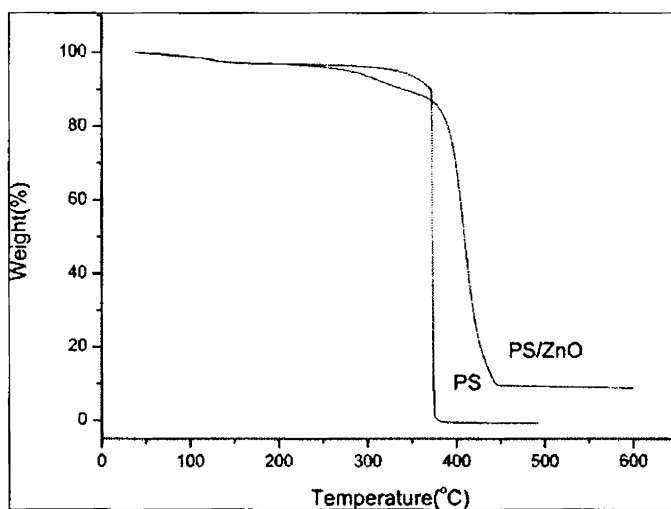
Figure 3.5: TGA curves of PS and ZnO/PS nanocomposite

Table 3.1: TGA data of PS and ZnO/PS nanocomposite

	$T_{0.1}$	$T_{0.3}$	$T_{0.5}$	$T_{0.7}$	$T_{0.9}$
PS	368	375	375	375	375
ZnO/PS	330	400	409	417	440

3.4.3 Optical characterization

The optical characterization carried out in the present work includes optical absorption, Diffuse Reflectance Spectroscopy (DRS) and Photoluminescence (PL) studies. The samples were characterized by optical absorption measurements using JASCO V 570 Spectrophotometer. Photoluminescence emission of ZnO and ZnO/PS nanocomposite was recorded at room temperature using Flouromax-3 Spectroflurimeter. The optical absorption and photoluminescence characteristics of the ZnO/PS nanocomposite films containing different weight percentages of ZnO, were studied in detail.

3.4.3 (a) DRS analysis

The optical band gap E_g of powder samples is estimated from the UV-Vis Diffuse Reflectance Spectroscopic (UV-Vis DRS) studies. Diffuse Reflectance Spectroscopy (DRS), also sometimes known as Elastic Scattering Spectroscopy, is a non-invasive technique that utilizes the interaction of light with the medium. Reflection and scattering produce a characteristic reflectance spectrum, providing information about the structure and composition of the medium. In the present study, measurements were taken using the DRS mode of JASCO V 570 spectrophotometer in the wavelength range from 190nm to 1000nm. The direct band gap of ZnO is estimated from the plot of [(k/s). hυ] ^{2} versus hυ, where hυ is the photon energy and k/s is the ratio of the absorption coefficient to the scattering coefficient.
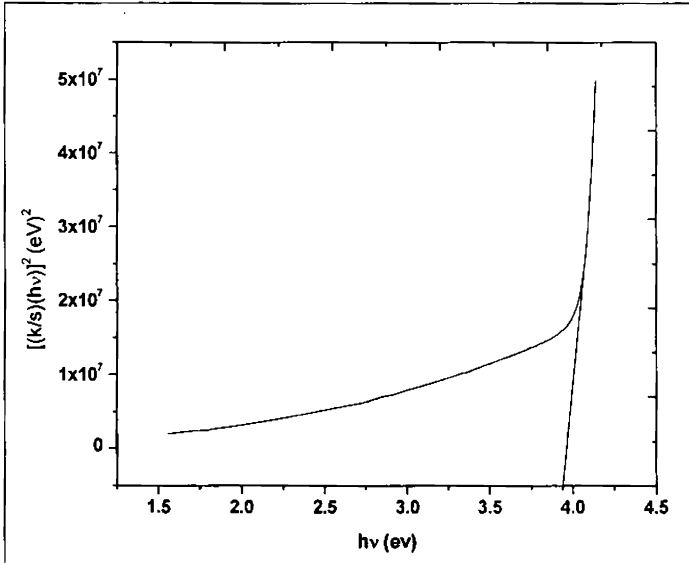
Figure 3.6: DRS plot for finding the band gap of ZnO powder, prepared at 60°C

The ratio, k/s is given by, $(1-R)^2/2R = k/s$ (Kubelka-Munk equation, the details of which is described in chapter 2), where R is the reflectance of the sample. By extrapolating the linear portion of the curve to meet at hυ=0, the band gap can be found out. The band gap of nanosized ZnO is found to be 3.93 eV.

3.4.3(b) UV-Vis absorption spectroscopy

The UV-visible absorption spectra of PS and ZnO/PS composite films are shown in figure 3.7. Pure PS film does not show any appreciable UV absorption, and there is only a broad, less intense absorption band. For the composite films, one can see UV absorption windows in all the samples, corresponding to different weight percentages of ZnO. The absorption window is found in the range 240-365 nm, and the intensity of UV absorption increases sharply with increase of ZnO content in the composite. The presence of nanosized zinc oxide enhances the UV absorption capacity of PS films. The ZnO content or dispersability enhances the UV shielding properties of the nanocomposite polymer. Furthermore, the absorption peak wavelengths of the composite films are substantially blue shifted relative to that of the bulk ZnO (~ 373 nm) due to the strong confinement effect [20]. In the case of nanocrystallites, the electrons, holes and excitons have limited space to move and their limited motion becomes possible only for definite values of energy. The highest occupied valence band and lowest unoccupied conduction band are shifted to a more negative and positive values respectively resulting in the widening of band gap. This leads to a blue shift of absorption band which can be observed through optical absorption and transmission studies.

The thickness of the PS and ZnO/PS nanocomposite films is measured using the thickness profiler (Dekdak 6M Stylus Profiler). The film thickness is found to lie in the range 0.8 to 1μm for all the films investigated in the present work. In this thickness range, the spin-coated films are also found to be homogeneous. In a recent work by Yao Tu et al. [15] ZnO/PS nanocomposite films are shown to exhibit quite high UV-shielding efficiency with the absorption of 99% of UV radiation in the wavelength range between 200 and 360 nm. In that work, however, the film thickness is very high which is about 360μm. The ZnO used is not pure, but ligand modified and the technique of film deposition is solution casting where one cannot have good control over the film thickness.
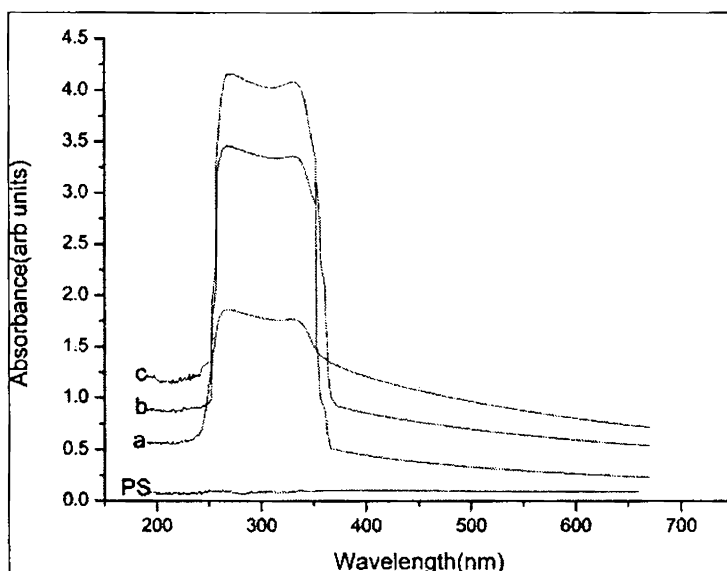
Figure 3.7: UV-visible absorption spectra of PS and ZnO/PS composite films (a,b, and c—ZnO/PS composite films with 5, 10, and 20 wt% of ZnO respectively).

In the present work, about 1μm thick spin-coated film of ZnO/PS nanocomposite is showing about 90% UV absorption in the wavelength range from 240 to 365 nm with 20% of ZnO loading in the composite. These films are highly transparent in the visible range and offer prospects of application as transparent UV radiation protectors in the wavelength range from 240 to 365 nm. The presence of ZnO nanoparticles thus enhances the UV absorption of the composite films and modifies the overall optical behavior of PS films.

3.4.3(c) Photoluminescence (PL) studies

Photoluminescence emission of ZnO, PS and ZnO/PS nanocomposite was recorded at room temperature using Flouromax-3 Spectroflurimeter consisting of Xenon arc lamp, monochromator and a CCD detector under an excitation at 325 nm. The PL emission spectra of these samples are shown in figure 3.8. The PL spectrum of ZnO depicts a sharp intense emission peak at 367 nm along with a broader but more intense emission peak in the longer wavelength side centered at 530 nm. A kink is also observed in the blue region around 450 nm. Pure PS film does not show any luminescence emission in this region as seen from the PL spectrum.
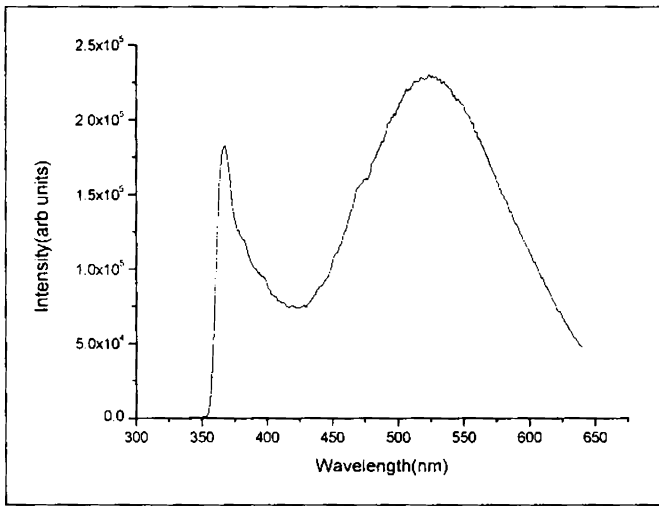
(i)
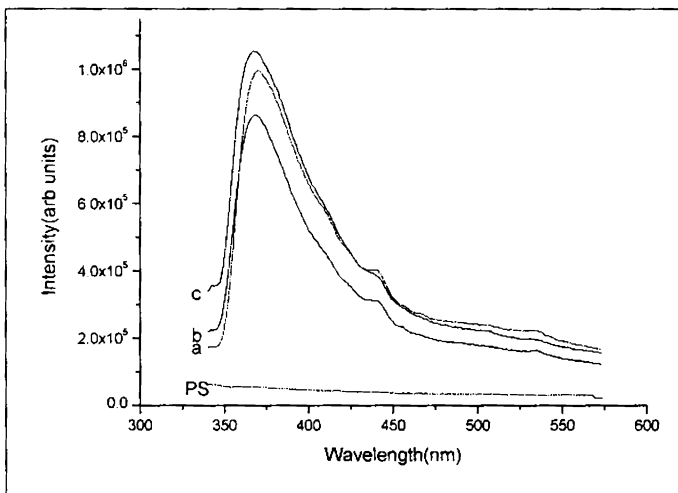
(ii)

Figure 3.8: PL emission spectra of (i) ZnO and (ii) PS and ZnO/PS nanocomposite films
(a, b and c—ZnO/PS composite films with 5,10, and 20 wt% of ZnO, respectively).

The broad PL band at around 530 nm has already been reported in bulk ZnO as well as in ZnO quantum dots by many researchers [21-24]. However, the origin of this broad luminescence is not fully established.

It is reported that the emission in the UV region is due to near band gap transition [25] and the emission in the green region corresponds to the impurity related emission from defect levels arising either due to oxygen vacancies or zinc interstitials [26-30]. The excitons can exhibit excited state transitions, in addition to their ground state transitions, which can result in additional emission peaks. The composite films show intense luminescence emission centered around 367 nm in the UV region and intensity of this emission peak is found to increase with the increase of ZnO content in the composite. The effect of different weight percentages of ZnO is only in the slight variations in the intensity of PL emission.

The intensity of the broad luminescence observed around 530 nm relative to that of the UV luminescence decreases considerably and is almost quenched in the composite films. The kink observed in the blue region of the ZnO spectrum becomes more visible in the spectra of the composite films. The green emission in ZnO originates mainly from the deep surface traps, which can almost be removed via surface passivation by the polymer matrix. The kink in the blue region of the PL spectrum of ZnO is not much observable because of the presence of the broad intense green emission. However, this kink is more prominent in the PL spectra of the composite films due to the considerable lowering of PL intensity in the green region. The suppression of green luminescence is due to the surface modification of ZnO nanocrystals by the polymer, whereby the deep surface traps are almost removed [22]. The observed blue emission in ZnO and the ZnO/PS composite arises from the presence of acetate impurities incorporated in ZnO, possibly during the synthesis process from the precursor zinc acetate. In ZnO, it appears only as a kink mainly

because of the presence of the broad and intense emission in the green region. Since the green emission is almost suppressed in the composite, the blue emission appears more pronounced. The intensity of the blue emission increases with increase in the ZnO content in the composite, and this observation also points towards the presence of acetate impurities on the ZnO surface, as the possible reason for this emission. The FT-IR spectra of the ZnO powder and ZnO/PS composite also support the incorporation of acetate impurities onto ZnO.

3.5 Conclusion

Zinc oxide (ZnO) nanoparticles were prepared by wet chemical method. The nanocrystalline nature of the prepared ZnO powder sample was confirmed by FESEM and XRD analysis. Using the nanosized ZnO, the polymer nanocomposite, ZnO/Polystyrene (PS) was synthesized and transparent films of this nanocomposite were deposited on glass substrates using spin coating technique, with thickness around 1micrometre. Good surface fictionalization of ZnO with the polymer has facilitated the homogeneous dispersion of ZnO particles in the polymer matrix.

The ZnO/PS nanocomposite films exhibit good UV shielding properties in the wavelength range from 240 to 365 nm, where a UV absorption window of about 125 nm has been observed. This aspect highlights the prospects of applications of the ZnO/PS nanocomposite films as UV protectors for UV shielding in plastics, textiles, paints, cosmetics, etc. The UV absorption of about 90% observed in the present work can be further enhanced by increasing the film thickness and also by using non toxic surfactants to achieve further surface modification of

ZnO. It may also be possible that the wavelength range of high UV absorption can be further extended, down to less than 180 nm. The present work offers ample scope for further studies with spin coated films of ZnO/PS, since the various parameters of spin coating can be suitably optimized to get the desired results. Another highlight of the present work is the observation that the polystyrene matrix itself brings about considerable surface modification of ZnO by almost removing the trap and impurity levels in ZnO. This effect is manifested as the quenching of the trap level related photoluminescence emission around 530 nm in the ZnO/PS composite films. In the composite films, the emission in the UV region is observed to have much higher intensity. The surface modification of ZnO by the polymer matrix thus almost quenches the emission in the visible region and confines the emission entirely to the near band edge.

References

[1] Alexandre, M.; Dubois, P. Mater Sci Eng 2000, 28, 1.

[2] Yi, G.-C.; Wang, C.; Park, W. I. Semicond Sci Tech 2005, 20, S22.

[3] Beek, W. J. E.; Wienk, M. M.; Janssen, R. A. J. J Mater Chem 2005, 15, 2985.

[4] Sahay, P. P. J Mater Sci 2005, 40, 4383.

[5] Jiaqiang, X.; Yuping, C.; Daoyong, C.; Jianian, S. Sensor Actuat B Chem 2006, 113, 526.

[6] Kong, L.; Li, F.; Zhang, L.; Yao, X. J Mater Sci Lett 1998, 17, 769.

[7] Hao, X. T.; Zhu, F. R.; Ong, K. S.; Tan, L. W. Semicond Sci Tech 2006, 21, 48.

[8] Shih, W. C.; Wu, M. S. J Cryst Growth 1994, 137, 319.

[9]   Radovanovic, R. V.; Norberg, N. S.; McNally, K. E.; Gamelin, D. R. J Am Chem Soc 2002, 129, 15192.

[10]   Alivisatos, A. P. Science 1996, 271, 933.

[11]   Sheng, W. C.; Kim, S.; Lee, J.; Kim, S. W.; Jensen, K.; Bawendi, N. G. Langmuir 2006, 22, 3782.

[12]   Lee, J.; Bhattacharyya, D.; Easteal, A. J.; Metson, J. B. Curr Appl Phys 2008, 8, 42.

[13]   Dong, W. C.; Byoung, C. K. Polym Adv Technol 2005, 16, 846.

[14]   Erjun, T.; Shaoying, D. Colloid Polym Sci 2009, 287, 1025.

[15]   Yao, T.; Li, Z.; Yi Zheng, J.; Chao, G.; Zhi Zhen, Y.; Ye Feng, Y.; Qing Ling, W. J Mater Chem 2010, 20, 1594.

[16]   Tang, E. J.; Liu, H.; Sun, L. M.; Zheng, E. L.; Cheng, G. X. Eur Polym Mater 2007, 43, 4210.

[17]   Sumetha, S. Science Asia 2008, 34, 031.

[18]   Yong, J. K.; Kyoung, H. K.; Chang, S. L.; Kwang, B. S. J Ceram Process Res 2002, 3, 146.

[19]   Siddheswaran, R.; Sankar, R.; Ramesh Babu, M.; Rathnakumari, M.; Jayavel, R.; Murugakoothan, P.; Sureshkumar, P. Cryst Res Technol 2006, 41, 446.

[20]   Haase, M.; Weller, H.; Henglein, A. J Phys Chem 1988, 92, 482.

[21]   Gong, V.; Gertrude, T. A.; Neumark, F.; Stephen O'Igor, L. Nanoscale Res Lett 2007, 2, 297.

[22]   Guo, L.; Yang, S.; Yang, C.; Yu, P.; Wang, J.; Ge, W.; Wong, G. K. L. Appl Phys Lett 2000, 76, 2901.

[23]   Wu, L.; Wu, Y.; Pan, X.; Kong, F. Opt Mater 2006, 28, 418.

[24]   Zhang, S. B.; Wei, S. H.; Zunger, A. Phys Rev B 2001, 63, 075205.

[25] U.Ozgur,I.Y.Alivov,C.Liu,A.Teke,M.A.Reshchikov,S.Dogan, V. Arutin, S .J.Cho and H.Morkoc, J.Appl.Phys. 2005, 98, 041301.

[26] E.G.Bylander, J.Appl.Phys. 1978, 49, 1168.

[27] K.Vanhesde, C.H.Seager, W.L.Warren, D.R.Tallent and J.A.Voigėt, Appl.Phys.Lett. 1996, 68, 404. [28]. M.Liu, A.H.Kitai and P.Mascher, J.Lumin. 1992, 54, 943.

[28] B.Lin, Z.Fu and Y.Zia, Appl.Phys.Lett. 2001, 79, 943.

[29] K.F.Lin, H.M.Cheng, H.C.Hsu, L.J.Lin and W.F.Hsieh, Chem. Phys. Lett. 2005, 409, 208.

.....ഈ൜.....

Chapter **4**

Size-dependent optical properties of transparent, spin-coated Zinc oxide/ Polystyrene nanocomposite films

Zinc oxide (ZnO) nanoparticles are synthesized using a simple chemical method at room temperature. A variation in molar concentration of the precursor, potassium hydroxide, from 0.25 to 0.01 mol l^{-1} is accompanied by a decrease in the average size of the nanoparticles from 35 to 5 nm. These nanoparticles are used for the deposition of ZnO/ polystyrene nanocomposite films using spin-coating technique on glass substrates. These nanocomposite films are found to be highly transparent throughout the visible region and absorb UV light in the region from 395 to190 nm, almost covering the near and middle UV ranges (400 to 200 nm). This observation highlights the possible prospects of these films in UV shielding applications. The wavelength corresponding to the onset of UV absorption is found to be blue shifted with a decrease in size of the ZnO particles in the composite films due to confinement effects. The photoluminescence spectra of the composite films also undergo changes as the ZnO particle size changes. The emissions at longer wavelength due to defects and impurity-related states in ZnO are almost quenched as a result of surface modification by the polymer matrix. The observed band gap enlargement with a decrease in size of the ZnO particles in the nanocomposite films is significant for band-gap engineering of nanoparticles for various applications.

4.1 Introduction

Semiconductor nanocrystals are interesting because of their size-dependent electronic and optical properties. The fascinating properties exhibited by nanoparticles, such as blue shift of the absorption spectrum, size-dependent luminescence, etc., are various manifestations of the so-called quantum confinement effects [1–3]. Zinc oxide (ZnO), a direct band-gap semiconductor with an energy gap of 3.37 eV and large room temperature exciton binding energy of 60 meV [4–6] is a promising candidate for applications in optical and optoelectronic devices [7–10]. It is well known that low-dimensional structures have superior optical properties over bulk materials due to the confinement effect [11]. Polymer-based nanocomposites are the subjects of considerable research due to the possibility of combining the advantages of both polymers and nanoparticles. There are several applications of polymeric nanocomposites based on their optical, electrical and mechanical properties [12, 13]. Inorganic/polymer nanocomposites benefit from physical flexibility and ease of processing, which are typical features of polymers. Further, nanocrystals dispersed in suitable solid hosts can be stabilized for long periods of time. Polystyrene (PS), which is flexible in thin-film form, is chosen as the host matrix, because of its ideal characteristics for investigating optical properties. It is one of the most extensively used plastic materials, in disposable cutlery, plastic models, CD and DVD cases, and smoke-detector housings.

UV radiation has effects, both beneficial and damaging, on human health. For instance, overexposure to UVB (280–315 nm in wavelength) radiation can cause sunburn and some forms of skin cancer via direct

DNA damage. UVA (315–400 nm) radiation does not damage DNA directly like UVB and UVC (100–280 nm) radiations, but it can generate highly reactive chemical intermediates which in turn can damage DNA. Many polymers used in consumer products, and many pigments and dyes, are degraded by UV light. Therefore, extensive research efforts have been made to develop transparent materials which are ideal for UV shielding applications. Inorganic/polymer nanocomposites are excellent candidates for this purpose. ZnO/PS nanocomposites have potential applications as antireflection coatings, as UV protecting sheets and films and as materials with enhanced thermal stability [14, 15]. There are reports on the UV shielding applications [16] and the thermal properties of ZnO/ PS nanocomposite films [17, 18]. However, a detailed investigation on the size-dependent optical properties of these nanocomposite films deposited using spin-coating technique has not been attempted. In the present work, ZnO nanoparticles have been synthesized at room temperature, contrary to the earlier reports mentioned above, where the synthesis of ZnO has been carried out at higher temperatures. These factors are the motivating forces behind the present investigations on the size-dependent optical properties of ZnO/PS nanocomposite films.

In the present study, ZnO nanoparticles of various average particle sizes were prepared by tuning the reaction conditions. These nanoparticles were then used for the deposition of ZnO/PS composite films using spin-coating technique. Spin-coating is an attractive technique in which one can control film thickness by suitably adjusting the viscosity of the solution and the spinning speed and get

homogeneous films with thickness around a few micrometers. Optical methods give rich experimental information about the energetic structure of these nanocomposites. The size-induced modifications of the optical absorption and photoluminescence (PL) spectra of the composite films are discussed.

4.2   Sample synthesis

ZnO nanoparticles were synthesized at room temperature using a simple chemical method. Zinc acetate (0.1 mol/litre) was dissolved in 100 ml of methanol with magnetic stirring and then potassium hydroxide (KOH) was added. The mixture was stirred for about 2 hrs and then washed and filtered. The filtrate was dried in an oven at 50^0 C for 5–6 hrs. A set of samples was prepared by varying the concentration of KOH from 0.25 to 0.01 mol/litre. The white powder samples obtained were determined to be pure ZnO nanocrystals of various average sizes using XRD analysis.

ZnO/PS nanocomposite solutions were prepared by adding 10 wt% of each ZnO powder sample into PS solutions (10% w/v) in toluene. The mixtures were then stirred for 2 hrs and then sonicated for 10 minutes. These solutions were used to deposit thin films of these nanocomposites by spin coating on ultrasonically cleaned and optically flat glass substrates (Spin 150).

4.3   Characterization
4.3.1 Structural analysis

The ZnO nanoparticles and ZnO/PS nanocomposite films were structurally characterized using XRD, TEM and FESEM analysis. The

size and structure of the nanoparticles, and the surface morphology of the composite films were investigated using these techniques.

4.3.1(a) XRD

The XRD patterns of ZnO nanocrystals and composite films were obtained using a Rigaku X-ray Diffractometer with Cu-Kα (1.5418 A°) radiation operating at 30 kV and 20 mA. Scanning was carried out in the 2θ range from 10–80 ° at a scan speed of 2° per minute.

The XRD patterns of ZnO nanoparticles prepared by varying the concentration of KOH precursor from 0.25 to 0.01 mol/litre are shown in figure 4.1. All the observed diffraction peaks in the XRD spectrum of ZnO nanoparticles can be indexed to match the standard diffraction pattern of wurtzite ZnO (JCPDS card no. 36-1451). The diffraction peaks corresponding to (100), (002), (101), (102), (110), (103), and (112) planes indicate the hexagonal structure of zinc oxide. The peaks get broadened as the particle size decreases and the extent of broadening is used to calculate the average size of the particles. The particle size is determined using the Scherrer relation (given in chapter 2) and it is found to decrease with decrease in KOH concentration. The precursor concentration decrease from 0.25M to 0.01M is accompanied by a decrease in average particle size from 35 to 5 nm (Table 4.1). The XRD patterns of the composite films appear alike and hence only one pattern is shown in figure 4.2, which consists of a broad non-crystalline peak of PS and sharp diffraction peaks of ZnO.
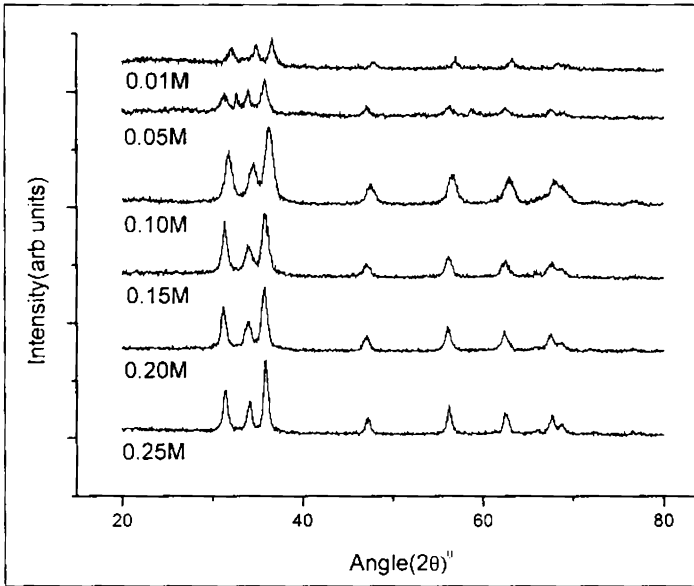
Figure 4.1: XRD patterns of ZnO particles of different average particle sizes (5-35 nm) prepared by varying the concentration of KOH precursor (0.25 to 0.01M)
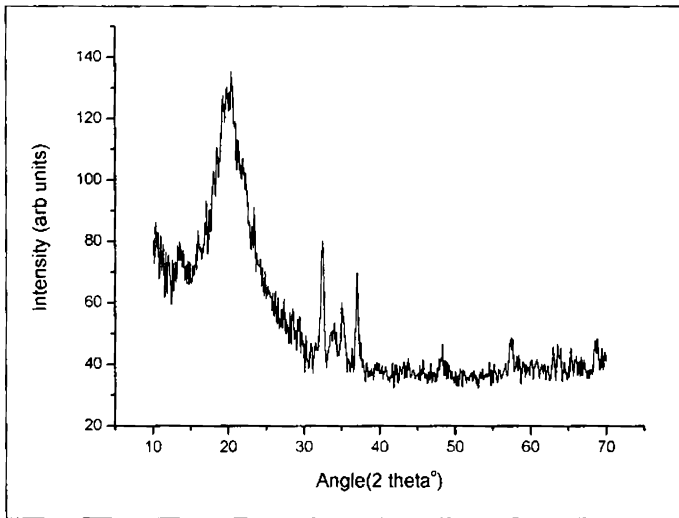
Figure 4.2: XRD pattern of ZnO/PS nanocomposite film.

4.3.1(b) Transmission Electron Microscopy (TEM) and Field Emission Scanning Electron Microscopy (FESEM) studies

The nanostructure of the ZnO particles and the surface morphology of the nanocomposite films were investigated using TEM and FESEM studies. Transmission electron microscope images of the ZnO particles were taken using JEOL 3010 instrument with a UHR pole piece. This gives a lattice resolution of 0.14 nm and a point-to-point resolution of 0.12 nm. Field emission scanning electron microscope images were obtained using a HITACHI SU 6600 Microscope with an accelerating voltage of 20 kV.

The TEM, HRTEM and FESEM images of ZnO nanoparticles and FESEM images of ZnO /PS nanocomposite films are shown in figure 4.3(a -f). The average particle size of the ZnO nanoparticles determined from the XRD peaks using the Debye-Scherrer formula is found to be close to that based on TEM and FESEM analysis. Figure 4.3b illustrates the surface morphology of ZnO/PS nanocomposite films and shows a continuous and fine-grained structure without any cracks. It is observed that the ZnO particles are homogeneously dispersed in the PS matrix. The size of the ZnO nanoparticles in the PS matrix corresponds to that of primary particles, and the extent of agglomeration is negligible.

(a)

(b)

(c)

(d)

(e)

(f)
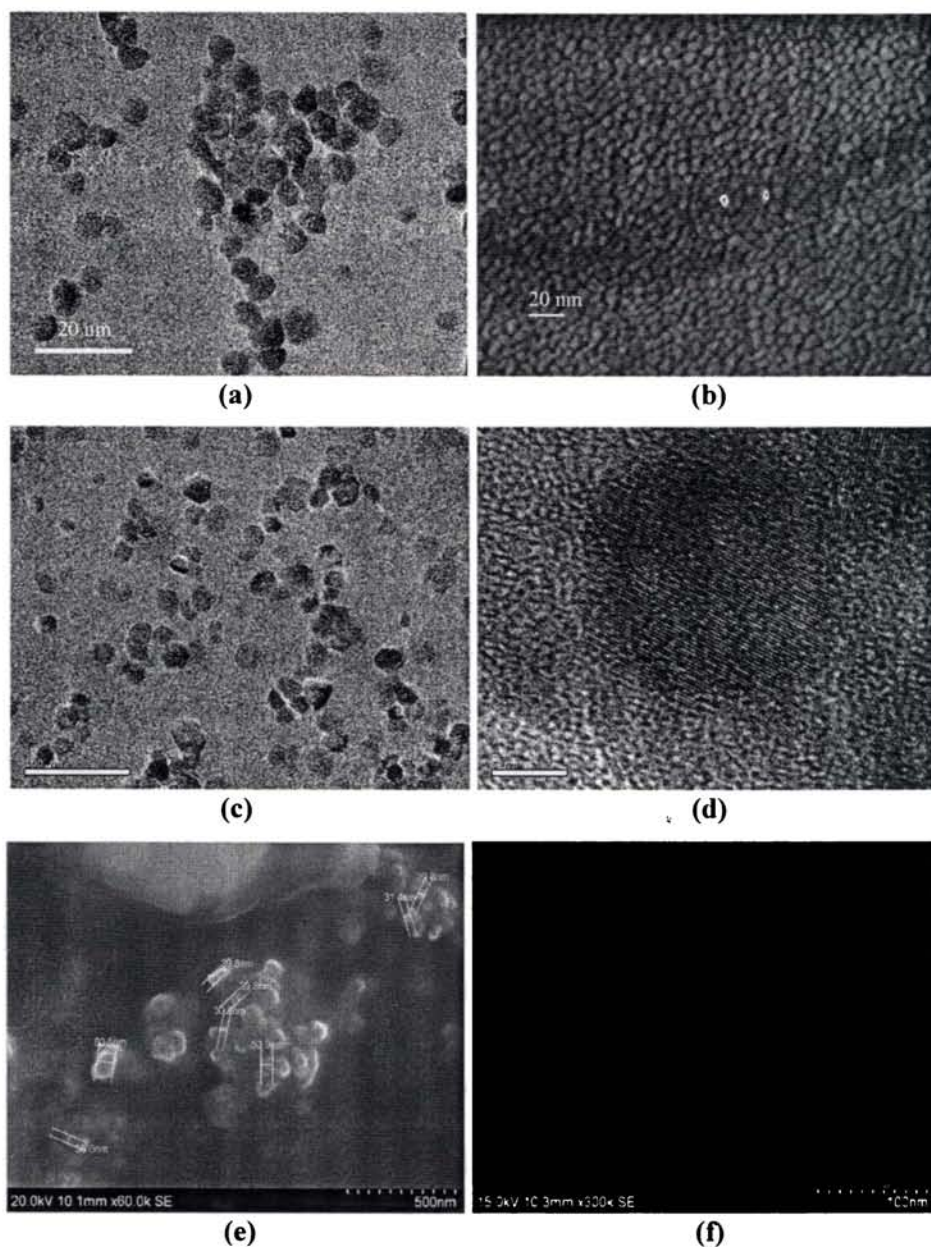
Figure 4.3: a) TEM image of ZnO particles of size ~ 5 nm b) FESEM image of ZnO/PS composite film containing ZnO crystals of size ~5 nm c) TEM image of ZnO particles of size ~15 nm d) HRTEM of ZnO (~15 nm size) e) & f) FESEM images of ZnO particles of size ~30 nm and the ZnO/PS nanocomposite film.

4.3.1(c) Raman spectroscopy studies

Raman spectra of the samples were recorded on a Micro Raman spectrometer, HORIBA JY (Lab RAM HR) using a laser of wavelength 633 nm as the excitation source. The Raman spectra of ZnO, PS and ZnO/PS composite are shown in figure 4.4. The peaks in the Raman spectra of ZnO at 418 cm^{-1} and at 435 cm^{-1} represent the Raman active modes of the wurtzite hexagonal ZnO [19]. Hence the results of Raman spectrum analysis are in good agreement with the XRD analysis. The characteristic peak of ZnO in the ZnO/PS composite film is broadened and shifted to higher frequency side compared to ZnO. This observation highlights the possibility of bonding between PS and ZnO in the composite.
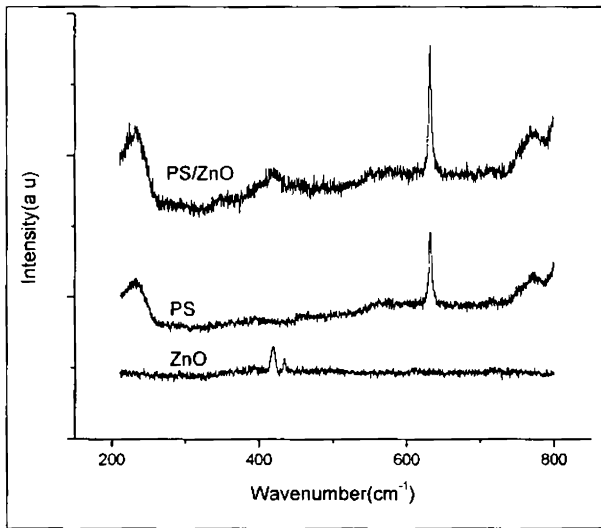
Figure 4.4: Raman spectra of ZnO, PS and ZnO/PS composite

4.3.2 Optical characterization

4.3.2(a) UV-Vis Absorption spectroscopy

The UV-Visible absorption spectra of PS and ZnO/PS composite films were obtained using JASCO-V' 570 spectrophotometer in the wavelength range 200 to 800 nm.

The spectra are shown in figure 4.5. Pure PS film does not show any appreciable UV absorption and there is only a broad, less intense absorption band in the UV range. As described earlier, (section 3.4.3) in the case of nanocrystallites, the electrons, holes and excitons have limited space to move and their limited motion becomes possible only for definite values of energy. The highest occupied valence band energy level and lowest unoccupied conduction band level are shifted to a more negative and positive values respectively resulting in widening of band gap. This leads to a blue shift of absorption band which can be observed through optical absorption and transmission studies. This size dependent shift in absorption band edge is shown in the figure.

For all the composite films, there is an absorption window of width over 100nm and the observed absorption window is found to shift towards the shorter wavelength side as the size of ZnO nanocrystals in the composite decreases. This implies that the ZnO nanocrystals in the composite are in the regime of spatial exciton confinement, where the electronic properties depend strongly on the particle size [20]. The excitonic peak is found to be blue shifted from 395 to 303 nm with decrease in particle size of ZnO and this can be attributed to the confinement effects [21, 22]. The extent of

confinement in a low dimensional structure is judged by the value of the exciton Bohr radius (a_B). Quantum confinement effects arise as soon as the dimension of a nanocrystal (R) becomes comparable to the exciton Bohr radius (a_B), leading to significant changes in the electronic and optical properties. Generally, one can differentiate between different regimes of confinement depending on the magnitude of crystallite size, as strongly confined regime ($R < a_B$), intermediate confined regime ($R \sim a_B$) and weakly confined regime ($R > a_B$). From the figure it is clear that the composite films containing ZnO particles of size 5 and 6.5 nm lie in the regime called intermediate regime ($R \sim a_B$) and those containing particles of size 15 to 35 nm lie in the other regime called the weak confinement regime ($R > a_B$) where R is the radius of the particle and a_B is the exciton Bohr radius in ZnO [23-26]. The value of a_B in ZnO is 2 nm. The absorption band edge of the composite films in the intermediate regime shifts from 307 to 303 nm and that in the weak confinement regime shifts from 395 to 350 nm towards the shorter wavelength side. For the composite films in the weakly confined regime (say, group A) the absorption window extends over ~100 nm and for those in the intermediate confined regime (say, group B) the window extends over ~115 nm.
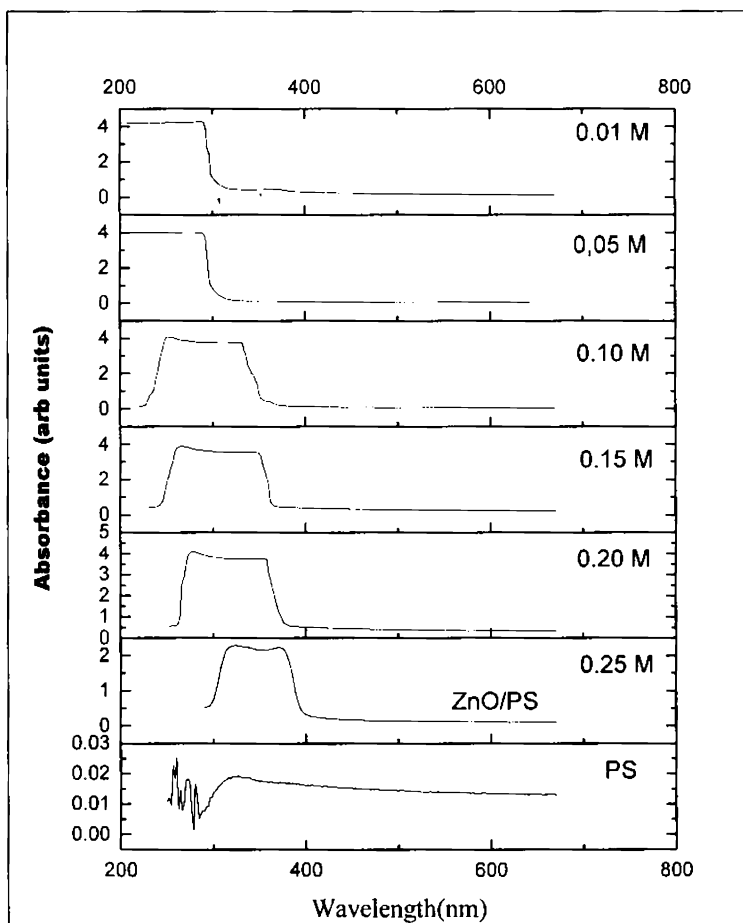
Figure 4.5: **UV-Vis absorption spectra of PS and ZnO/PS nanocomposite films containing ZnO nanoparticles prepared by varying the concentration of KOH precursor (0.25 to 0.01M)**

The composite films in group A absorb almost all the UVA radiation, whereas the UVB and part of UVC radiations are found to be absorbed by films in group B. The films in both groups together are capable of absorbing UV radiation in the range from 395 to 190 nm, covering completely UVA and UVB regions and part of UVC region, thus showing prospects of acting as efficient UV filters. .The saturation of the absorption spectra corresponding to lower precursor molarities

and hence lower particle size cannot be identified sharply due to the limitation of the apparatus used, where the lowest wavelength available is 190 nm.

4.3.2(b) Optical band gap

The optical band gap of the composite films is estimated from the plot of $(\alpha h\upsilon)^2$ vs hυ (Figure 4.6) for the absorption coefficient α which is related to the band gap E_g as

$$(\alpha h\upsilon)^2 = k(h\upsilon - E_g),$$

where hυ is the incident light energy and k is a constant. Extrapolation of the linear part of the plot onto the hυ axis gives E_g. The optical band gap values of the composite films are found to be size dependent and there is widening of the band gap with decrease in the size of ZnO particles in the composite [22, 27]. The blue shift of the absorption edge of the composite films from 395 to 303 nm is associated with a band gap enlargement from 3.2 to 4.15 eV. This is due to the confinement effects and the two regimes can be well distinguished in the figure.
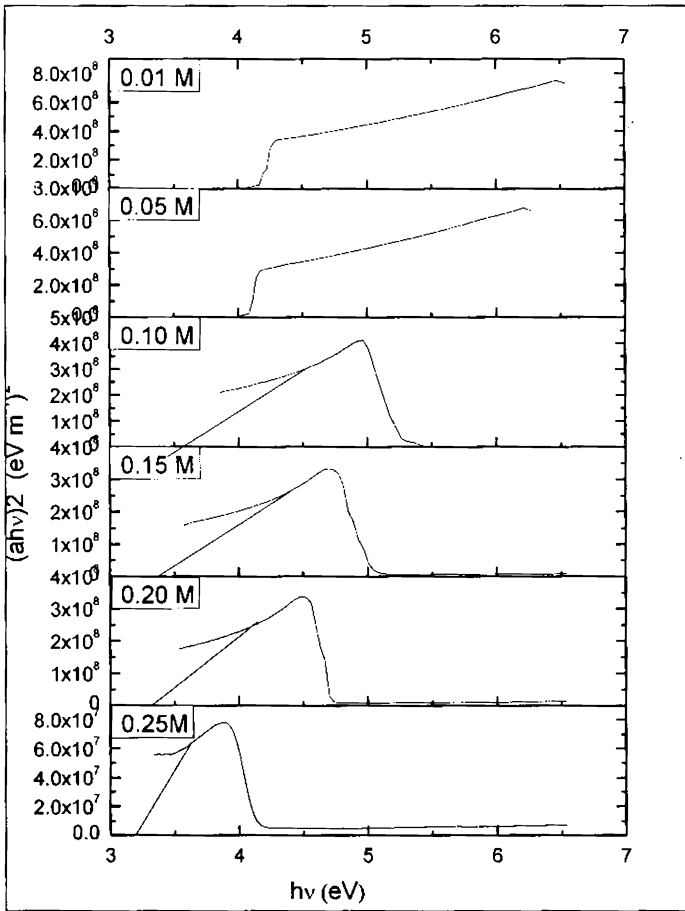
Figure 4.6: Plots of $(\alpha h\upsilon)^2$ vs $h\upsilon$ of the PS/ZnO composite films for band gap determination

4.3.2(c) Photoluminescence (PL) studies

The PL spectra of ZnO and ZnO/PS nanocomposites were obtained using Flouromax-3 Spectroflurimeter consisting of Xenon arc lamp, monochromator and a CCD detector. The PL spectra are shown in figures 4.7&4.8. Generally, ZnO exhibits emissions, both in the UV region (corresponding to near band-edge emission) and in the visible region [28-32]. In the spectra of the composite films, the UV emission band is assigned to a direct band gap transition.
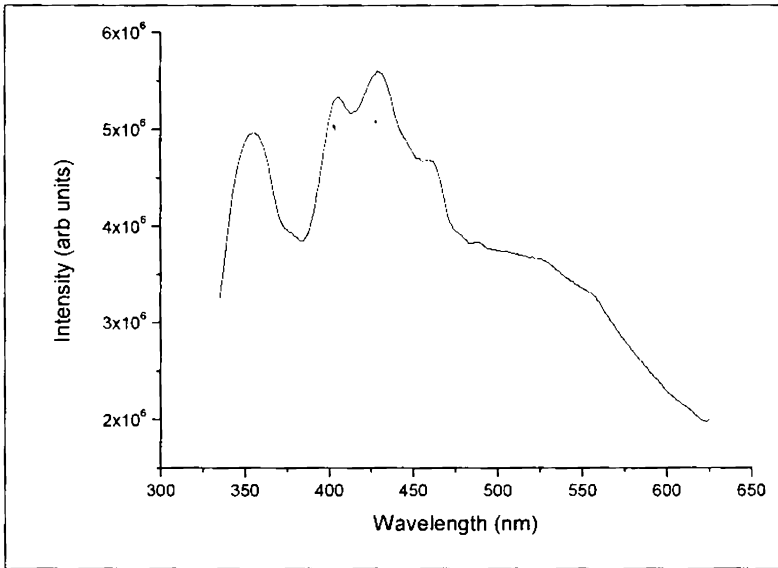
Figure 4.7: The PL spectrum of ZnO nanoparticles

Like the absorption spectrum, the UV emission band is found to shift towards the lower wavelength side as the size of ZnO nanoparticles in the composite decreases [33], which is due to the quantum confinement of ZnO nanoparticles present in the film. For the composite films, there are no sharp and intense emission peaks in the visible region. However, in the spectrum of ZnO, shown in figure 4.6, there are intense emission peaks in the visible region which arise mainly from the defect states in ZnO. These defect related emission peaks are almost quenched in the spectra of the composite films, indicating surface modification of ZnO nanoparticles by the polystyrene matrix.

The sample was excited at wavelength 325 nm

several quantum particle systems [28, 34]. The dependence of the spectral characteristics of ZnO/PS nanocomposite films and the ZnO particle size are summarized in table 4.1.

Table 4.1: Spectral characteristics of ZnO/PS nanocomposite films

KOH molarity	Absorption edge	Optical band gap	PL emission peak	Particle size
M	nm	eV	nm	nm
0.25	395	3.20	390	35
0.20	374	3.38	386	30
0.15	366	3.42	383	22
0.10	350	3.55	380	15
0.05	307	4.05	370	6.5
0.01	303	4.15	364	5.0

The possibility of tuning PL emission through size variations can find applications in the realization of nanoscale devices like LEDs and photo detectors covering a broad spectral range [2]. Furthermore, the emissions in the visible region observed in the PL spectrum of ZnO (Figure 4.7), which originate from the presence of surface traps and impurities in ZnO [5,35,36] are found to be almost quenched in the PL spectra of the composite films (Figure 4.8). This is due to the surface modification of the ZnO nanoparticles by the polystyrene matrix, which almost quenches the defect related emissions and facilitates near band edge emission. From the FT-IR studies of ZnO and ZnO/PS composite, described earlier [16] (section 3.4.1), it is observed that the characteristic vibration peak of ZnO at ~420 cm^{-1} gets shifted to higher frequency side in the ZnO/PS composite. The Raman peak corresponding to ZnO vibration, observed at 418 cm^{-1}, becomes broader and is modified and
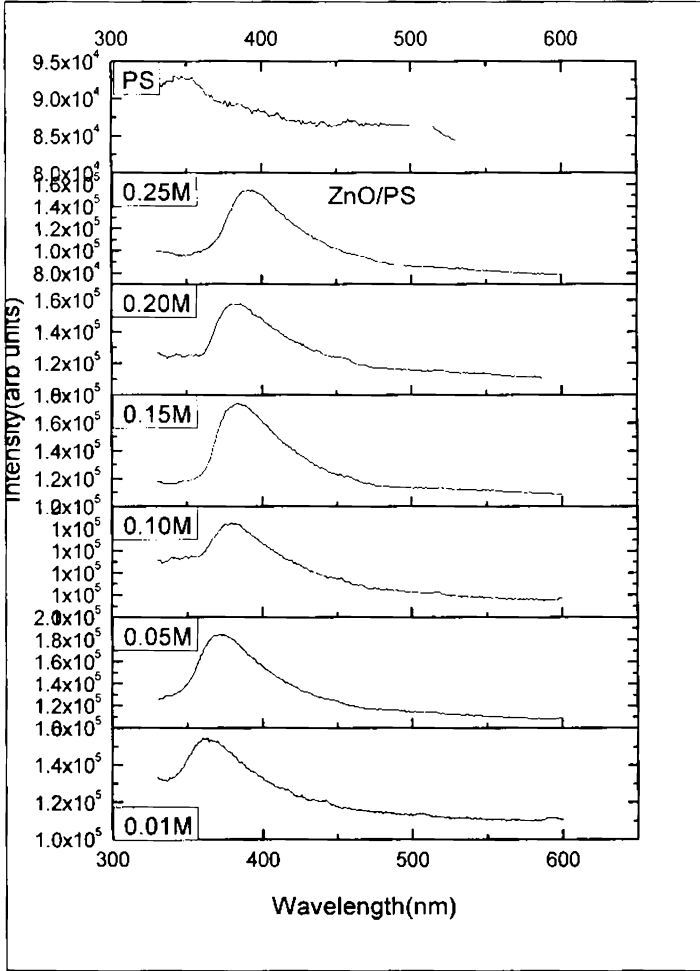
Figure 4.8: The PL spectra of PS and ZnO/PS nanocomposite films.

The emission peaks of the composite films, containing ZnO particles in the weak confinement regime shift from 390 to 380 nm, and those corresponding to the intermediate confinement regime shift from 370 to 364 nm. These are attributed to the size dependent optical characteristics of ZnO nanoparticles. Such size dependent optical properties of semiconductor nanoparticles in the quantum regime are well known and similar observations have previously been made for

shifted to higher frequency side in the ZnO/PS composite. The observed modifications in the ZnO vibration frequency in the ZnO/PS composite, compared to pure ZnO, as seen from FT IR and Raman studies, provide ample evidence for strong bonding between PS and ZnO. This bonding is responsible for the surface modification of ZnO by the polystyrene matrix, which removes most of the defect states by compensating for the unsatisfied valencies.

4.4 Conclusions

The synthesis of ZnO nanoparticles by the chemical method at room temperature is a reproducible and comparatively simple method. It allows control on the size of the particles through variations in precursor concentration. The ZnO/PS nanocomposite films prepared by spin coating are found to be homogeneous and the ZnO particles are well dispersed in the polymer matrix. The composite films exhibit good UV shielding properties and absorb about 90% of UVA, UVB and part of UVC radiations, in the range from 395 to 190 nm with 10% ZnO loading in the composite. The band gap enlargement from 3.2 to 4.15 eV is observed with a decrease in the size of ZnO particles in the composite films, indicating that the ZnO nanoparticles are in the regime of spatial exciton confinement. The size dependency of photoluminescence emission makes it possible to tune the emission to suit any specific application by changing the nanoparticle size, which has tremendous significance in photonics. Development of novel synthesis methods and stabilization of monodispersed semiconductor nanoparticles in transparent matrices offer good opportunities for innovative experimental research.

References

[1]   Gaponenko S V, Optical Properties of Semiconductor Nanocrystals. Cambridge University Press, Cambridge, pp. 1–51 (1998).

[2]   Gudiksen M S, Wang J and Lieber C M, J Phys ChemB 106:4036 (2002).

[3]   Ashcroft N WandMerminN D, Solid State Physics. Harcourt College Publishers, Orlando, FL, pp. 626–628 (1976).

[4]   Yi G C,Wang C and ParkW I, Semicond Sci Technol 20:S22 (2005).

[5]   Stroyuk O L, Dzhagan V M, Shvalagin VV and Kuchmiy SY, J Phys Chem C 114:220 (2010).

[6]   Huang M H,Mao S,Feick H,Yan H,WuY,Kind H, et al, Science 292:1897 (2001).

[7]   Moon TH, Jeong MC, LeeW and Myoung JM, Appl Surf Sci 280:240 (2005).

[8]   Ozgur U, Alivov YI, Liu C, Teke A, Reshchikov MA, Dogan S, et al, J Appl Phys 98:41301 (2005).

[9]   Pearton SJ, Abernathy CR, Overberg ME, Thaler GT, Norton DP, Theodoropoulou N, et al, J Appl Phys 93:1 (2003).

[10] Tsukazaki A,Ohtomo A,Onuma T,Ohtani M,Makino T, Sumiya M, et al, NatureMater 4:42 (2005).

[11] Alivisatos AP, Science 271:933 (1996).

[12] Beecroft L and Ober CK, ChemMater 9:1302 (1997).

[13] Kumar RV, Elgamiel R, Diamant Y and Gedanken A, Langmuir 17:1406 (2001).

[14] Lu N, Lu X, Jin X and Lu C, PolymInt 56:138 (2007).

[15] Shim J-W, Kim J-W, Han S-H, Chang I-S, Kim H-K, Kang H-H, et al, Colloids Surf 207:105 (2002).

[16]   Jeeju PP and Jayalekshmi S, J Appl PolymSci 120:1361 (2011).

[17]   Yao T,Zhou L, Jin YZ,Gao C,Ye ZZ,Yang TF, et al, JMater Chem20: 1594 (2010).

[18]   Chee DW and Kim BC, PolymAdv Technol 16:846 (2005).

[19]   Vossmeyer T, Katsikas L, Giersig M, Popovic I, Diesner K, Chemseddine A, et al, J Phys Chem 98:7665 (1994).

[20]   Sun Y-L, Bian J-M, Li Q-Wi and Luo Y-M, JInorgMater 25:1116 (2010).

[21]   Yao T and Woo JC (eds), Physics and Applications of Semiconductor QuantumStructures. IOP Publishing, Bristol (2001).

[22]   Luna-Moreno D, de la Rosa-Cruz E, Cuevas FJ, Regalado LE, Salas P, Rodr´ıguez R, et al, OptMater 19:275 (2002).

[23]   Davies JH, The Physics of Low-Dimensional Semiconductors. Cambridge University Press, Cambridge (1997).

[24]   Ogava S, Nagano H and Petek H, Phys Rev Lett 88:116801 (2002).

[25]   Abramowitz M and Stegun IA, Handbook of Mathematical Functions, vol. 55. Dover Publications, New York (1972).

[26]   Murray CB, North DJ and Bavendi MG, JAmChemSoc 115:8706 (1993).

[27]   Colvin VL, Alivisatos AP and Tobin JG, Phys Rev Lett 66:2786 (1991).

[28]   Brus L, J Phys Chem 90:2555 (1986).

[29]   Bylander EG, J Appl Phys 49:1168 (1978).

[30]   Vanhesde K, Seager CH, Warren WL, Tallent DR and Voiget JA, Appl Phys Lett 68:404 (1996).

[31]   Liu M, Kitai AH and Mascher P, JLumin 54:943 (1992).

[32]   Lin B, Fu Z and Zia Y, Appl Phys Lett 79:943 (2001).

[33]   Lin KF, Cheng HM, Hsu HC, Lin LJ and HsiehWF, Chem Phys Lett 409:208 (2005).

[34]   Han S, Henryk T and Venkatesh N, Phys Rev B 69:245401 (2004).

[35]   Gong Y, Andelman T, Neumark GF, O'Brien S and Kuskovsky IL, Nanoscale Res Lett 2:297 (2007).

[36]   Guo L, Yang S, Yang C, Yu P,Wang J, Ge W, et al, Appl Phys Lett 76:2901 (2000).

.....ဆဏ.....

Size dependent nonlinear optical properties of Zinc Oxide-Polystyrene nanocomposite films

The investigations carried out on the third-order nonlinear behavior of ZnO/PS nanocomposite films, containing ZnO particles with size in the range 6.5– 35 nm, by Z-scan technique are included in this chapter. ZnO/PS nanocomposite shows a self-defocusing type nonlinearity and good nonlinear absorption at 532 nm. The observed optical nonlinearity is explained based on two-photon absorption. The third-order optical susceptibility ($\chi^{(3)}$) increases with increasing particle size (R) due to the size dependent enhancement of exciton oscillator strength. These films also show a self-defocusing type negative nonlinear refraction in closed aperture Z-scan experiment. The good nonlinear response of these composite films, combined with the improved stability of ZnO nanoparticles in the polymer matrix offer prospects of application of these composite films in the fabrication of stable non-linear optical devices.

5.1 Introduction

Nanoscale materials are under active research over the past few decades, owing to their interesting versatile properties, quite different from those of the bulk form [1]. Semiconductor nanocrystals have been investigated extensively due to their promising applications in optoelectronics and photonics. The effects of particle size on optical properties are more pronounced in semiconductor nanoparticles.

Specifically, oxide semiconductor nanocrystals are currently being studied widely, considering their tunable electrical and optical properties and the potential applications in many areas, such as field emission displays, solar cells and gas sensors [2-4]. The linear and nonlinear optical properties of nanostructured semiconductors are the topics of current theoretical and experimental interest [5]. With the advent of the widespread usage of optical detectors and sensors for scientific and industrial purposes, the need has rapidly arisen for optical limiting devices that protect the photosensitive components from intense optical radiation while remaining inactive for low intensity levels. Amongst the various nonlinear optical (NLO) materials investigated, direct band gap semiconductors, such as zinc oxide have attractive nonlinear properties that make them ideal candidates for NLO based devices. Zinc oxide is having many applications in transparent electronics, photovoltaics, display devices and laser fabrication [4, 6].

Investigations into the nonlinear optical properties of the composite films containing semiconductor nanoparticles have attracted considerable attention due to their practical applications in optical switching and optoelectronic devices [7-11]. Polymers are chosen as

suitable host materials because they usually exhibit long-term stability and possess flexible reprocessability. Attractive optical properties such as fluorescence, electroluminescence and optical nonlinearity have been observed in these organic-inorganic composites.

The studies of nonlinear processes in photonic materials are significant in the context of their technological applications, especially in areas such as passive optical power limiting, optical switching, and the design of logic gates. Optical limiting (OL) is an important application of nonlinear optics, useful for the protection of human eyes, optical elements and optical sensors from intense laser pulses. Optical limiting occurs when the absolute transmittance of a material decreases with increase in input fluence. The optical limiting property occurs mostly due to absorptive nonlinearity which corresponds to the imaginary part of third order susceptibility [12]. ZnO based nanocomposites are good candidates for optical limiting against broadband laser pulses. Optical limiting can be achieved by one or more of the nonlinear optical mechanisms such as excited state absorption (ESA), free-carrier absorption (FCA), two photon absorption (TPA), thermal defocusing/scattering, photo refraction, nonlinear refraction, and induced scattering [13]. Optical limiting performance is enhanced by coupling two or more of the nonlinear optical mechanisms like self-defocusing in conjunction with TPA in semiconductors [14] or TPA of one molecule with ESA in another molecule [15].

Although optical nonlinearity has been reported in many semiconductor nano composites [16, 17], this phenomenon in ZnO/PS nanocomposite films has not been subjected to detailed investigations

yet. Hence attempts have been made, in the present work, to investigate in detail, the optical nonlinearity of polymer-modified nanocrystalline ZnO, synthesized by a wet-chemical synthesis process. Polystyrene (PS) is chosen as the host polymer material because of its excellent solubility in ordinary solvents and chemical stability. In the present work, the nonlinear optical properties of the ZnO/PS nanocomposite films are investigated by employing the Z-scan technique using nanosecond laser pulses at 532 nm. The dependence of the non linear effects on the size of the ZnO nanoparticles in the composite films is analyzed in detail.

5.2 Optical characterization

The UV-Visible transmission spectra of the films were recorded on a JASCO-V 570 spectrophotometer in the wavelength range 200 to 800 nm.

The transmission spectra of pure PS and ZnO/PS nanocomposite film are shown in figure 5.1. The composite film shows transparency around 70% in the visible region. The photograph of the freestanding ZnO/PS nanocomposite film with the printing beneath is shown in the inset of figure 5.1. It is clear that the absorption of the ZnO/PS nanocomposite film comes mainly from the ZnO nanoparticles, especially below 400 nm. ZnO/PS nanocomposite film exhibits strong absorption around 350 nm and the optical band gap of the composite films is estimated from the plot of $(\alpha h \upsilon)^2$ vs. $(h \upsilon)$ for the absorption coefficient α [20]. An increase in the band gap with decrease in particle size of ZnO is observed which is attributed to the quantum size effect [21].The band gap of ZnO nanoparticles increases as the size decreases, with a decrease in the concentration of KOH solution (Figure 5.2).
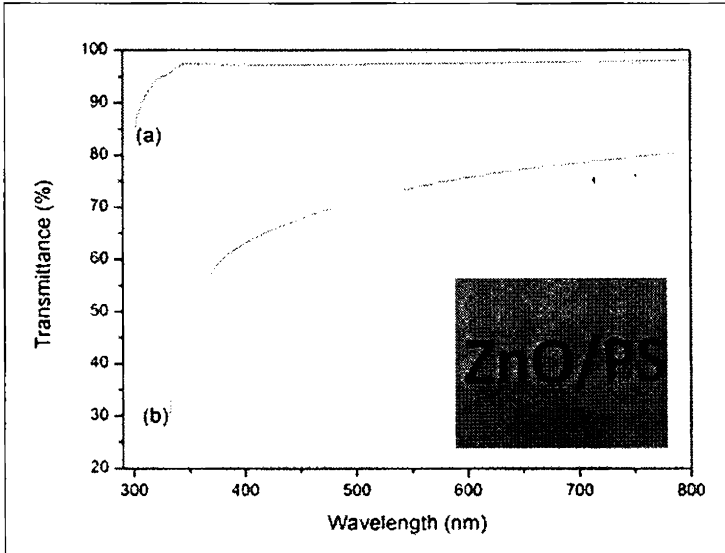
Figure 5.1: The transmission spectra of (a) PS film (b) ZnO/PS nanoc
film (Inset shows the photograph of ZnO/PS freestanding
the printing beneath it).
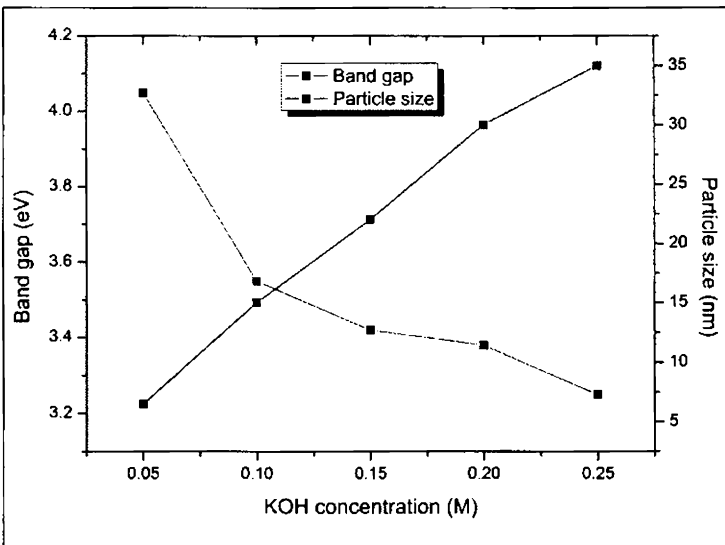
Figure 5.2: Dependence of band gap energy and particle size of Zn
composite film on KOH concentration.

5.3 Nonlinear optical (NLO) studies

The optical nonlinearity of the nanocomposite films was studied by Z-scan technique. This method was used for measuring the sign and magnitude of nonlinear refractive index and nonlinear absorption coefficient [18, 19]. A Q-switched Nd-YAG laser with a pulse width of 7ns at 532 nm was used in the experiment. A lens of focal length 23 cm was used to focus the laser pulses. Samples in the form of thin film were used for the experiment. The sample was moved in the direction of light incidence near the focal spot of the lens. The transmitted beam energy, reference beam energy and their ratio were measured simultaneously by an energy ratio meter (Rj7620, Laser Probe Corp.) having two identical pyroelectric detector heads. The linear transmittance of the far field aperture S, defined as the ratio of the pulse energy passing the aperture to the total energy was measured to be approximately 0.21. The data was analyzed by using the procedure described by Sheik Bahae et al. [18] and the nonlinear coefficients were obtained by fitting the experimental Z-scan plot with the theoretical plots. The experimental set up and other details are given in chapter 2.

5.3.1 Open aperture Z-scan

Nonlinear optical properties of ZnO/PS nanocomposite films, containing ZnO nanoparticles having different particle size, were investigated by the Z-scan technique. Figure 5.3(a-e) shows the nonlinear absorption of ZnO/PS nanocomposite films at a typical laser energy of 25μJ for an irradiation wavelength of 532 nm. The open-aperture curve exhibits a normalized transmittance valley, indicating the presence of induced absorption. The observed nonlinearity is found to be

of the third-order, as it fits to a two photon absorption process (TPA). The corresponding net transmission is given by [18]

$$T(z) = \frac{c}{q_{0\sqrt{\pi}}} \int_{-\infty}^{\infty} ln(1 + q_0 e^{-t^2}) dt,$$ ---------------------------(5.1)

where q_0 $(z, r, t) = \beta I_0$ (t) L_{eff}.

Here, $L_{eff} = 1 - e^{-\alpha L} /\alpha$, is the effective thickness with linear absorption coefficient α and nonlinear absorption coefficient β, and I_0 is the irradiance at focus. The solid curves in figure 5.3(a-e) represent the theoretical curves having best fit to the experimental data. The experimentally obtained values of nonlinear absorption coefficient β at a pulsed energy of 25μJ are shown in table 5.1.

From the open aperture Z-scan curves it is found that the ZnO/PS nanocomposite films do exhibit a large induced absorption behavior. It is observed that as the band gap decreases (that is, as the particle size increases) the rate of two photon absorption increases which is attributed to an inverse proportionality between β and the third power of band gap [13]. Hence the dip in the open aperture curve increases with increase in particle size leading to the observed increase in the limiting efficiency with increase in the particle size. Although similar investigations have been reported in ZnO/PMMA nanocomposite films [22], in the present case, the curves of ZnO/PS films show a better fit to the theoretical equations for TPA, compared to the former. The transmittance minimum reported is about 0.65 for ZnO/PMMA films. For ZnO/PS films of the present work, the transmittance minimum is about 0.43, which highlights the better optical limiting efficiency of the latter compared to the former.

The nonlinear coefficients are calculated as described in chapter 2 (given in table 5.I), and show fairly high values of nonlinear parameters. The nonlinear absorption coefficient substantially increases as the size of the ZnO particles in the nanocomposite increases.

Generally, induced absorption can occur due to a variety of processes, like two photon absorption, free carrier absorption, transient absorption, inter band absorption, photo ejection of electrons and nonlinear scattering, which are reported to be operative in nanoclusters. In the present study, the theory of two photon absorption (TPA) process fits well with the experimental curve and hence TPA can be established as the basic mechanism. The reduced normalized transmittance values obtained (Figure 5.3) for larger particles show that the samples can be used as efficient optical limiters. Optical limiting devices (optical limiters) protect light-sensitive detectors such as eye or CCD cameras, from possible damage caused by intense light exposure.
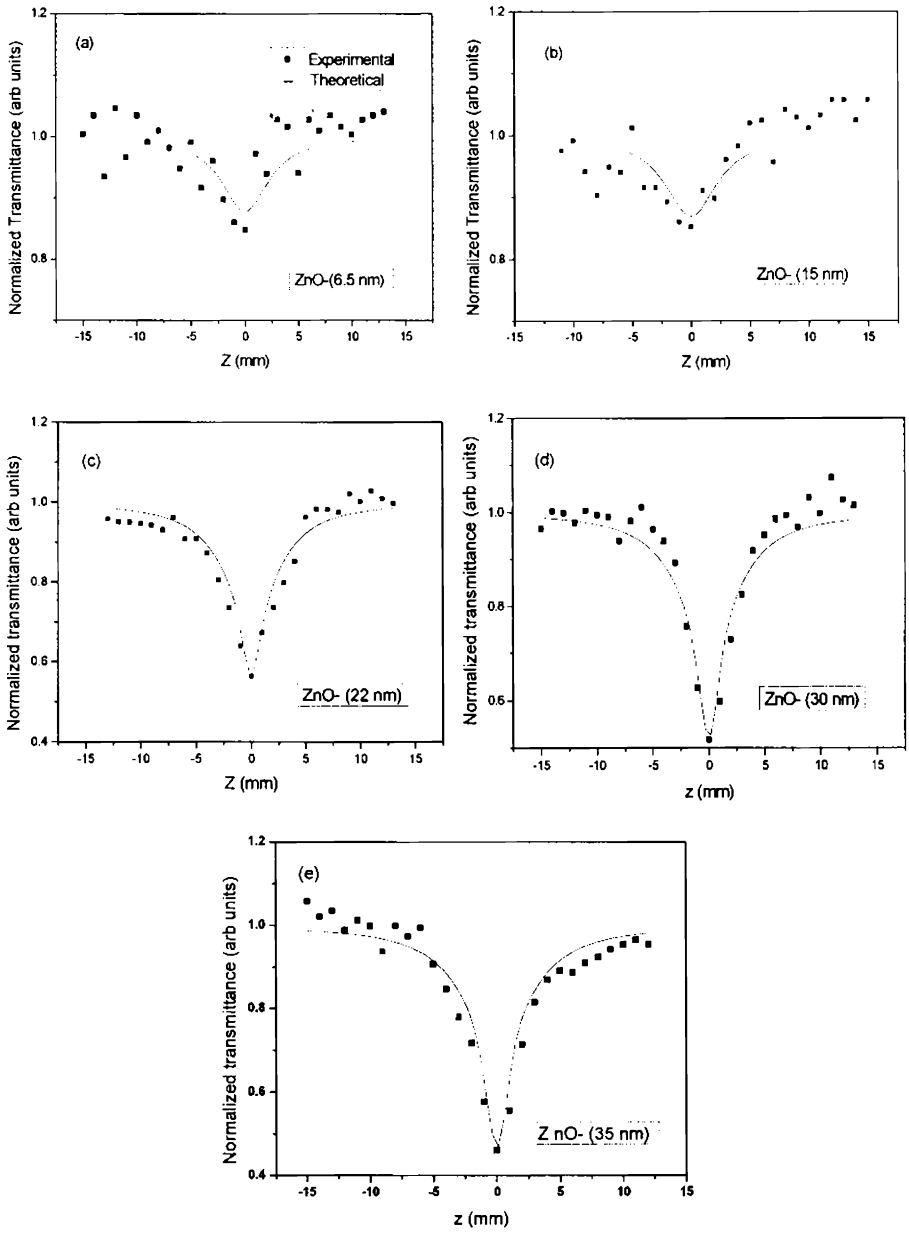
Figure 5.3(a-e): Open aperture Z-scan curves of ZnO/PS nanocomposite films containing ZnO particles of different size.

5.3.2 Closed aperture Z-scan

The closed aperture Z-scan traces of ZnO/PS nanocomposite films for an irradiance wavelength of 532 nm from pulsed Nd-YAG laser of energy 25μJ are given in figure 5.4. The closed-aperture curve exhibits a peak to valley shape, indicating a negative value of the nonlinear refractive index n_2 [23]. For samples with appreciable refractive and absorptive nonlinearities, closed aperture measurements show contributions from both, i.e. the intensity-dependent changes in the transmission and in refractive index [18]. By dividing the normalized closed aperture transmittance data by the corresponding normalized open-aperture data, one can retrieve the phase distortion created due to the change in refractive index.

The value of the difference between the normalized peak and valley transmittance, T_{p-v} can be obtained by the best theoretical fit from the results of divided Z-scan curve. The nonlinear refractive index n_2 is calculated from T_{p-v} in closed aperture Z-scan using equation (5.2) and is tabulated in table 5.1,

$$T_{p-v} = 0.406(1 - S)^{0.25} |\Delta\Phi_0|, \text{ where } |\Delta\Phi_0| = (2\pi/\lambda) \, n_2 \, I_0 \, L_{\text{eff}} \quad \text{-----(5.2)}$$

where S is the linear transmittance of the far field aperture and λ is the excitation wavelength. From the closed aperture Z-scan fit, $\Delta\Phi_0$ can be obtained.

The peak-valley trace in the closed aperture Z- scan shows that these samples have self-defocusing (negative, $n_2 < 0$) nonlinearity, as reported for ZnO/PMMA nanocomposite [22].

The nonlinear refractive index is also found to increase as the size of the ZnO particles in the nanocomposite increases.
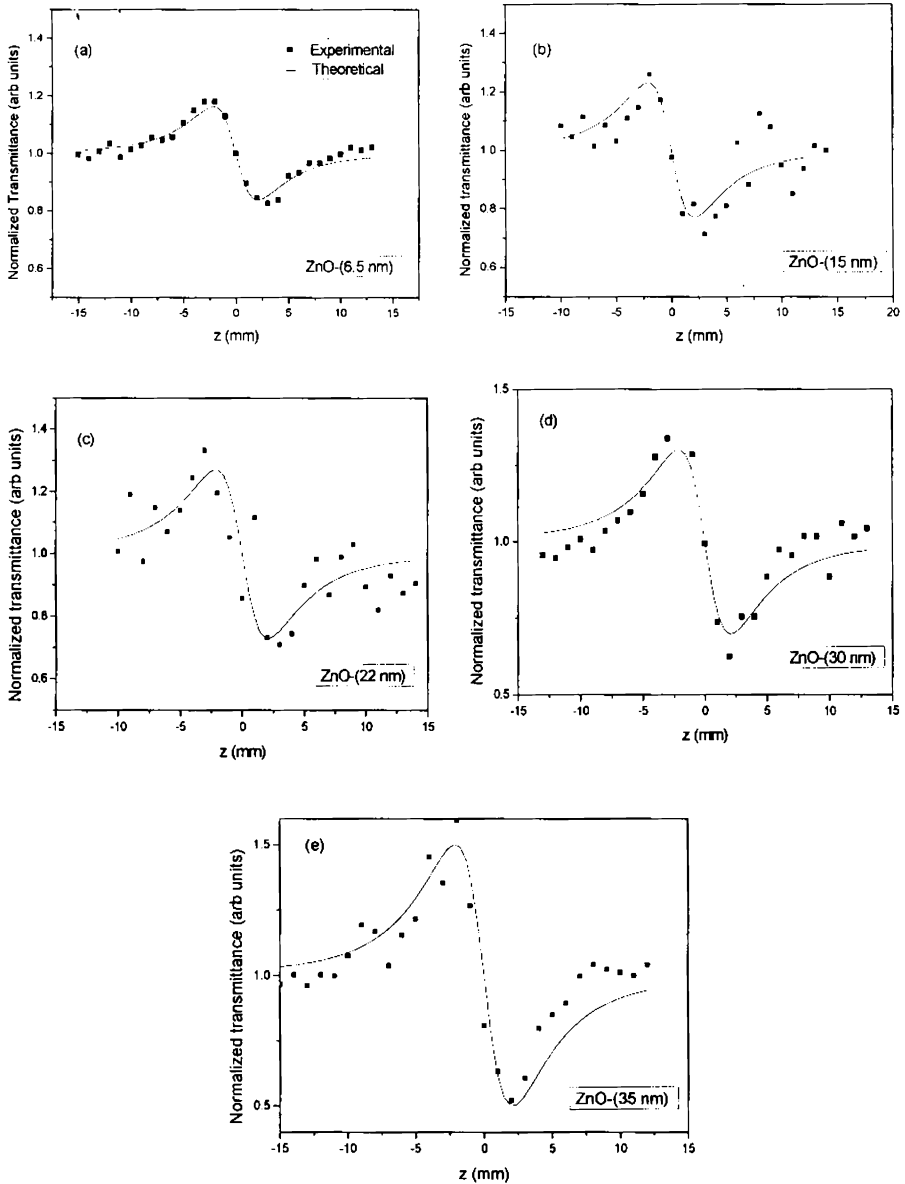
Figure 5.4 (a-e): Closed aperture Z-scan curves of ZnO/PS nanocomposite films containing ZnO particles of different size

5.3.3 Size dependent enhancement of third order nonlinear susceptibility

By analyzing the open aperture and closed aperture Z-scan data, using the procedure described in chapter 2, the nonlinear susceptibility is calculated.

The nonlinear refractive index n_2 is related to the real part of nonlinear susceptibility, Re ($\chi3$) by the relation,

$$Re\ (\chi3) = n_0\,n_2/3\pi\quad (esu) \text{--} (5.3)$$

The imaginary part of third order susceptibility Im ($\chi3$) determines the strength of the nonlinear absorption. The nonlinear absorption coefficient, β is related to Im ($\chi3$) by the relation

$$
\begin{aligned}
Im\ (\chi3) &= \ \varepsilon_0\,n_0^2\,c^2\,\beta\,/\,\omega\ (m^2\,V^{-2}) \\
&= \ n_0^2\,c^2\,\beta\,/\,240\,\pi^2\,\omega \quad (esu) \text{------------------------} (5.4)
\end{aligned}
$$

where n_0 is the linear refractive index, ε_0 is the permittivity of free space and c the velocity of light in vacuum.

From the real and imaginary parts of ($\chi3$), the modulus of third order nonlinear susceptibility can be found out using equation (5.5).

$$|\ (\chi3)\ | = [\ [Re\ (\chi3)]^2 + [Im\ (\chi3)]^2]^{1/2} \text{------------------------} (5.5)$$

The magnitude of ($\chi3$) is significantly affected by the crystallite size and it determines the strength of nonlinearity of the material.

The third order nonlinear susceptibility values of ZnO/PS composite films at a pulsed energy of 25μJ for a wavelength of 532 nm

are tabulated in table 5.1.These values are within an error of 7% arising mainly by the uncertainty in intensity measurements on the samples and the fitting error.

There is enhancement in the nonlinear susceptibility values with increase in particle size. The enhancement of nonlinear optical properties with increasing particle dimension in the weak confinement regime, essentially originates from the size dependent enhancement of oscillator strength of coherently generated excitons [24]. In the weak confinement regime the Coulomb interaction between the electron and hole yields an exciton which is confined as a quasiparticle. The optical nonlinearity arises from the exciton-exciton interaction. Theoretical studies have shown that the confinement of excitonic envelope wave function gives rise to the enhancement in oscillator strength for an exciton within the nanoparticle by a factor of R^3/a_B^3, where R is the radius of the nanoparticle and a_B, the exciton Bohr radius [24].The effect of large oscillator strength is brought out only in the weak confinement regime. This size dependent oscillator strength has been experimentally confirmed in CuCl quantum dots [25, 26]. Such oscillator strength effect will result in an enhancement of the nonlinear susceptibility, and hence $\chi 3$ depends on the crystallite size [27, 28]. Hence, in the present study, the observed enhancement of nonlinear optical properties with increase in particle size can be attributed to the size dependent enhancement of exciton oscillator strength.

The nonlinear susceptibility is found to be size dependent, without showing any saturation behaviour in the size range of the present investigation. The observed high susceptibility values measured by the

Z-scan technique establish the fact that the ZnO/PS nanocomposite films investigated in the present work have good nonlinear optical response and can be chosen as ideal candidates with high prospects of applications in nonlinear optics [29, 30].

Table 5.1: Variation of band gap and nonlinear parameters with the ZnO nanoparticle size in the composite

KOH concentration (M)	Particle size nm	Band gap (eV)	β (cm/GW)	n_2 (10^{-10} m^2/W)	$(\chi 3)$ (10^{-12} esu)
0.05	6.5	4.05	82	-4.30	5.71
0.10	15	3.55	89	-6.08	6.17
0.15	22	3.42	258	-7.15	7.28
0.20	30	3.38	270	-7.99	8.81
0.25	35	3.30	281	-13.3	14.0

5.4 Conclusion

The nonlinear optical properties of ZnO/PS nanocomposite films are investigated for optical limiting application. The composite films show a self-defocusing type (negative refractive index, n_2) nonlinearity and good nonlinear absorption behaviour. The observed optical nonlinearity is explained based on two-photon absorption. The dependence of the nonlinear parameters like nonlinear absorption coefficient, nonlinear refractive index and third order susceptibility on the ZnO particle size has been investigated and these parameters are found to be enhanced for larger particle size in the range of 6.5 to 35 nm. The observed nonlinear behaviour of the nanocomposite films is much pronounced compared to that of bulk ZnO. The fairly low transmittance

of about 0.43 observed for these nanocomposite films is ideal for the fabrication of efficient optical limiters in sensor protection applications.. The ZnO nanoparticles embedded in the polystyrene matrix are highly stable and stable optical devices can be fabricated.

References

[1]   C. C Baker, A. Pradhan, S. Ismat Shah, Encyclopedia of Nanoscience and Nanotechnology Vol 5, p-463 (American Scientific Publishers, California 2004)

[2]   J. Hu, L.S. Li, W. Yang, Science 292 (2001) 2060-2063.

[3]   H. Wu, X. Peng, A.P. Alivisators, Adv. Mater. 11 (1999) 623-927.

[4]   W. Lee, H.I. Yoo, J.K. Lee, Chem. Commun. 24 (2001) 2530-2531.

[5]   Y. Kayanuma, Phys. Rev. B 38 (1988) 9797-9805.

[6]   L. Guo, J. X.Cheng, X.Y.Li, Y. J.Yan, S. H. Yang, C. L. Yang, Mat. Sci. Eng. C.16 (2007) 123-127.

[7]   J.. Pyun and K. Matyjaszewski Chem. Mater 13 (2001) 3436-3454

[8]   P.P Jeeju, S Jayalekshmi J. Appl. Polym. Sci. 120 (2011) 1361-1366.

[9]   R. F. Haglund, L.Yang,R. H. Magruder III, J. E. Wittig, K. Becker, and R. A. Zuhrl, Opt. Lett. 18, 373 (1993)

[10]   Hache and M. Bourgeois, Appl. Phys. Lett. 77 (2000) 4089-4091

[11]   Y. Hamanaka, K. Fukata, A. Nakamura, L. M. Liz-Marzán, P.Mulvaney, Appl. Phys. Lett 84 (2004) 4938-4940.

[12]   L. Irimpan, B. Krishnan, A. Deepthy, V. P. N. Nampoori, and P. Radhakrishnan, J. Appl. Phys. 103 (2008) 094914 1-8.

[13]   L.W. Tutt, T.F. Boggess, Prog.Quanta.Electr. 17 (1993) 299-338.

[14]   E. W. Van Stryland, H. Vanherzeele, M. A. Woodall, M. J. Soileau, A. L. Smirl, S. Guha, T.F. Boggess, Opt. Eng. 24 (1985) 613-623.

[15] M. P. Joshi, J. Swiatkiewicz, F. Xu, P. N. Prasad, B. A. Reinhardt, R. Kannan, Opt. Lett. 23 (1998) 1742-1744.

[16] M. S. Neo, N. Venkatram, G. S. Li, W. S. Chin, and Ji Wei, J. Phys. Chem. C 113 (2009) 19055-19060.

[17] C. Wang, L. Guan, Y. Mao, Y. Gu, J. Liu, S. Fu and Q. Xu, J. Phys. D: Appl. Phys. 42 (2009) 045403.

[18] M.S. Bahae, A.A. Said, E.W. van Stryland, Opt. Lett. 14 (1989) 955-957.

[19] R. Viswanatha, S. Sapra, B. Satpati, P.V. Satyam, B.N. Dev, D.D. Sharma, J. Mater. Chem. 14 (2004) 661-668.

[20] P. P. Jeeju, A. M. Sajimol, V.G. Sreevalsa, S. J.Varma, S.Jayalekshmi, Polym. Int. 60 (2011) 1263-1268.

[21] S. Furukawa, T. Miyasato, Phys. Rev. B 38 (1988) 5726-5729.

[22] R. Sreeja, Jobina John, P.M. Aneesh, M.K. Jayaraj, Optics Communications 283 (2010) 2908-2913.

[23] H. S. Waff, K. Park, Phys. Lett. A 32 (1970) 109-110.

[24] E. Hanamura, Phys. Rev. B 37 (1988) 1273-1279.

[25] A Nakamura, H Yamada and T Tokizaki, Phys. Rev. B 40 (1989) 8585-8588.

[26] T Itoh, M Furumiya and C Gourdon;, Solid State Commun. 73 (1990) 271-274.

[27] T. Kataoka, T. Tokizaki and A. Nakamura; Phys. Rev. B 48 (1993) 2815-2818.

[28] L. Irimpan, A Deepthy, Bindu Krishnan, V P N Nampoori and P Radhakrishnan, Applied Physics B: Lasers and Optics 90 (2008) 547-556.

[29] D. Jezequel, J. Guenot, N. Jouini and F. Fievet; J.Mater.Res. 10 (1995) 77-83.

[30] E W Seelig, B Tang, A Yamilov, H Cao and R P H Chang; Materials Chemistry and Physics 80 (2002) 257-263.

.....ℰℭℛ.....

Chapter 6

On the linear and nonlinear optical properties of thermally stable, ZnO/PS-PMMA nanocomposite films

The linear and nonlinear optical properties of highly transparent and thermally stable zinc oxide (ZnO)/ poly (styrene) - poly (methyl methacrylate) (PS-PMMA) nanocomposite films have been investigated and the details are given in this chapter. ZnO nanoparticles of size around 10 nm, as confirmed from Transmission electron spectroscopy (TEM) studies are used to synthesize the ZnO/PS-PMMA nanocomposite samples. The nanocomposite films, deposited by spin coating technique are characterized by XRD, FT-IR, AFM, UV-Vis-NIR spectroscopy, TGA, Photoluminescence (PL) spectroscopy and Z- scan technique. In present work, the host matrix used is the blend of the two polymers, PS and PMMA. Both of these polymers are highly transparent and environmentally stable and proven to be excellent for forming nanocomposites with ZnO.   Hence, in the present work, the nanocomposite samples of ZnO with PS-PMMA blend have been synthesized and their linear and nonlinear optical properties, investigated. Excellent optical limiting and efficient UV shielding are found to be the significant advantageous characteristics of these composite samples.

6.1 Introduction

Recently, nanocomposite materials have received a lot of attention and close scrutiny of scientists and researchers. The driving force behind the fabrication of novel composites is to achieve functional properties for promising applications in many fields of technology such as optoelectronics, electrochemistry, coating technology and catalysis [1]. Nanocomposite materials are multiphase solids where one of the phases has a dimension less than 100 nm. These materials typically consist of an inorganic (host) solid containing an organic component or vice versa, or they may also consist of two or more inorganic/organic phases in some combinational form with the constraint that at least one of the phases is nanosized. The development of polymer-based nanocomposites, which exhibit interesting optical properties, such as tailored absorption/ emission or strong optical nonlinearities has attracted great interest because of their potential optoelectronic applications [2].

Nanostructures of ZnO have attracted significant attention due to their proposed applications in the low voltage and short-wavelength electro-optical devices, transparent ultraviolet protection films, gas sensors, optical limiters and spintronic devices [3-5]. A great deal of research has been focused on the development of ZnO/polymer nanocomposite materials using different polymer systems. Polystyrene (PS) and polymethyl methacrylate (PMMA) are transparent thermoplastic materials, with lots of prospects for making composite materials with nanostructured ZnO. Introduction of ZnO filler into polymeric matrices can modify the optical, electrical, and mechanical properties [6-8]. Composite materials consisting of zinc oxide and

polymers exhibit the merits of blending the advantageous properties of zinc oxide with the processability and flexibility of polymers.

In the present study, PS/PMMA blend is used for making ZnO-polymer nanocomposite. PS/PMMA blend is a well-known immiscible combination for which bulk and surface phase separation has been observed [9, 10]. However, due to the low entropy of mixing, polymeric blends are mostly incompatible and exist as phase separated under appropriate conditions. In incompatible polymer blends, the thin film of the blend may undergo phase separation even during preparation. This behavior has been observed in a variety of incompatible blend systems [11, 12].In the present work, highly transparent thin films of ZnO/PS-PMMA composite are prepared by spin-coating technique. Although there are a few reports on the synthesis and various properties of this sort of nanocomposite materials [13-17], there are no detailed studies on the nonlinear optical characterization of ZnO/PS-PMMA nanocomposite films. The work presented in this chapter is an attempt to investigate in detail the linear and nonlinear optical properties of the spin-coated ZnO/PS-PMMA nanocomposite films and see how the choice of the polymer blend in the nanocomposite is influencing the optical characteristics. The results obtained are compared with those of the ZnO/PS and ZnO/PMMA composite films.

6.2   Synthesis details

ZnO nanoparticles were synthesized using the method described in chapter 4, and were found to be of average size ~10 nm by XRD analysis. The ZnO/PS-PMMA nanocomposite solution was prepared by adding 10 wt% of ZnO powder sample into the polymer blend solution

(10% w/v) of PS and PMMA (PS wt% = 50, Mw-175,000 g/mol; PMMA wt% = 50, Mw-140,000 g/mol) in toluene and stirring the mixture for two hours and then sonicating for ten minutes to ensure that the ZnO nanoparticles could be dispersed well. This solution was used to deposit thin films by spin coating on ultrasonically cleaned and optically flat glass substrates (Spin 150). The thin film samples were dried in an oven at 60°C. The nanocomposite films of ZnO/PS and ZnO/PMMA were also prepared using the method described in chapter 4.

6.3   Structural characterization

6.3.1 XRD analysis

X-ray diffraction spectra (XRD) of the samples were taken on a Rigaku X-ray Diffractometer   with Cu - Kα (1.5418 A°) radiation operating at 30 kV and 20 mA. Scanning was carried out in the 2θ range from 10 to 70° at a scan speed of 5° per minute (2° per minute for the films).

The XRD patterns of ZnO nanparticles, PS-PMMA blend and ZnO/PS-PMMA nanocomposite films are shown in figure 6.1. The average ZnO particle size is determined from the X-ray line broadening using the Scherrer equation, $\beta = k\lambda / d\cos\theta$,   where β is the full width at half maximum (FWHM) in radians of the diffraction peak, λ is the X-ray wavelength, k is a constant (0.89), θ is the Bragg angle of the peak and d is the average particle size . The particle size is found to be ~10 nm. The XRD pattern of the composite film consists of a broad non-crystalline peak of the polymer blend and sharp diffraction peaks of ZnO. The XRD pattern of PS-PMMA blend does not show any crystalline peak. The

presence of ZnO in the composite produces neither new peaks nor any peak shifts with respect to the polymer blend, showing that nano ZnO filled PS-PMMA composite consists of phase separated structures.
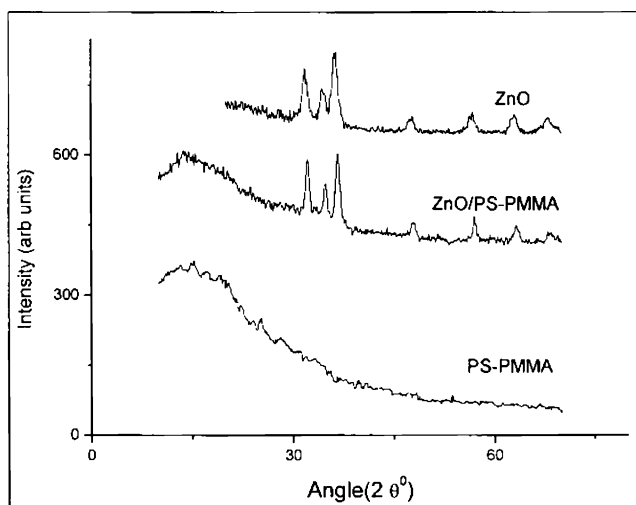
Figure 6.1: XRD patterns of a) ZnO particles b) ZnO/PS-PMMA and c) PS-PMMA blend

6.3.2 TEM and AFM analysis

The morphology and size of the synthesized ZnO particles were studied by transmission electron microscopy (TEM). The micrographs were taken using JEOL 3010 instrument with a UHR pole piece. This gives a lattice resolution of 0.14 nm and a point to point resolution of 0.12 nm. The TEM and HRTEM images of ZnO nanoparticles are shown in figure 6.2 (a & b). The morphology of ZnO is hexagonal. The average particle size of ZnO determined from the XRD peaks using the Debye-Scherrer formula is found to be close to the one estimated from TEM analysis.
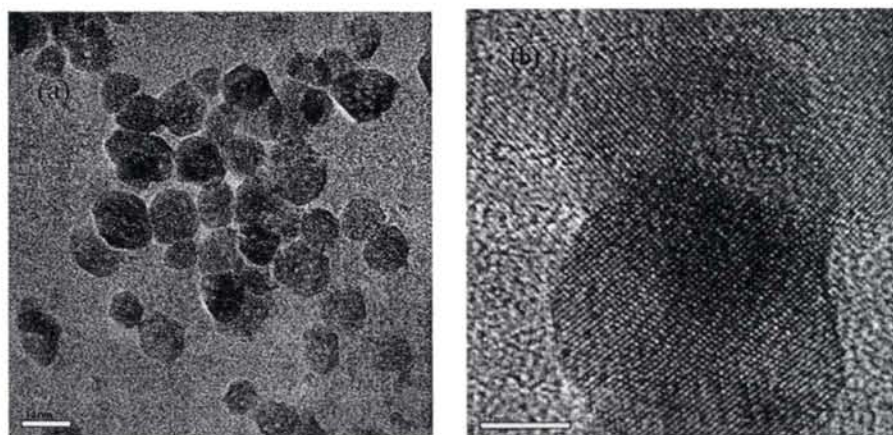
Figure 6.2: a) TEM and b) HRTEM images of ZnO particles of size ~ 10 nm

The AFM pictures of the ZnO/PS-PMMA nanocomposite films are shown in figure 6.3. AFM images of the composite films were obtained with Park XE-100 Atomic Force Microscope The uniform dispersion of the nanoparticles in the polymer blend matrix (Figure 6.3a) and the smooth surface morphology of the films (Figure 6.3b) are clear from the AFM images. The rms roughness estimated is around10 nm. The morphology of PS-PMMA blend has already been reported by Saziye Ugur et al. [18]. According to them the morphology of PS-PMMA corresponds to that of an interpenetrating network through the whole volume of the sample. The ZnO particles are evenly dispersed in both PS and PMMA which is clear from the AFM image. The AFM pictures confirm the formation of a bi-continuous phase structure where both components form phases that partly or fully form a continuous phase.
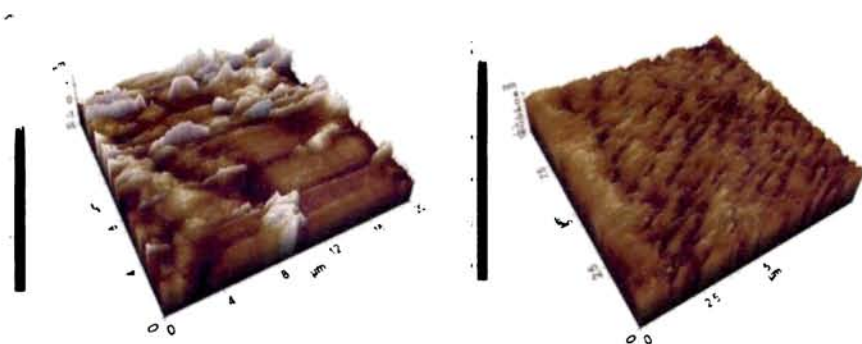
Figure 6.3: AFM pictures of ZnO/PS-PMMA nanocomposite film

6.3.3 FT IR analysis

The chemical structure of the synthesized ZnO particles and the composite film was studied using Fourier transform infrared (FT-IR) spectroscopy. The spectra of the samples were obtained with AVTAR 370 DTGS FT-IR spectrophotometer in the wave number range 400–4000 cm^{-1}.

Figure 6.4 shows the FT-IR spectra of ZnO, PS-PMMA and ZnO/PS-PMMA nanocomposite. FT-IR analysis was used to characterize the functional groups of the nano-ZnO and ZnO/PS-PMMA nanocomposite. The spectrum of the nanocomposite exhibits the characteristic vibrations corresponding to polymeric groups and ZnO. In the spectrum of ZnO, the bands observed at 424, 453, and 527 cm^{-1} are assigned to Zn-O vibrations [19-21] out of which the bands at 453 and 527 cm^{-1} are present in the ZnO/PS-PMMA composite spectrum confirming the presence of ZnO in the composite.

The bands centered at 1338 and 1412 cm^{-1} observed in the ZnO spectrum are attributed to the stretching vibrations of C= O and C= C

groups in acetate species. The characteristic vibration bands of aromatic C = C of styrene units are observed at 1452, 1493, and 1601 cm^{-1} in the spectra of PS-PMMA and ZnO/PS-PMMA but the relative intensity of these peaks in the composite has slightly changed. In the spectrum of the composite, the absorption band at 1735 cm^{-1} is characteristic of C=O stretching vibration from PMMA. The peak at 1151 cm-^{1} is due to the C-O-C stretching vibration of the polymer blend linkage [22, 23].The peaks due to the adsorbed acetate species cannot be clearly distinguished in the ZnO/PS-PMMA spectra. This could be due to the presence of the polymer blend matrix in which the ZnO nanoparticles are homogeneously dispersed. The bands at 1382 and 1450 cm^{-1} correspond to symmetrical bending vibration and asymmetrical bending vibration of methyl group, respectively. The absorption band around 3424 cm^{-1} is assigned to OH vibration on the ZnO surface. The bands centered at 2924 and 2850 cm^{-1} observed in PS-PMMA and ZnO/PS-PMMA spectra are assigned to the asymmetric and symmetric stretching vibrations of CH$_2$. respectively.

The PS-PMMA matrix can bring about considerable surface modification of the ZnO nanoparticles by eliminating most of the adsorbed species on the surface. The changes in the relative intensities of the bands in the region 1500 cm^{-1}, in the composite can be due to the minute presence of adsorbed species on the surface of the ZnO nanoparticles.
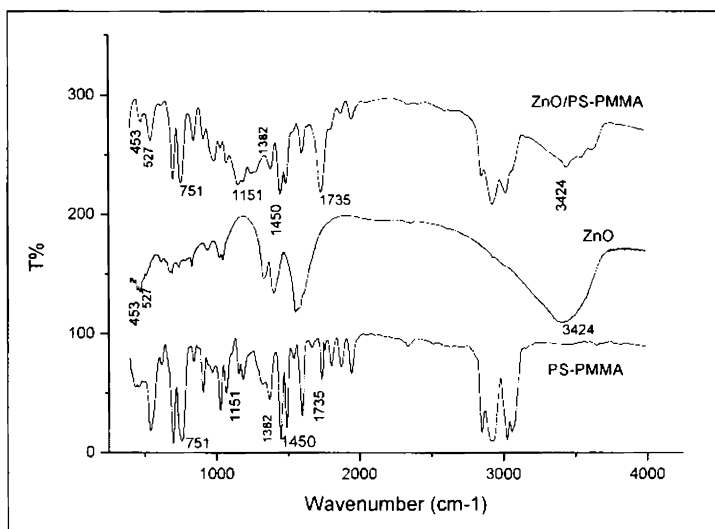
Figure 6.4: FT-IR spectra of a) ZnO/PS-PMMA nanocomposite b) ZnO and c) PS-PMMA blend.

The absorption bands corresponding to aromatic C-H stretching are observed in the range 2900-3200 cm^{-1}. Because the characteristic bands of PS-PMMA and ZnO are both observed in the ZnO/PS-PMMA spectrum, it is clear that ZnO is well dispersed in the PS-PMMA matrix

6.4 Thermal analysis

Thermo gravimetric analysis (TGA) of the samples was carried out on a Diamond TG/DTA instrument. Samples were heated to $1000^{0}C$ at a scan rate of $10^{0}C$ per minute in nitrogen atmosphere. The thermal degradation profiles of PS-PMMA and ZnO/PS-PMMA nanocomposite under nitrogen atmosphere are given in figure 6.5. The percentage weight loss of the samples at different temperatures is summarized in table 6.I. The presence of the nanosized ZnO increases the degradation temperature of the polymer composite. The degradation onset temperature (T_{onset}) of ZnO/PS-PMMA composite, measured as the

temperature required for percentage degradation is higher than that of PS-PMMA blend beyond 25% degradation. $T_{0.1}$, $T_{0.2}$ ....$T_{0.9}$ denotes the temperatures for10%, 20% ...90% degradation in weight, respectively (Table 6.1). The composite is more thermally stable compared to PS-PMMA blend. The dispersion of ZnO nanoparticles in the polymer blend enhances the thermal stability of the composite.
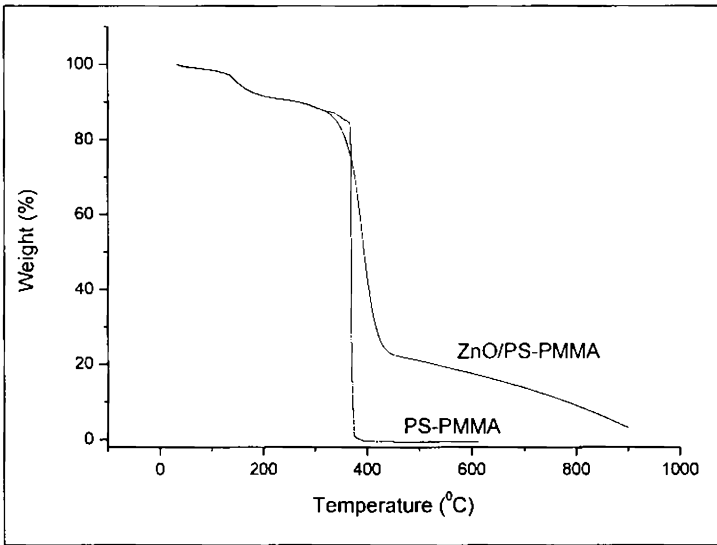
Figure 6.5: TGA curves of PS-PMMA and ZnO/PS-PMMA nanocomposite.

Table 6.1: TGA data of PS-PMMA and ZnO/PS-PMMA nanocomposite

	$T_{0.1}$	$T_{0.2}$	$T_{0.3}$	$T_{0.4}$	$T_{0.5}$	$T_{0.6}$	$T_{0.7}$	$T_{0.8}$	$T_{0.9}$
PS-PMMA	268	368	369	369	370	370	370	371	372
ZnO/PS-PMMA	264	359	377	386	394	404	417	527	859

6.5 Optical studies

6.5.1 UV-Visible absorption spectroscopy

UV-Visible absorption spectra of the samples were recorded on a JASCO-V 570 spectrophotometer in the wavelength range 200 to 800 nm.

The UV-Visible absorption spectra of the polymer blend and the ZnO/polymer nanocomposite films are shown in figure 6.6. Pure PS-PMMA blend films do not show any appreciable UV absorption, but an absorption window is found in the range 200-365 nm for the ZnO/PS-PMMA composite films. The ZnO/PS-PMMA films exhibit excellent UV absorption of about 94% spread over a uniform absorption window of about 165 nm width. Furthermore, the absorption peak wavelength of the composite films is substantially blue shifted relative to that of bulk ZnO (~ 373nm) due to the strong confinement effect [24].

The thickness of the nanocomposite films measured using the thickness profiler (Dekdak 6M Stylus Profiler) is found to lie in the range 1 to 5 μm for all the films investigated in the present work. In this thickness range, the spin coated films are also found to be homogeneous. In a recent work by Junlin Ge et al. [17] ZnO/PS-PMMA nanocomposite films are shown to exhibit UV-shielding efficiency in the wavelength range from 300 to 360 nm. Furthermore, the thickness of their films is very high, which is about 200 μm, and the technique of film deposition is solution casting where one cannot control the film thickness properly. In the present work, about 5 μm thick spin-coated film of ZnO/PS-PMMA nanocomposite is showing about 94% UV absorption in the wavelength range between 200 and 365 nm with 10% of ZnO loading in the composite. These films are highly transparent in the visible range and offer prospects of application as transparent UV radiation protectors in the wavelength range from 200 to 365 nm. The presence of ZnO nanoparticles, thus, enhances the UV absorption of the composite films and modifies the overall optical behaviour of polymer blend films.
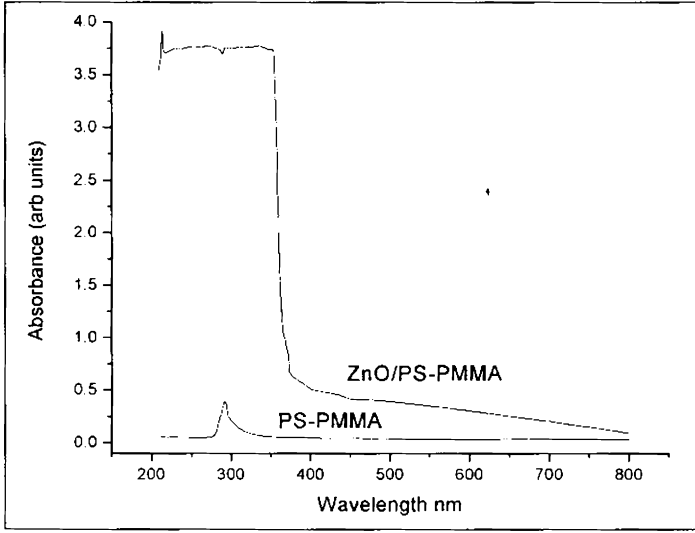
Figure 6.6: UV-Vis absorption spectra of PS-PMMA and ZnO/ PS-PMMA composite films
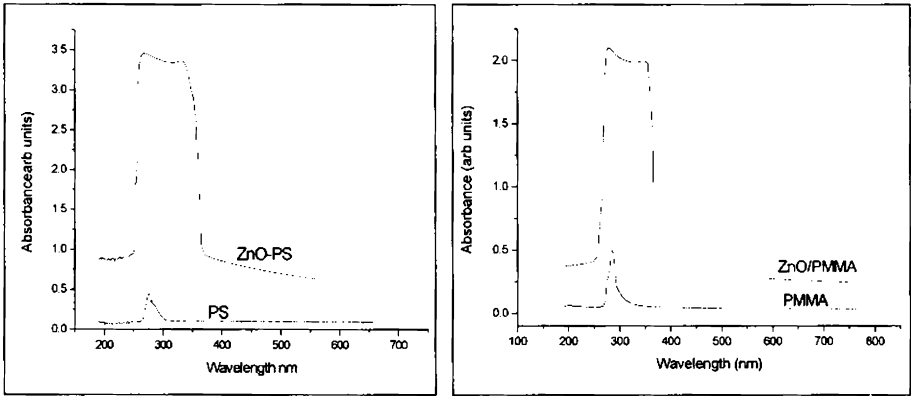
Figure 6.7: UV-Vis absorption spectra of ZnO/PS and ZnO/PMMA nanocomposite films

UV-Vis absorption spectra of ZnO/PS and ZnO/PMMA nanocomposite films prepared under the same conditions are shown in figure 6.7 for comparison. An absorption window is found in the range 255-365 and 250-366 nm for the ZnO/PMMA and ZnO/PS composite

films respectively. Among these ZnO/polymer nanocomposites, ZnO/PS-PMMA shows the highest intensity of UV absorption with maximum width for the absorption window The excellent optical characteristics observed in ZnO/PS-PMMA nanocomposite can be related to the formation of an interpenetrating network (IPN) of PS and PMMA in the polymer blend. The formation of IPN offers better possibilities for getting extended regions of pi conjugation which can influence the optical properties significantly.

6.5.2 Photoluminescence

The room temperature photoluminescence emission spectra of ZnO nanoparticles and the composite samples were obtained with Fluoromax-3 Spectroflurimeter using Xe lamp as excitation source under an excitation at 325 nm. The photoluminescence emission spectra of ZnO and ZnO/PS-PMMA nanocomposite films are shown in figure 6.8. The PL spectrum of ZnO depicts an intense emission peak at 370 nm along with a broader but more intense emission peak in the longer wavelength side centred about 522 nm. A kink is also observed in the blue region around 460 nm. The broad PL band at around 522 nm has already been reported in bulk ZnO as well as in ZnO quantum dots by many researchers [25-27]. The composite films show intense luminescence emission centered around 375 nm in the UV region. The intensity of the broad luminescence observed around 522 nm relative to that of the UV luminescence decreases considerably and is almost quenched in the spectrum of the composite film. The kink observed in the blue region of the ZnO spectrum is less visible in the spectrum of the composite film.

The emission peak in the visible region observed for ZnO nanoparticles is due to the defect levels in ZnO. Since ZnO is nanostructured, there is the possibility of the formation of higher concentration of surface defects. This is the reason for the enhanced intensity of the emission peak in the visible region compared to the near band edge emission in the UV region. In the nanocomposite, due to the surface passivation effect of the polymer blend matrix, most of the dangling bonds will be compensated for. This in turn results in the observed quenching of the emission peak in the visible region in the ZnO/PS-PMMA nanocomposite. Subsequently, the emission gets completely confined to the near band edge emission in the UV region, in the nanocomposite. The polymer blend film alone does not show appreciable PL emission. The ZnO nanoparticles, in combination with PS-PMMA, can bring about functionalities suitable for the realization of efficient light emitting diodes, photo detectors, and other optoelectronic devices.

The photoluminescence emission spectra of ZnO/PS, ZnO/PMMA and ZnO/PS-PMMA nanocomposite films together are shown in figure 6.9 for comparison. Among the nanocomposite systems studied, the ZnO/PS-PMMA composite shows the highest intensity of photoluminescence emission.
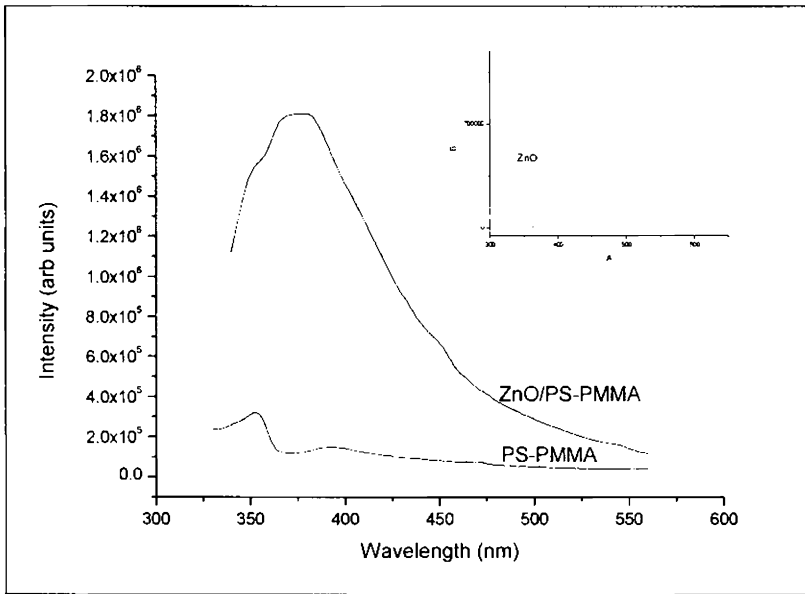
Figure 6.8: PL emission spectra of PS-PMMA and ZnO/PS-PMMA nanocomposite films (Inset shows PL emission spectrum of ZnO)
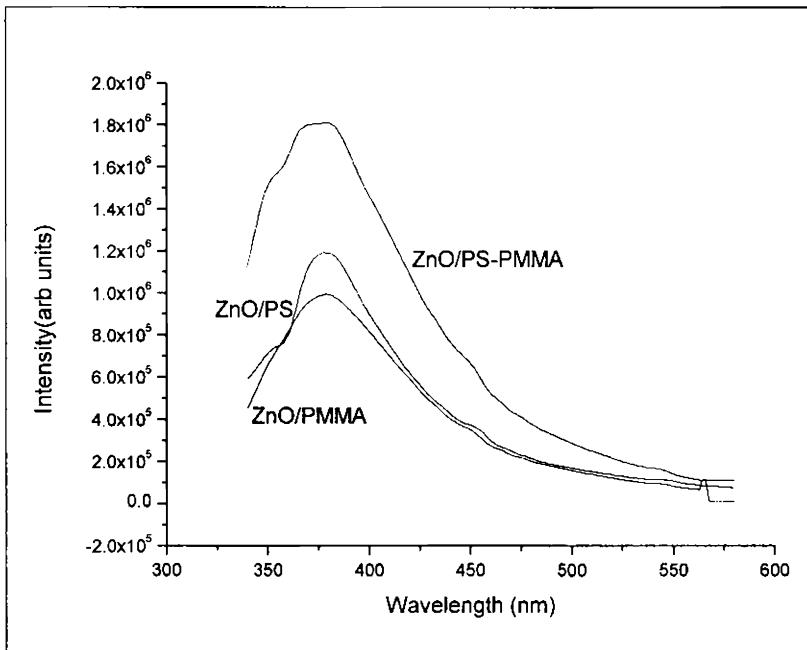
Figure 6.9: The PL spectra ZnO/PS, ZnO/PMMA and ZnO/PS-PMMA nanocomposite films

6.6 Nonlinear optical studies

6.6.1 Open aperture Z-scan

Nonlinear optical properties of ZnO/PS-PMMA nanocomposite films were investigated by the Z-scan technique. Figure 6.10(a) shows the nonlinear absorption of ZnO/PS-PMMA nanocomposite films at typical laser energy of 25 μJ for an irradiation wavelength of 532 nm. The open-aperture curve exhibits a normalized transmittance valley, indicating the presence of induced absorption. The observed nonlinearity is found to be of the third order, as it fits to a two photon absorption process (TPA). The corresponding net transmission is given by

$$T(z) = \frac{C}{q_0\sqrt{\pi}} \int_{-\infty}^{\infty} \ln[(1 + q_0] \, e^{-t^2}) \, dt$$

-------------------------------- (6.1)

where $q_0(z, r, t) = \beta I_0(t) L_{eff}$.

Here, $L_{eff} = 1 - e^{-\alpha L}/\alpha$, is the effective thickness with linear absorption coefficient α and nonlinear absorption coefficient β, L is the sample length and I_0 is the irradiance at focus [28]. The solid curve in Fig. 6.10(a) represents the theoretical fit to the experimental data. The experimentally obtained value of nonlinear absorption coefficient β at a pulsed energy of 25μJ is shown in table 6.2.

From the open aperture Z-scan curve it is found that, the ZnO/PS-PMMA nanocomposite films do exhibit large induced absorption behaviour. The observed dip in the open aperture curve shows the transmittance limiting efficiency of the nanocomposite films. Although similar investigations have been reported in ZnO/PMMA nanocomposite films [15], the transmittance minimum reported is only about 0.65. In

one of our earlier investigations the transmittance minimum obtained for ZnO/PS nanocomposite film is about 0.43 (chapter 5). In the present work, the curves of ZnO/PS-PMMA films show a better fit to the theoretical equations for TPA, and the' transmittance minimum is about 0.25, which highlights the better optical limiting efficiency of the latter compared to the former ones. The calculated nonlinear parameters are given in table 6.2. The comparatively much lower transmittance value obtained for ZnO/PS-PMMA composite films (Figure 6.10a) shows that these films can be used as efficient optical limiters. Optical limiting (OL) devices protect light-sensitive sensors, such as eye or CCD cameras, from possible damage caused by intense light exposure. The observed improvements in the nonlinear optical properties of ZnO/PS-PMMA nanocomposite films compared to ZnO/PS and ZnO/PMMA nanocomposite films can be associated with the formation of an interpenetrating network (IPN) of PS and PMMA in the PS-PMMA polymer blend.

6.6.2 Closed aperture Z-scan

Figure 6.10b gives the closed aperture Z-scan trace of ZnO/PS-PMMA nanocomposite film for an irradiance wavelength of 532 nm from pulsed Nd- YAG laser of energy 25 μJ. The closed-aperture curve exhibits a peak to valley shape, indicating a negative value of the nonlinear refractive index n_2 [29]. For samples with appreciable refractive and absorptive nonlinearities, closed aperture measurements show contributions from both, i.e. the intensity-dependent changes in the transmission and the refractive index [28]. By dividing the normalized closed aperture transmittance data by the corresponding normalized

open-aperture data, one can eliminate the effect of nonlinear absorption and the resulting curves can be fitted with the theoretical equation for pure nonlinear refraction.
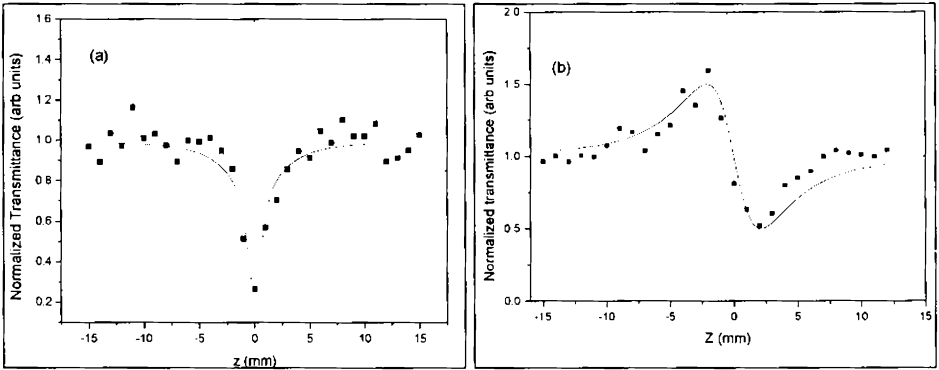
Figure 6.10: The open aperture (a) and closed aperture (b) Z scan curves of ZnO/PS-PMMA nanocomposite film

The value of the difference between the normalized peak and valley transmittance, T_{p-v} can be obtained by the best theoretical fit from the results of divided Z-scan curve. The nonlinear refractive index n_2 is calculated from T_{p-v} in closed aperture Z-scan using Eq. (6.2) and is given in table 6.2,

$$T_{p-v} = 0.406(1 - S)^{0.25} |\Delta\Phi_0|, \text{ where } |\Delta\Phi_0| = (2\pi/\lambda) \, n_2 \, I_0 \, L_{eff}, \text{ ---- (6.2)}$$

where S is the linear transmittance of the far field aperture and λ is the excitation wavelength. From the closed aperture Z-scan fit, $\Delta\Phi_0$ can be obtained.

The peak-valley trace in the closed aperture Z- scan curve shows that the samples have self-defocusing (negative, $n_2 < 0$) type optical nonlinearity, as reported for ZnO/PMMA nanocomposite [15].

6.6.3 Determination of nonlinear susceptibility

The nonlinear susceptibility is calculated by the analysis of the open aperture and closed aperture Z-scan data using the procedure described in chapter 2.

The nonlinear refractive index n_2 is related to the real part of nonlinear susceptibility, Re ($\chi 3$) by the relation,

$$Re \ (\chi 3) = n_0 n_2 / 3\pi \quad (esu), \ \text{-- (6.3)}$$

where n_0 is the linear refractive index.

The imaginary part of third order susceptibility, Im ($\chi 3$) determines the strength of the nonlinear absorption. Equation (4) given below, relates the nonlinear absorption coefficient β to Im ($\chi 3$)

$$\begin{aligned} Im \ (\chi 3) &= \ \varepsilon_0 \, n_0^2 \, c^2 \, \beta \, / \, \omega \quad (m^2 \ V^{-2}) \\ &= \ n_0^2 \, c^2 \, \beta \, / \, 240 \, \pi^2 \, \omega \quad (esu) \ \text{------------------------ (6.4)} \end{aligned}$$

where, ε_0 is the permittivity of free space and c the velocity of light in vacuum.

From the real and imaginary parts of ($\chi 3$), the modulus of third order nonlinear susceptibility can be found out.

$$| \ (\chi 3) \ | \ = [\ [Re \ (\chi 3)]^2 + [Im \ (\chi 3)]^2]^{1/2} \ \text{------------------------ (6.5)}$$

The magnitude of ($\chi 3$) is significantly affected by the molecular orientation and it determines the strength of nonlinearity of the material.

The third order nonlinear susceptibility value of ZnO/PS-PMMA composite film at a pulsed energy of 25 µJ for a wavelength of 532 nm is given in table 6.2. The observed higher susceptibility value of ZnO/PS-PMMA films measured by the Z-scan technique, compared to both ZnO/PS and ZnO/PMMA films, establishes the fact that the ZnO/PS-PMMA nanocomposite films have better nonlinear optical response and can be chosen as ideal candidates with high prospects of applications in nonlinear optics [30.31].

Table 6.2: Linear and nonlinear optical parameters of ZnO/PS-PMMA nanocomposite film along with those of ZnO/PS and ZnO/PMMA nanocomposite films

	Band gap (eV)	β (cm/GW)	n_2 ($\chi 3$) (10^{-9} m^2/W)	(10^{-11}esu)
ZnO/PS-PMMA	3.46	1562	- 6.25	8.15
ZnO/PS	3.42	1468	-3.09	5.19
ZnO/PMMA	3.43	1499	-2.68	4.34

The open aperture and closed aperture Z-scan curves of ZnO/PMMA and ZnO/PS nanocomposite films are shown in figure 6.11. The transmittance minimum observed for the ZnO/PMMA and ZnO/PS nanocomposite films are 0.41 and 0.37 respectively (Figure 6.11a&c), whereas the value obtained for ZnO/PS-PMMA is much lower and is 0.25 (Figure 6.10a). The closed-aperture curves exhibit a peak to valley shape, indicating a negative value of the nonlinear refractive index n_2 for both the ZnO/PMMA and ZnO/PS nanocomposite films.
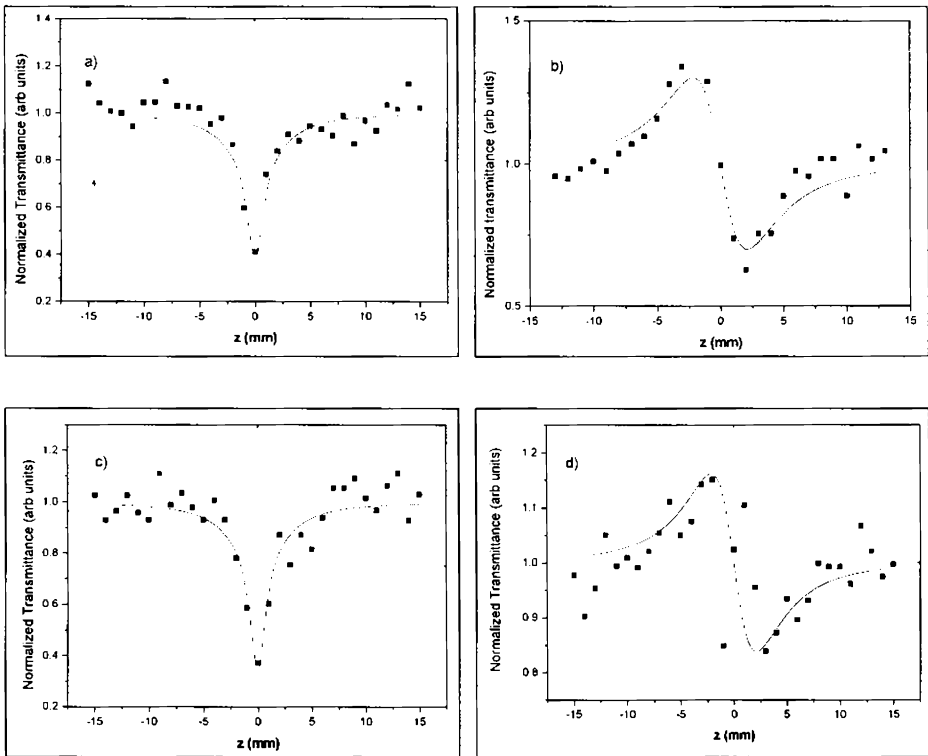
Figure 6.11: The open aperture (a & c) and closed aperture (b & d) Z scan curves of ZnO/PMMA and ZnO/PS nanocomposite films respectively.

6.7 Conclusion

In the present work, ZnO nanoparticles and transparent ZnO/PS-PMMA nanocomposite films have been prepared using simple and reproducible methods. The ZnO/PS-PMMA composite films with ZnO content of 10 wt % exhibit strong UV absorption (around 94%),wide UV absorption window of width around 165 nm and high transmittance (around 93%) in the visible region. These nanocomposite films with strong UV absorption and high transmittance in the visible region offer prospects of applications as optical coating materials for UV protection and shielding. Furthermore, these composite films are found to be more

thermally stable compared to films of PS-PMMA blend. The composite films show a self-defocusing type (negative refractive index, n_2) optical nonlinearity and good nonlinear absorption behaviour. The linear and nonlinear optical characteristics of these films are compared to those of ZnO/PS and ZnO/PMMA films prepared under the same conditions. The much lower transmittance of about 0.25 observed for the ZnO/PS-PMMA nanocomposite films is ideal for the fabrication of efficient optical limiters in sensor protection applications. The main factor contributing to the excellent optical characteristics of the ZnO/PS-PMMA nanocomposite is assumed to be the formation of an interpenetrating network (IPN) of PS and PMMA in the polymer blend.

References

[1] Subhranshu Sekhar Samel and Smrutisikha Bal, J. of Minerals & Mate. Characterization and Engineerung 7 (2008) 355.

[2] Arango, A. C.; Johnson, L. R.; Bliznyuk, V. N.; Schlesinger, Z. Adv Mater. 12 (2000) 1689.

[3] Moon T. H, Jeong M. C, Lee. W and Myoung J. M, Appl. Surf. Sci. 280 (2005)240.

[4] Ozgur U, Alivov YI, Liu C, Teke A, Reshchikov MA, Dogan S, et al, J Appl. Phys. 98 (2005) 41301.

[5] Pearton S. J, Abernathy C. R, Overberg M. E, Thaler G. T, Norton D. P, Theodoropoulou N et al, J Appl. Phys. 93 (2003) 1.

[6] Lee, J.; Bhattacharyya, D.; Easteal, A. J.; Metson, J. B., Curr Appl. Phys. 8 (2008) 42.

[7] Dong, W. C.; Byoung, C. K., Polym. Adv. Technol. 16 (2005) 846.

[8] Erjun, T.; Shaoying, D. Colloid Polym. Sci. 287 (2009) 1025.

[9] S.W alheim, M. Boltau, J.Mlynek, G. Krausch, U.Steiner ,Macromolecules 30 (1997) 4995–5003.

[10] J.J. Schmidt, J.A. Gardella, L. Salvati, Macromolecules 22 (1989) 4489.

[11] G.Krausch, Mater.Sci.Eng. 14 (1995) 1

[12] J.S. Gutmann, P. MuK ller-Buschbaum, D.W. Schubert, N. Stribeck, M. Stamm, J. Macromol.Sci.Phys.Ed. 38 (1999) 563.].

[13] Yao, T.; Li, Z.; Yi Zheng, J.; Chao, G.; Zhi Zhen, Y.; Ye Feng, Y.; Qing Ling, W. J Mater. Chem. 20(2010) 1594.

[14] Jeeju P. P. and Jayalekshmi S, J Appl. Polym. Sci. 120 (2011) 1361.

[15] R. Sreeja, Jobina John, P.M. Aneesh, M.K. Jayaraj, Opt. Commun. 283 (2010) 2908.

[16] J. Antonio Paramo, Yuri M. Strzhemechny, Alojz Anžlovar, Majda Žigon, and Zorica Crnjak Orel, J. of Appl. Phys. 108 (2010) 023517.

[17] Junlin Ge, Xiaofei Zeng, Xia Tao, Xue Li, Zhigang Shen, Jimmy Yun, Jianfeng Chen, J Appl Polym Sci. 118 (2010) 1507.

[18] Saziye Ugur, Onder Pekcan, J Appl. Polym. Sci. 100 (2006) 2104.

[19] Sumetha, S. Science Asia 34 (2008) 031.

[20] Yong, J. K.; Kyoung, H. K.; Chang, S. L.; Kwang, B. S. J Ceram. Process Res. 3 (2002)146.

[21] Siddheswaran, R.; Sankar, R.; Ramesh Babu, M.; Rathnakumari, M.; Jayavel, R.; Murugakoothan, P.; Sureshkumar, P. Cryst. Res. Technol. 41 (2006) 446

[22] Rong, M. Z.; Zhang, M. Q.; Wang, H. B.; Zeng, H. M. Appl Surf Sci 2002, 200, 76.

[23]. Tang, E.; Cheng, G. X.; Ma, X. L. Powder Technol 2006, 161, 209.

[35] M Haase ; H Weller and A Henglein, J. Phys. Chem. 92 (1988) 482.

[24] M Haase ; H Weller and A Henglein, J. Phys. Chem. 92 (1988) 482.

[25] Vinyan Gong ; Tamar Andelman Gertrude ; F Neumark ; Stephen O'Igor L.Kuskovsky, Nanoscale Res. Lett. 2 (2007) 297.

[26] Lin Guo ; S.Yang ; Chunlei Yang ; Ping Yu; Jaiannong Wang ; Weikun Ge and George K L Wong, Appl. Phys. Lett. 76, 20 (2000) s2901.

[27] L Wu; Y Wu; X. Pan; F Kong, Opt. Mater. 28(4) (2006) 418.

[28] M.S. Bahae; A.A. Said; E.W. van Stryland. Opt. Lett. 14 (1989) 955.

[29] H.S. Waff; K. Park., Phys. Lett. A., 32 (1970)109.

[30] D. Jezequel; J. Guenot; N. Jouini and F; Fievet; J.Mater.Res., 10 (1995) 77.

[31] E W Seelig; B Tang; A Yamilov; H Cao and R P H Chang. Mater. Chem. Phys. 80 (2002)257.

.....ഇൗ.....

Novel polypyrrole films with excellent crystallinity and good thermal stability

Polypyrrole has drawn a lot of interest due to its high thermal and environmental stability in addition to high electrical conductivity. The present work highlights the enhanced crystallinity of polypyrrole films prepared from the redoped sample solution. Initially hydrochloric acid (HCl) doped polypyrrole was prepared by chemical oxidative polymerization of pyrrole using ammonium peroxidisulphate (APS) as oxidant. The doped polypyrrole was dedoped using ammonia solution and then redoped with camphor sulphonic acid (CSA). Films were coated on ultrasonically cleaned glass substrates from the redoped sample solution in meta-cresol. The enhanced crystallinity of the polypyrrole films has been established from X-ray diffraction studies. The results of Raman spectroscopy and Differential scanning calorimetry (DSC) studies, and Thermo gravimetric analysis (TGA) of the samples support the enhancement in crystallinity. Percentage crystallinity of the samples has also been estimated from XRD and DSC data. The present work is significant, since crystallinity of films is an important parameter for selecting polymers for specific applications.

7.1 Introduction

Conducting polymers have attracted a great deal of attention in the last few decades because of their unusual and tunable electrical and optical properties. The electrically conducting polymers are capable of electrical charge transfer to the same extent as an electrical conductor or a semiconductor. Due to their fascinating electrical and optical properties, conducting polymers have played indispensable roles in specialized industrial applications in spite of their short history. However, the major aspects useful for most applications are not the metal or semiconductor like electrical properties alone, but the combination of electrical conductivity and polymeric properties such as flexibility, low density and ease of structural modification that suffice for many commercial applications. The possibility of synthesizing materials capable of simultaneously presenting the properties of organic polymers and those of crystalline semiconductors has attracted the interest and efforts of both academic and industrial researchers.

Of all known conducting polymers, polypyrrole (PPy) is one of the most extensively studied polymers, since monomer pyrrole can be easily oxidized for polymerization, is commercially available and possesses good redox properties. Polypyrrole is frequently used in commercial applications, due to the long-term stability of its electrical conductivity and the possibility of forming copolymers or composites with optimal mechanical properties. In the last few years, investigations have centered mainly on the improvement of the physical properties of polypyrrole, such as processability, stability or mechanical integrity. Several techniques including blend or composite formation are being optimized

in order to prepare processable materials which can be used and processed like common polymers. The possibilities of improving the physical properties of PPy as well as its good intrinsic properties make this material a serious candidate for use in specific technological applications such as batteries, super capacitors, electrochemical (bio) sensors, conductive textiles and fabrics, mechanical actuators, electromagnetic interference shielding devices, anti-static coatings and drug delivery systems [1,2]. Polypyrrole coatings have excellent thermal stability and are good for use in carbon composites [3] Chemical and electrochemical polymerization techniques are the two widely used methods to synthesize polypyrrole. In the chemical polymerization process, monomer pyrrole is oxidized by oxidizing agents or catalysts in the presence of suitable dopants, to produce the conducting form of the polymer. The advantage of chemical synthesis is that it offers mass production at reasonable costs. This is often difficult to achieve with electrochemical methods. On the other hand, electrochemical methods offer the possibilities of synthesizing polymers with better conducting properties. Recent years have witnessed the development of improved synthesis and processing routes for the preparation of more ordered and homogeneous polypyrrole samples, both in bulk and thin film forms [4-6].

7.2 Semi crystalline polymers

Polymer crystallinity is one of the important properties of all polymers since crystallinity influences many of the polymer characteristics, including mechanical strength, opacity and thermal properties. Crystallinity measurement provides valuable information for both materials research and quality control in material processing [7-12].

Polymers exist both in crystalline and amorphous forms. The polymer chains are not aligned with each other over their whole length, and the alignment is limited only to small crystallite regions [13]. Such polymers are the so-called semi-crystalline polymers having both crystalline and amorphous regions. Semi-crystalline polymers are interesting because they combine the strength of crystalline polymers with the flexibility of amorphous ones. They are generally strong with the ability to bend without breaking. As the polymer crystallinity increases, its level of secondary bonding also increases. This in turn increases the stiffness (elastic modulus) and strength of the polymer. On the other hand, ductility declines as crystallinity increases. Factors affecting crystallinity are

- Linearity of the polymer chain

- Presence of more than one monomer type

- Arrangement of side groups on the backbone

- Processing conditions

Crystallinity in polymers is a measure of the extent of the crystalline regions with respect to amorphous ones. The percentage crystallinity is an important parameter, which influences the optical, thermal, and mechanical properties of a polymer. DSC is an advantageous technique, which provides a rapid method for determining polymer crystallinity based on the heat required to melt the polymer. XRD technique is also used to establish the nature of the polymer and estimate the extent of crystallinity present in the polymer.

This chapter deals with a detailed study of the crystallinity in polypyrrole film samples, prepared from the redoped PPy solution in meta-cresol. A quantitative assessment of the crystallinity in these films has been carried out using DSC and XRD analysis. The Raman spectroscopic analysis supports the conclusions drawn from DSC and XRD studies.

7.3   Synthesis of PPy samples

Polypyrrole was prepared by oxidative polymerization of pyrrole using ammonium peroxidisulphate as oxidant. Freshly distilled pyrrole was dissolved in the dopant acid (HCl) solution. Ammonium peroxidisulphate (APS) dissolved in water was added drop by drop to it with continuous stirring for 4-5 hours. The polymerization was carried out at 0^0C temperature with an oxidant /monomer molar ratio of 1:1. The black precipitate obtained was filtered, washed and dried under vacuum for 12 hours. The HCl doped polypyrrole powder was reduced by ammonia solution and the resulting precipitate was filtered, washed and dried to obtain the dedoped polypyrrole powder. The dedoped PPy powder was mixed with CSA in a mortar for redoping. This redoped sample dissolved in meta-cresol (m-cresol) was used to prepare films on glass substrates by solution casting.

7.4   Characterization of PPy samples
7.4.1 XRD analysis

The X-ray diffraction (XRD) studies of the samples were done on a Rigaku X-ray Diffractometer   with Cu – Kα (1.5418 A°) radiation operating at 30 kV and 20 mA. Scanning was carried out in the 2θ range

from 0 to 60° at a scan speed of 2^0 per minute. The XRD patterns of the PPy samples are shown in figure 7.1. The CSA redoped PPy film shows exceptionally higher crystallinity compared to the HCl doped and dedoped samples. The peaks in HCl doped PPy and dedoped PPy (Figure 7.1 (a) and (b)) are mostly of amorphous nature. However, the peaks appear with excellent sharpness in the XRD pattern of CSA redoped polypyrrole film as shown in figure 7.1(c).
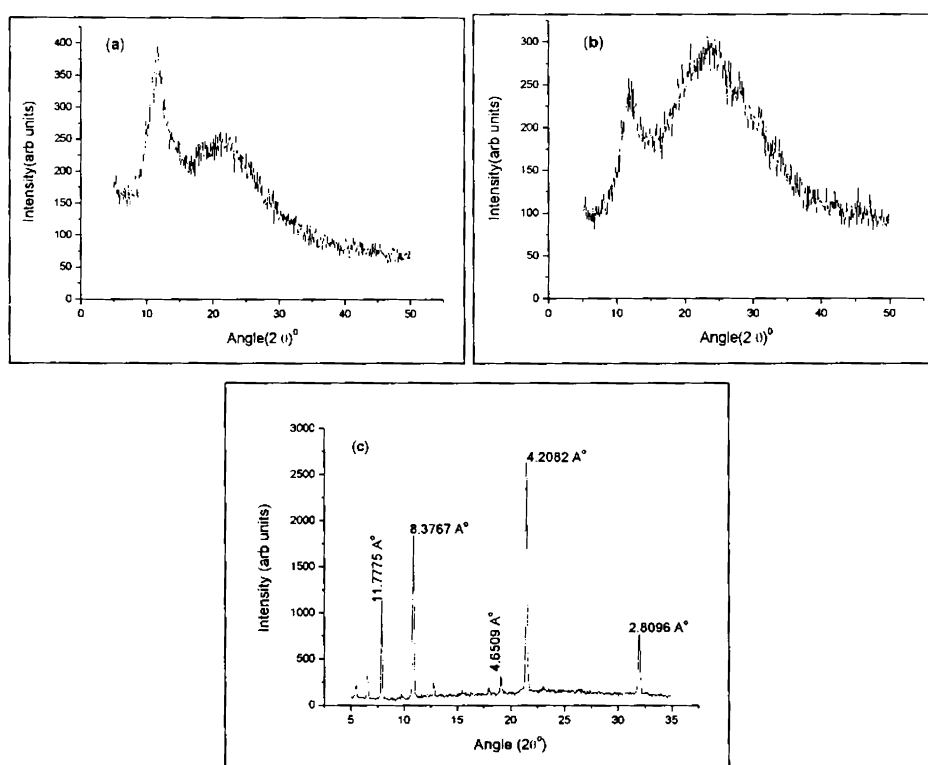
Figure 7.1: XRD patterns of (a) HCl doped PPy (b) Dedoped PPy and (c) CSA redoped PPy film prepared from meta-cresol solution.

In figure 7.1(c), the prominent peaks observed at about 10.5 ^{0}, 21^0 and 32^0 correspond to the d spacing values 8.377, 4.208 and 2.809 A° respectively. These d values correspond to the interlayer distance from

pyrrole to pyrrole ring, from pyrrole ring to the camphor sulphonate dopant, and the face-to-face stacking distance, respectively [14, 15]. The d-value of 16.7Å corresponding to the peak at 5.34^0 is an indication of the order closely associated with the dopant ions between the polymer chains. The peaks are indexed by calculating hkl indices as in the case of crystalline samples. The hkl indices suggest a simple cubic structure, and the dimension of the fundamental repeating unit is found to be 1.67nm (Table 7.1).

Table 7.1: Indexing of hkl planes from XRD peaks of PPy film

hkl planes	d(nm)	a(nm)
100	1.67341	1.67341
110	1.17775	1.6656
200	0.83767	1.67534
320	0.46509	1.6769
400	0.42082	1.6832
531	0.28096	1.66218

The XRD pattern of CSA redoped polypyrrole film exhibits extraordinarily high crystallinity, which has not been reported earlier .One of the reasons for the excellent crystallinity of the CSA redoped film can be the secondary doping effect of the solvent meta-cresol. Other reasons for the enhanced crystallinity can be (a) the effect of controlled doping (redoping using one molar CSA) by which more crystallite regions are formed and (b) ultrasonication. The enhanced crystallinity in turn improves the electrical conductivity of the sample also [16].

Majority of polymers diffracts X-rays like any crystalline substance, but behaves like amorphous materials giving very broad and diffuse XRD patterns. Unlike simple inorganic compounds, polymers do not have a perfectly ordered crystal lattice formation and are not fully crystalline. In fact, they contain both crystalline and amorphous regions, and consequently the X-ray diffraction spectra are found to be a mixture of sharp as well as diffused patterns. The sharp peaks correspond to crystalline and ordered regions and the diffuse and broad ones refer to amorphous regions. Crystallinity of a polymer is expressed in terms of the crystalline fraction of the sample [17]. The crystallinity is calculated by separating intensities due to amorphous and crystalline phases of the diffracted graphs. The total area of the diffracted pattern is divided into crystalline (A_c) and amorphous (A_a) components. Percentage crystallinity (X_c %) is estimated as the ratio of crystalline area to total area [13].

$$X_c\% = \left[A_c / \left(A_c + A_a\right)\right]. \ 100 \ (\%) \ \text{-------------------- (7.1)}$$

The percentage crystallinity values obtained for the PPy samples are given in table 7.2.

Table 7.2: Percentage crystallinity of PPy samples using XRD analysis

Sample	A_c	A_a	X_c %
HCl doped PPy (bulk)	2092.35	3136.67	40
Dedoped PPy (bulk)	1548.65	4197.35	27
CSA redoped PPy film	2766.7	1555.8	64

Numerous X-ray diffraction studies have been conducted on PPy films to characterize the degree of molecular order. It has been reported that the degree of alignment increases as the applied potential and

temperature of polymerization decreases in electrochemical polymerization of pyrrole [18]. The mechanical properties of PPy films have been observed to improve under such conditions. Thus, there may be some correlation between molecular order and the mechanical properties of PPy films. A greater degree of order has been observed when the films are mechanically stretched [19, 20]. The stretching is believed to orient the molecular chains in the direction of the applied stress. In the present work, about 64% crystallinity has been observed in chemically synthesized, CSA redoped films of PPy from m-cresol, without being mechanically stretched or subjected to any other types of strain.

7.4.2 Atomic force microscopy (AFM) studies

The AFM images of the CSA redoped PPy films were obtained with Park XE-100 Atomic Force Microscope. The AFM image is shown in figure 7.2. Some extent of ordering of polymer chains in PPy film is seen in the AFM picture.
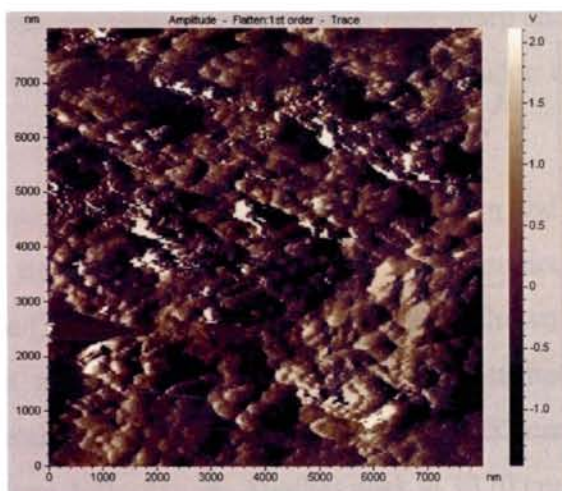
Figure 7.2: AFM picture of polypyrrole film

7.4.3 FT-IR analysis

Fourier transform infrared (FT- IR) spectra of the samples were obtained with AVTAR 370 DTGS FT- IR spectrophotometer in the wave number range 500 – 4000 cm^{-1}. FT-IR investigations have been carried out to confirm the polymerization of the monomer and redoping of CSA during the synthesis process.

The FT IR spectrum of HCl doped PPy, shown in Figure 7.3(a), indicates the typical characteristics of PPy, which are consistent with the reported data [21-23]. The bands at 1555 and 1474 cm^{-1} correspond to the stretching vibrations of C=C and C-N of PPy respectively. The band at 1198 cm^{-1} corresponds to the breathing vibration of the pyrrole ring. The band of C-H in-plane deformation vibration is located around 1043 cm^{-1} while the band of C-H out-of-plane deformation vibration is found at 921 cm^{-1}. The strong absorption at 3400 cm^{-1} is due to N-H stretching and the characteristic absorption band of PPy at 1126 cm^{-1} is due to C-C stretching. [24-27]
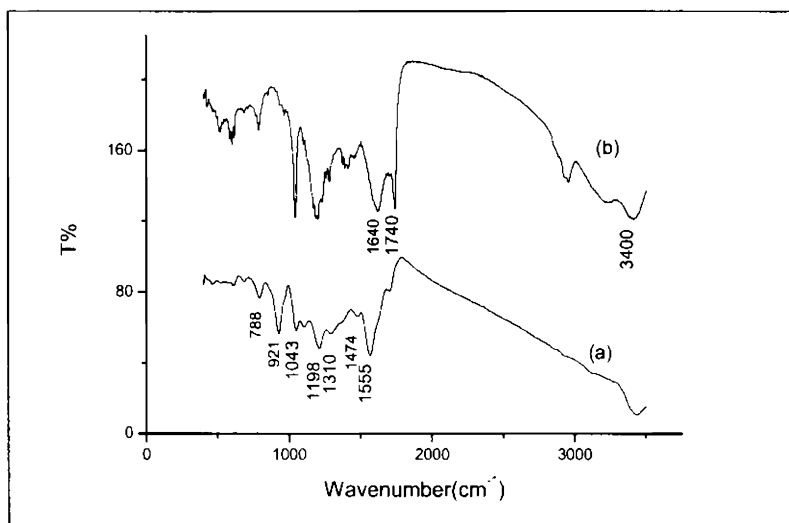

Figure 7.3: FT IR spectra of (a) HCl doped PPy and (b) CSA redoped PPy

Figure 7.3(b) shows the FT-IR spectrum of CSA redoped PPy sample. The bands in the range 500-700 cm^{-1} correspond to S-O and C-S stretching modes, which indicate the presence of sulfonic acid groups in the polymer backbone [27]. The absorption bands at about 1040 and 1740 cm^{-1} are due to the SO$_3$ group and C=O stretching vibrations respectively, in the camphor sulfonate [28]. Most of the absorption bands of CSA are overlapped by those of PPy, but the CSA absorption at 1640 cm^{-1} is clearly seen (Figure 2 (b) [24]. The bands at 1560 and 1472cm^{-1} correspond to the stretching vibrations of C=C and C-N of PPy respectively. From the FT- IR spectra, it is clear that polymerization as well as CSA doping have taken place during the synthesis process.

7.4.4 Raman spectral studies

Raman spectroscopic study is one of the important tools to obtain structural information on polymers. In most cases, Raman scattering is sensitive to the degree of crystallinity in a sample. Typically, a crystalline material yields a spectrum with very sharp and intense Raman peaks, while an amorphous material shows broader and less intense Raman peaks.

The Raman spectra of CSA redoped PPy film and HCl doped PPy are shown in figure 7.4. Many researchers have studied Raman spectra of polypyrrole [29-31]. The most important peak shown in figure 7.4 (a) is the one at about 1580cm^{-1}, which can be attributed to the C=C backbone stretching of PPy. The peak at about 1052 cm^{-1} is assigned to the C–H in plane deformation. Another peak at 1370 cm^{-1} is attributed to the ring-stretching mode of PPy. The bands located at about 940 and 990

cm^{-1} are assigned to the ring deformation associated with dication (bipolaron) and radical cation (polaron), respectively [32- 34].

Two broad bands centered around 1370 and 1590 cm^{-1} are observed in the Raman spectrum of PPy bulk sample (Figure 7.4(b)), whereas narrow and sharp peaks are found in the spectrum of CSA redoped PPy film (Figure 7.4(a)). Most of the peaks observed in the spectrum of the PPy film are very sharp compared to those reported in literature [35-37]. The sharpness of the Raman lines observed in the spectrum of PPy film is a consequence of the enhanced crystallinity of the film. In other words, Raman spectroscopy studies support the enhancement in crystallinity of the PPy films, established through the XRD analysis.
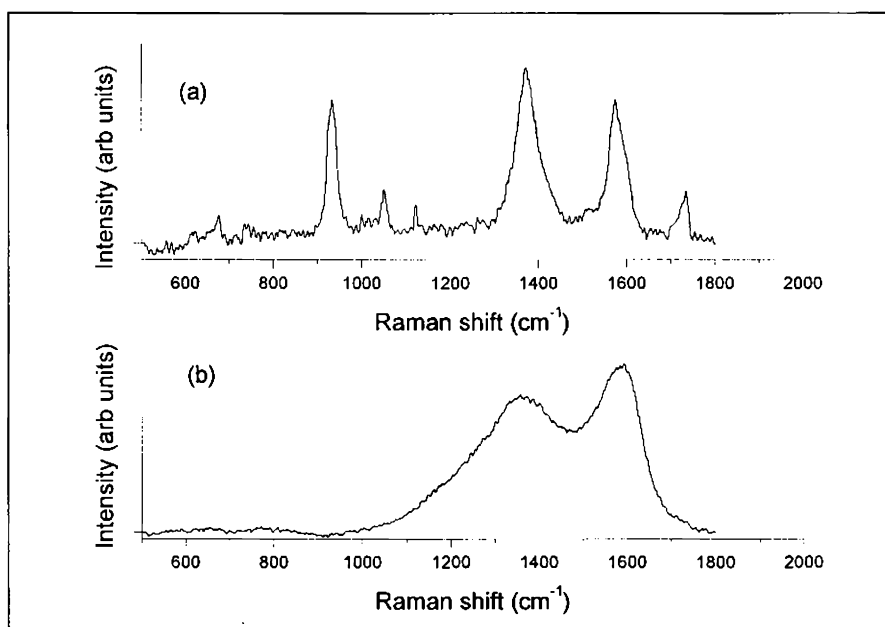
Figure 7.4: Raman spectra of (a) CSA redoped PPy film and(b) HCl doped PPy

7.4.5 Thermal studies

7.4.5 (a) Differential scanning calorimetry (DSC)

The measurement of a polymer's crystalline content (given as percentage crystallinity) by DSC is a straightforward and easy-to-perform test. This simply involves taking a small quantity of the polymer (generally 10 mg) and heating it at a steady rate (10° C/minute). The DSC curve of CSA redoped sample in m-cresol is shown in figure 7.5. DSC evaluation can be used to estimate the extent of crystallinity in the sample by two methods [38].

Method 1: Let the heat of crystallization be H_C, and the total heat given off during melting be H_T,

$$H= (H_T\text{-} H_C) \text{ Joules, } \text{---}(7.2)$$

where H is the heat given off by that part of polymer, which is already in crystalline state. By dividing H by Hc_1 (specific heat of melting), where Hc_1 is the amount of heat given off when 1gram of polymer is melted, the total amount of polymer that is crystalline below T_C, the crystallization temperature, is obtained.

$$H/Hc_1 = \text{Joules / Joules per gram} = \text{ Mc grams } \text{--------} (7.3)$$

The percentage of crystallinity in the polymer sample is

$$(M_C/M_t) \times 100 = \% \text{ crystallinity in the sample ----------- } (7.4)$$

where, Mt is the total mass of sample taken.

The percentage crystallinity of the sample estimated from DSC data as per equation (7.4) is about 61%. The values of the glass

transition temperature T_g and of the melting point T_m are respectively 120 ^{0}C and 314 ^{0}C for the PPy films (Figure 7.5(b)). The increase in the value of T_g (from 100 to 120^0 C) of the redoped PPy film from that of the HCl doped sample also supports the enhancement in crystallinity of the former.
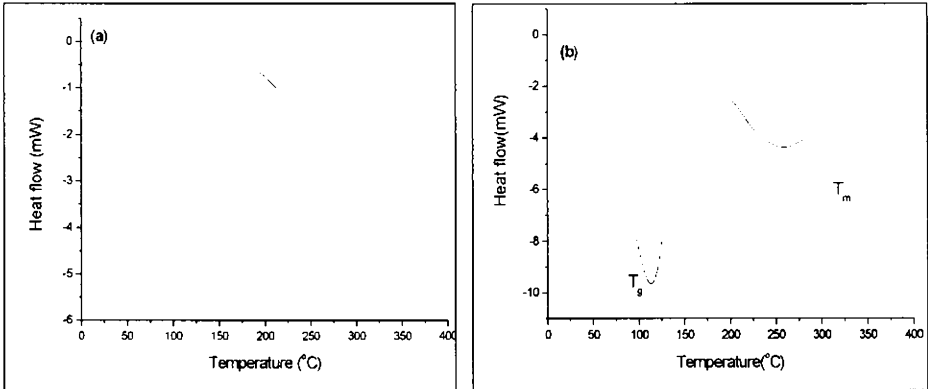
Figure 7.5: DSC curves of (a) HCl doped PPy and (b) CSA redoped film sample

Method 2: The percentage crystallinity can also be estimated from the heat of melting. The experimental heat of melting (H_m) is evaluated by integrating the area under the melting peak and then comparing to a reference value ($H_m°$), which represents the heat of melting of the theoretically 100% crystalline sample

$$\% \text{ crystallinity} = (H_m/ H_m°) \times 100 \ (\%) \ \text{-------------------} \ (7.5)$$

The percentage crystallinity of the sample calculated, following method 2 is about 63%.

7.4.5 (b) Thermo gravimetric analysis (TGA)

Thermo gravimetric analysis determines the weight changes of a sample as a function of temperature or time. The TGA curves (Figure 7.6)

show the enhancement in thermal stability of the redoped film sample compared to the doped powder sample. The increase in crystallinity of the CSA redoped film sample is evident from the more or less sharp weight loss of this sample (Figure 7.6 (b). The thermal stability of HCl doped PPy (Figure 7.6 (a) is less than that of the CSA redoped PPy (Figure 7.6 (b) film sample in m-cresol. The increase in thermal stability of the redoped film sample is attributed to the enhanced crystallinity of the sample, brought about by controlled doping.
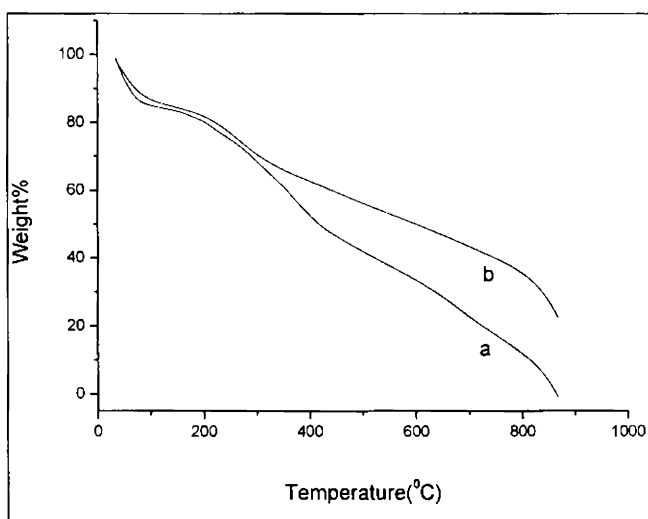
Figure 7.6: TGA curves of (a) HCl doped PPy and (b) CSA redoped PPy film

7.4.6 Electrical Conductivity studies

The four-point probe technique is the most common method for measuring the resistivity/conductivity of samples with appreciable conductivity. The room temperature DC electrical conductivity of HCl doped PPy sample in the form of pressed pellet (diameter-13 mm) and CSA redoped PPy film has been measured using a standard four-probe setup. The conductivity of the redoped polypyrrole film is 8.5 S/cm,

which is found to be about 30 times higher than that of the HCl doped PPy, which is around 0.27 S/cm.

The observed increase in the electrical conductivity of the CSA redoped film samples can be attributed to the secondary doping effect of the solvent, m-cresol and the effects of controlled CSA doping(redoping using one molar CSA) , by which more crystallite regions are formed. This in turn improves the mobility of charge carriers and hence increases the conductivity of the sample [16].

7.5 Conclusions

Highly crystalline polypyrrole films have been prepared from CSA redoped sample solution in m-cresol. Crystalline peaks have been identified in the XRD pattern of the CSA redoped film samples, which correspond to the distance between pyrrole rings, the distance from the pyrrole ring to the camphor sulphonate dopant and the face-to-face stacking distance. The extent of crystalinity has been assessed using the DSC and XRD data. The sharp peaks in the Raman spectrum of the PPy film also support the observed increase in crystallinity of the film samples. The thermal analysis establishes the higher stability of the CSA redoped PPy film compared to the HCl doped sample. The d.c. electrical conductivity of the redoped polypyrrole film is about 30 times higher than that of the HCl doped pellet sample. The secondary doping effect of the solvent, m-cresol and the controlled doping using CSA facilitate the enhancements in crystallinity and conductivity. The observation of extra ordinarily high extent of crystallinity in the CSA redoped PPy film is the highlight of this chapter. Semi-crystallinity is desirable for most polymers because semi crystalline polymers combine the strength of

crystalline polymers and the flexibility of amorphous ones. Crystallinity influences many of the polymer properties, and hence it plays an important role while selecting polymers for specific applications. The present work is quite significant from this point of view.

References

[1]   Hart Singh Nalwa, Handbook of Organic conductive molecules and polymers Vol 2 1997 (Chichester: Wiley)

[2]   Seung Hyun Cho, Ki Tae Song and Jun Young Lee, Handbook of Conjugated Polymers; Theory, Synthesis, Properties, and Characterization (Edited by Tejre A . Skotheim and John R. Reynolds) Chap 8 Recent Advances in Polypyrrole.

[3]   Iroh. J. O, Williams. C, Formation of thermally stable polypyrrole-naphthalene/benzene sulfonate-carbon fiber composites by an electrochemical process.Synth. Met. 99,1999, 1-8 K Lee, S Cho, S H Park, A J Heeger, C W Lee, S H Lee, Metallic transport in polyaniline, Nature 441(2006) 65-8

[4]   J Jang, J Bae, K Lee, "Synthesis and characterization of polyaniline nanorods as curing agent and nanofiller for epoxy matrix composite," Polymer 46 (2005) 3677-3684

[5]   H Liu, X B Hu, J Y Wang, R I Boughton, Structure, Conductivity, and Thermo⁻power of Crystalline Polyaniline Synthesized by the Ultrasonic Irradiation Polymerization Method, Macromolecules 35 (2002) 9414-9419)

[6]   L. E. Alexander, X-Ray Diffraction Methods in Polymer Science, Krieger Publishing Company, Malabar, FL, 1985.

[7]   N. Kasai and M. Kakudo, X-Ray Diffraction by Macromolecules, Kodansha and Springer,Tokyo, 2005, 393–417.

[8]   N. S. Murthy and H. Minor, General procedure for evaluating amorphous scattering and crystallinity from X-ray diffraction scans of semicrystalline polymers, Polymer 1990, 31, 996–1002.

[9] N. S. Murthy, H. Minor, M. K. Akkapeddi, and B. V. Buskirk, Characterization of polymer blends and alloys by constrained profile-analysis of X-ray diffraction scans, J.Appl. Polym. Sci.1990, 41, 2265–2272.

[10] K. B. Schwartz, et al., Crystallinity and unit cell variations in linear high-density polyethylene, Adv. X-Ray Anal. 1995, 38, 495–502.

[11] N. S. Murthy and R. Barton Jr., Polymer industry, Industrial Applications of X-Ray Diffraction, edited by F. H. Chung and D. K. Smith, Marcel Dekker, New York, 2000, 495–509.

[12] Raghavendra R Hegde, M G Kamath, Atul Dahiya, Polymer Crystallinity, www.utk.edu

[13] Carrasco, PM, Grande, HJ, Cortazar, M, Alberdi, JM, Areizaga, J, Pomposo, JA, ''Structure– Conductivity Relationships in Chemical Polypyrroles of Low, Medium and High Conductivity.'' Synth. Met., 156 420–425 (2006).

[14] Cheah, K, Forsyth, M, Truong, VT, ''Ordering and Stability in Conducting Polypyrrole.'' Synth. Met., 94 215–219 (1998).

[15] A B Kaiser,Electronic transport properties of conducting polymers and carbon nanotubes, Rep. Prog. Phys.64 (2001) 1-49

[16] Gowariker V R, Viswanathan N V,Jayadev Sreedhar Polymer Science, New age international (P) Ltd Publishers New Delhi 1986

[17] Wettermark, U.G., Worrell, G.A. and Chem, C.S. Polym. Mater. Sci. Eng. 1991, 64:267.

[18] Ogasarara, M., Funahashi, K., Demura, T., Hagiwara, T. and Iowata, K. Synthetic Metals. 1986, 14:61.

[19] Hagiwara, T., Hirasaka, M., Sato, K. and Yamaura, M. Synthetic Metals. 1990, 36:241.

[20] Acik M, Baristiran C and Sonmez G Mater. Sci. 41 4678, 2006

[21]   Omastova M, Trchova M, Pionteck J, Prokes J and Stejskal J (Effect of polymerization conditions on the properties of polypyrrole prepared in the presence of sodium bis(2- ethylhexyl) sulfosuccinate) Synth. Met. 143, 153-161, 2004

[22]   Min-Kyu Song,Young-Taek Kima, Bum-Seok Kim, Jinhwan Kim, Kookheon Char and Hee-WRhee, Synthesis and characterization of soluble polypyrrole doped with alkylbenzenesulfonic acids,   Synth. Met. 141, 315-319   2004)

[23]   Youqing Shen, Melxiang Wan (Soluble Conducting Polypyrrole Doped withDBSA-CSA Mixed Acid) Journal of Applied Polymer Science, Vol. 68, 1277–1284 (1998))

[24]   Rashmi Saxena, Manasvi Dixit, Kananbala Sharma, Narendra S, Saxena and Thaneshwar P Sharma (Effect on Annealing on Thermal & Optical Properties of Polypyrrole) Proc. American Institute of Physics 978-0-7354-0523-3/08/\$23.00

[25]   Kousik Dutta, S.K. De (Transport and optical properties of SiO2-polypyrrole nanocomposites Solid State Communications 140 (2006) 167-171

[26]   Kwan Sik Jang, Hoosung Lee, Bongjin Moon (Synthesis and characterization of water soluble   Polypyrrole doped with functional dopants) Synthetic Metals 143 (2004) 289-294

[27]   Anuar Kassim, Zarina Bte Basar and H N M Ekramul Mahmud, (Effects of preparation temperature on the conductivity of polypyrrole conducting polymer) Proc. Indian Acad. Sci. (Chem. Sci.), Vol. 114, No. 2, April 2002, pp 155–162

[28]   R. Kostic, D. Radovic, S.A. Stepanyan, I.E. Davidova and L.A. Gribov, " Vibrational Spectroscopy of Polypyrrole, Theoretical Study", J. Chem. Phy, Vol. 102 (8), 1995.

[29]   Yu-C. Liu and B. J. Hwang, "Identification of oxidized polypyrrole on Raman spectrum", Synthetic Metals, Vol. 113, 2000, pp. 203-207.

[30] D. Y. Kim, J. Y. Lee, D. K. Moon and C. Y. Kim, "Stability of Reduced Polypyrrole", Synthetic Metals, Vol. 69, 1995, pp. 471-474.

[31] J. Duchet, R. Legras, S. Demoustier-Champagne, Synth. Met. 98 (1998) 113.

[32] A.B. Goncalves, A.S. Mangrich, A.J.G: Zarbin, Synth. Met. 114 (2000) 119.

[33] M.J.L. Santos, A.G. Brolo, E.M. Girotto , Study of polaron and bipolaron states in polypyrrole by in situ Raman spectroelectrochemistry, Electrochimica Acta 52 (2007) 6141–6145

[34] J. Mikat, I. Orgzall, and H. D. Hochheimer, Raman spectroscopy of conducting polypyrrole under high pressure, Phys. Rev. B, volume 65, 174202(1-8) (2002)

[35] Fenge´n Chen,1 Jiaxin Zhang,1 Fan Wang,2 Gaoquan Shi1 , Raman Spectroscopic Studies. on the Structural Changes of Electrosynthesized Polypyrrole Films During Heating and Cooling Processes, Journal of Applied Polymer Science, Vol. 89, 3390–3395 (2003)

[36] J. Ferreira a, M.J.L. Santos a, R. Matos a, O.P. Ferreira b, A.F. Rubira a, E.M. Girotto, Structural and electro chromic study of polypyrrole synthesized with azo and anthraquinone dyes, Journal of

[37] Electro analytical Chemistry 591 (2006) 27–32)

[38] Varma-Nair M., Wunderlich, B., The ATHAS Data Bank Update, J. Phys. Chem., 1991, (20(2), 349

.....෫ාൔ.....

$\mathcal{Chapter}$ **8**

Conclusion and future prospects

The conclusions drawn from the present investigations are summarized in this chapter. The significant outcomes of the present study are highlighted. The future prospects of the present investigations are also addressed.

8.1 Conclusions

The present study involves two phases of research activities. In the first phase, the linear and nonlinear optical properties of ZnO/polymer nanocomposites are investigated in detail. The second phase of work is centered on the synthesis and related studies on highly crystalline polypyrrole films.

Nanocomposites represent a novel class of nanostructures with profound technological significance. Organic/inorganic nanocomposites are generally organic polymer composites with inorganic nanoscale fillers. They combine the advantages of the inorganic materials such as rigidity, thermal stability etc and those of the organic polymers like flexibility, processability etc. Generally, these nanocomposites are endowed with the special properties of the nanofillers, leading to materials with quite innovative characteristics. Recent interest in polymer matrix based nanocomposites has emerged from the interesting observations involving carbon nanotubes, carbon nanofibers, graphene, nanocrystalline metals and a host of additional nanoscale inorganic fillers or fiber modifications. Polymer nanocomposites offer excellent opportunities to explore new functionalities beyond those of conventional materials.

Zinc oxide possesses large exciton binding energy at room temperature which makes this material very attractive from the point of view of optical device applications. One of the important routes to synthesize ZnO nanocrystals is the colloidal chemical method. Chemical methods have many advantages such as low cost, relatively low precipitation temperature and the flexibility of particle size selection by

changing precursor molarity. In the present study, nanosized ZnO is synthesized using wet chemical method at two different temperatures.

ZnO is a highly pursued material owing to its wide range of applications in transparent electronics, optoelectronics and many branches of photonics. The radiation hardness of ZnO to MeV proton irradiation makes it an important material in space applications. Transparent semi conducting thin films of ZnO are used in solar cells, gas sensors, displays and UV filters. ZnO finds application in protection against laser threats and signal processing, because of high third order optical nonlinearity.

The field of nanocomposites has been recognized as one of the most promising and rapidly emerging research areas. These materials typically consist of an inorganic (host) solid containing an organic component or vice versa. They may also consist of two or more inorganic/organic phases in some combinational form with at least one of the phases having nano dimension. The mechanical, electrical, optical, electrochemical and catalytic properties of the nanocomposites differ markedly from those of the component materials. Out of the different types of nanocomposites, polymer nanocomposites find special attention due to the unique properties of polymer systems such as light weight, ease of production and flexibility. A defining feature of polymer nanocomposites is that the small size of the fillers leads to an enormous increase in interfacial area as compared to traditional composites. The interfacial area creates a significant volume fraction of interfacial polymer with properties different from the bulk polymer even at low loadings of the nanosized filler material. Interfacial structure is known to

be different from bulk structure, and in polymers filled with nanoparticles possessing high surface areas, most parts of the polymers are present near the interfaces, in spite of the small weight fraction of the filler. This is one of the reasons why the nature of reinforcement is different in nanocomposites and is manifested even at very low loadings of the filler. The crucial parameters which determine the effects of fillers on the properties of composites are filler size, shape, aspect ratio and filler-matrix interactions.

In the present work, zinc oxide/polymer nanocomposites were prepared by adding certain amount of nanosized ZnO into polymer solutions in toluene followed by stirring and ultrasonication. Thin films were deposited, from the ZnO/polymer composite solutions, on glass substrates using spin coating technique. The polymer systems used in the present study are polystyrene (PS), poly methylmetacrylate (PMMA) and PS/PMMA blend. The ZnO/polymer nanocomposite films, investigated in the present work are found to be transparent and flexible.

The structural and morphological studies of ZnO nanoparticles and ZnO/polymer nanocomposite films were carried out using FT IR, XRD, FESEM and TEM analysis. These studies confirm the formation of ZnO nanoparticles having size in the range 5 to 35nm, and the uniform dispersion of ZnO nanoparticles in the polymer matrix. The thermal studies using TGA show that the ZnO/polymer nanocomposites are more thermally stable compared to the polymers. The optical properties of ZnO/PS nanocomposite films were investigated using UV-Visible absorption spectroscopy and photoluminescence studies. The UV-Vis absorption spectra of the nanocomposite films show UV absorption

window of width around 125 nm (240-365 nm) for all the weight percentages of ZnO in the composite. The ZnO content or dispersability enhances the UV shielding properties of the nanocomposite. The absorption edge wavelengths of the nanocomposite films are substantially blue shifted relative to that of the bulk ZnO (~ 375 nm) due to the confinement effect. The composite films show intense luminescence emission around 367 nm under an excitation at 325 nm and the intensity of emission increases with increase of ZnO content in the composite. The green emission observed in the spectrum of ZnO has been found to be quenched in the spectra of the nanocomposite films due to surface modification of ZnO nanoparticles by PS matrix, whereby the surface traps are almost removed. ZnO/PS nanocomposite films, in view of the strong UV absorption over a wide wavelength range, find prospects of application as efficient UV protectors.

Size-dependent optical properties of zinc oxide/ polystyrene nanocomposite films were also investigated using ZnO nanoparticles having different average particle size. The chemical synthesis of ZnO nanoparticles at room temperature, used in the present work, is a reproducible and comparatively simple method. It allows control on the size of the ZnO particles through variations in precursor concentration. The average particle size determined from the XRD peaks using the Debye-Scherrer formula is found to be close to the value based on TEM and FESEM analysis. In the UV-Visible absorption spectra of the composite films, the observed absorption window is found to shift towards the shorter wavelength side as the size of ZnO in the composite decreases. The absorption edge is found to be blue shifted from 395 to

303 nm with decrease in particle size of ZnO due to the confinement effects. The blue shift of the absorption edge, from 395 to 303 nm is associated with a band gap enlargement from 3.2 to 4.15 eV which is significant in band gap engineering applications. The ZnO/PS nanocomposite films containing ZnO nanoparticles of different average sizes together are capable of absorbing UV light in the range from 395 to190 nm, covering completely UVA (315–400 nm), UVB (280–315 nm) and part of UVC (100–280 nm) regions, thus showing prospects of acting as efficient UV filters. ZnO exhibits two kinds of emissions, one in the UV region corresponding to near band-edge emission and the other in the visible region. The defect related peaks in the green region, observed in the PL spectrum of ZnO, are quenched in the spectra of the nanocomposite films showing the surface modification by the polymer matrix. The possibility of tuning PL emission through size variations can find applications in realizing efficient nanoscale devices like LEDs and photo detectors, covering a broad spectral range.

Optical nonlinearity especially the third order nonlinearity, is very important in semiconductor nanocrystals, because it becomes considerably pronounced in nanomaterials compared to the bulk and, is useful for the development of new materials for applications in ultrafast optical devices. Attempts have been made in the present work to investigate the nonlinear optical (NLO) properties of ZnO/PS nanocomposite films using Z-scan technique. Nonlinear optical properties of ZnO/PS nanocomposite films, containing ZnO nanoparticles having different particle sizes were studied. The observed nonlinearity is found to be of the third-order, as it fits to a two photon

absorption process (TPA). It is observed that as the ZnO particle size increases the transmittance minimum decreases. The dip in the open aperture Z-scan curve increases with increase in ZnO particle size in the ZnO/PS nanocomposite films, leading to the observed increase in the optical limiting efficiency. The closed-aperture Z-scan curve exhibits a peak to valley shape, indicating a negative value of the nonlinear refractive index. The nonlinear parameters like nonlinear absorption coefficient, nonlinear refractive index and third order susceptibility are found to increase with increase in ZnO particle size. The observed enhancement of nonlinear optical properties with increase in ZnO particle size can be attributed to the size dependent enhancement of exciton oscillator strength.The fairly low transmittance of about 0.43 observed for the nanocomposite film with ZnO particles of size 35 nm is ideal for the fabrication of efficient optical limiters in sensor protection applications.

Enhanced linear and nonlinear optical characteristics have been observed in ZnO/PS-PMMA nanocomposite films prepared from the ZnO/PS-PMMA nanocomposite solution obtained by adding 10 wt% of ZnO powder sample into the PS-PMMA polymer blend (PS wt% = 50, PMMA wt% = 50) solution (10% w/v) in toluene. The ZnO/PS-PMMA composite films exhibit strong absorption (around 94%) in the UV region, wide UV absorption window of width around 165nm and high transmittance (around 93%) in the visible region. The composite films are more thermally stable compared to films of PS-PMMA blend. The composite films show a self-defocusing type (negative refractive index) nonlinearity and good nonlinear absorption behaviour. The linear and

nonlinear optical characteristics of these films are compared to those of ZnO/PS and ZnO/PMMA films prepared under the same conditions. The much lower transmittance of about 0.25 observed for ZnO/PS-PMMA nanocomposite films is more ideal for the fabrication of efficient optical limiters in sensor protection applications. The composite films show intense luminescence emission centred around 375 nm in the UV region. The ZnO nanoparticles, in combination with PS-PMMA, can bring about functionalities suitable for realizing efficient light-emitting diodes, photo detectors, and other optoelectronic devices. The main factor contributing to the excellent optical characteristics of the ZnO/PS-PMMA nanocomposite is assumed to be the formation of an interpenetrating network (IPN) of PS and PMMA in the polymer blend.

The second phase of the research work is focused on the synthesis and characterization of polypyrrole (PPy, a highly pursued conducting polymer) films with exceptionally high crystallinity. For the synthesis of polypyrrole films, HCl doped polypyrrole, after dedoping with ammonia solution was redoped with CSA and dissolved in meta-cresol. This solution was used to deposit polypyrrole thin films on glass substrates by solution casting. The film samples were characterized using techniques such as AFM, XRD, Raman analysis, FT-IR, DSC, TGA, UV-Vis-NIR absorption spectroscopy and four-probe conductivity measurement. The XRD pattern of CSA redoped polypyrrole film exhibits extraordinarily high crystallinity. The possible factors contributing towards the exceptional crystallinity are assumed to be the secondary doping effect of the solvent meta-cresol, the effect of controlled doping (redoping using one molar CSA) by which more crystallite regions are formed and

ultrasonication. The peaks in the XRD pattern of the PPy films were indexed by calculating hkl indices. The hkl indices suggest a simple cubic structure, and the dimension of the fundamental repeating unit is found to be 1.67 nm. The extent of crystallinity has been assessed using the DSC and XRD data. The estimated percentage of crystallinity in the present study is around 64%. The sharp peaks observed in the Raman spectrum of the PPy film provide further support for the increase in crystallinity of the CSA redoped PPy film samples, compared to the conventional HCl doped polypyrrole. The thermal analysis (TGA) establishes the higher thermal stability of the CSA redoped PPy film compared to the HCl doped powder sample. The room temperature d c electrical conductivity of the redoped polypyrrole film is about 30 times higher than that of the HCl doped PPy sample. The secondary doping effect of the solvent, m-cresol and the controlled doping using CSA facilitate the enhancements in crystallinity and electrical conductivity of the CSA redoped PPy films. It is the first time that PPy films with such exceptionally high extent of crystallinity have been synthesized and reported. Crystallinity influences many of the polymer properties, and hence it plays an important role while selecting polymers for specific applications. The present work is quite significant from this point of view.

8.2 Future prospects

The present work offers ample scope for further investigations, based on the results of the present studies and the conclusions drawn there from. The synthesis conditions of ZnO/PS-PMMA nanocomposite films can be further optimized to get highly transparent, freestanding

films with excellent UV shielding properties. Investigations can be extended to find the optimum size range of ZnO particles in the polymer nanocomposites to get the best optical response.

Extensive investigations to establish the nature of crystallinity in polypyrrole and other conducting polymers can be carried out and possible theoretical models can be predicted. Polypyrrole is known to be an excellent EMI shielding polymer. The relation between the extent of crystallinity and EMI shielding properties in PPy can be investigated in detail. The synthesis conditions of polypyrrole can be modified to get smaller sized PPy nano rods/tubes for various nanoscale applications.

.....ഇരു.....